Modeling and Optimization of Degradation of Dyes Present in Textile Waste Water using Supported Photocatalyst

A

Thesis

Submitted for the award of

DOCTOR OF PHILOSOPHY

Submitted by

Alok Garg

(Regn. No. - 951201002)

Under the supervision of

Dr. Pramod K. Bajpai
Former-Distinguished Professor

Dr. Vikas K. Sangal
Associate Professor

Department of Chemical Engineering
Thapar University, Patiala 147004, (Punjab), India

(October, 2016)

Dedicated to

My Family

CERTIFICATE

This is to certify that thesis entitled **"Modeling and Optimization of Degradation of Dyes Present in Textile Waste Water using Supported Photocatalyst"**, being submitted by Mr. Alok Garg, to the Department of Chemical Engineering, Thapar University, Patiala for the award of degree of **DOCTOR OF PHILOSOPHY**, is a record of bonafide research work carried out by him. Mr. Alok Garg has worked under our guidance and supervision and has fulfilled the requirements for the submission of this thesis, which to my knowledge has reached the requisite standard.

The results embodied in the thesis have not been submitted in part or full to any other University or Institute for the award of any degree or diploma.

Dr. Pramod K. Bajpai
Ex-Distinguished Professor
Department of Chemical Engineering
Thapar University, Patiala

Dr. Vikas K. Sangal
Associate Professor
Department of Chemical Engineering
Thapar University, Patiala

ACKNOWLEDGEMENTS

I would like to express my sincere gratitude to my both the thesis supervisors Dr. P. K. Bajpai, Former Distinguished Professor, Department of Chemical Engineering and Dr. V. K. Sangal, Associate Professor, Department of Chemical Engineering, Thapar University, Patiala, for their guidance, enthusiasm and insight in supervising the thesis. Their keen observations and valuable advice have provided incredible contribution to this thesis. Moral support & encouragement from them, useful criticism and constant help extended by them in the hours of need had been immensely useful. The enormous knowledge that I gained during their inspiring guidance would be valuable to me for all my future endeavors.

I am thankful to Dr. Prakash Gopalan, Director, Thapar University, for his generous financial assistance and facilitation of my research work. I would like to take this opportunity to put on record my respect to Dr. R. K. Gupta, Head, Department of Chemical Engineering, Thapar University for his constant support.

My sincere and grateful thanks are also due to Dr. R. K. Sharma, Dr. D. Gangacharyulu, Dr. Rajeev Mehta, Dr. H. Bhunia, Dr. Bonamali Pal, Dr. V. P. Singh and Dr. B. N. Chudasama for their moral support during my research.

I owe my grateful thanks to my friends, especially Dr. Sushant Upadhyay, Dr. J. P. Kushwaha, Dr. Sanghmitra Barman, Dr. Neetu Singh, Mr. Parminder Singh, Mr. Devender Kumar, Mr. Kundan Lal Rana, Dr. Dwarka Nath Ratha and Dr Ashish Kumar and many others who generously helped and encouraged me during my research work.

I am also thankful to the technical staff of the Department who helped me during the course of my research work. I am extremely grateful to the celebrated authors whose research work freely consulted and referred in my research work. I am also thankful to INUP at IIT Bombay (sponsored by DeitY, MCIT, Government of India) for FESEM and XPS analysis of the reported work.

I sincerely thank the Thapar University, Patiala for providing financial support and conducive environment to undertake this research work.

I wish to express my indebtedness to my wife Ms. Pooja, who have been always a source of strength and whose affection and patience enabled me to complete this thesis. I also owe a sense of apology to my daughter Anaya, whom I could not give their share of my time during this work. My thesis was made possible with the support from my family members. Needless to say that it was because of the efforts of my parents today I stand where I am.

I fully understand that the research experience and knowledge that I have gathered during the course of my Ph.D. programme would be highly useful throughout my professional career. This work was possible due to contributions of many. I am thankful to all of them and extremely sorry if anyone is left out in the acknowledgement. I thank the Almighty God for providing me an opportunity, strength and ambience to successfully accomplish this work.

(Alok Garg)

ABSTRACT

Synthetic dyes are mostly used in different industries like textile, paper etc. These dyes are discharged in the aqueous streams from the effluents of different industries like leather, textiles and paper etc. These dyes produce major environmental pollution problems by discharging polluting and potential carcinogenic substances. The dyeing and finishing industries are the major sources of pollutants in the industrial sector. Due to the toxicity and determination of the dyes, their removal from the textile wastewater has become an issue of interest during the last decades.

The complete mineralization of the dyes is not possible by conventional methods. The present study of water decontamination processes are concerned with the oxidation of the dyes. These methods depend on the formation of highly reactive chemical species that mineralize a number of recalcitrant molecules into non-toxic compounds and are called advanced oxidation processes (AOPs). Heterogeneous photocatalytic process employs the near UV irradiation to photo-excite a semiconductor photocatalyst. Using semiconductor based photocatalysis, organic contaminants (textile dyes) can be totally mineralized, reacting with the oxidizers to produce carbon dioxide, water and dilute concentration of simple mineral acids. Among the various semiconductors employed, the anatase phase of TiO_2 is known to be a good photocatalyst for the degradation of several pollutants due to its high photosensitivity and large bandgap. Despite the positive attributes of various photocatalysts, there are some drawbacks associated with their use. One of the major drawbacks is the band edge absorption threshold which does not allow the utilization of visible light. Bandgap tailoring by doping and codoping is the most efficient and frequently used approach. Photocatalytic degradation of organic dyes depends on temperature, agitation, catalyst loading, initial dye concentration, pH, geometry of reactor, flow behavior, radiation flux etc. Due to complexity of the processes, they are difficult to be modeled using conventional mathematical modeling. Artificial neural network (ANN) and response surface methodology (RSM) are the techniques that can be used for modeling and optimization of the photocatalytic treatment processes of water and wastewater. Immobilized

TiO_2 is an alternative solution to suspended TiO_2 systems mainly because of the convenience of not requiring additional post-treatment recovery of catalyst after the reaction process.

The present thesis deals with the modeling and optimization of the photocatalytic degradation (UV/TiO_2) of single dye and binary mixture using ANN and RSM. For improving the photocatalytic degradation of textile dyes, different metal ions have been doped and codoped on TiO_2, and immobilization of TiO_2 on solid support has been carried out.

Photocatalytic treatment of three textile dyes (RB5, AB113 and AR114) and binary dye mixture of AB113 and AR114 were carried out using suspension of commercially available TiO_2 catalyst under ultraviolet irradiation in a shallow pond reactor with UV light irradiation (UV-C). Two different methods, namely multivariate calibration and first order derivative spectrophotometric were used to quantify each dye separately in binary dye solutions. An artificial neural network (ANN) model was developed to predict the behavior of the process. Six operational parameters for single dye solution (TiO_2 dose, initial dye concentration, pH of the dye solution, area to volume ratio, UV light intensity and time) and five operational parameters (initial concentration of AB113 dye, initial concentration of AR114 dye, TiO_2 dose, pH of the dye solution and time) were employed as input parameters. The decolorization and degradation efficiencies for single dye solution and decolorization efficiency of AB113 and AR114 were employed as output of the network. The outcomes have been validated experimentally indicating that the ANN provided reasonable predictive performance. The parameteric optimization was done, by using multi-response optimization with desirability function approach, to simultaneously maximize the decolorization and degradation efficiency. Optimization of photocatalytic decolorization and degradation of dye and dye mixture by RSM effectively copes with interaction between optimizing variables and its prediction agreed well with the results of ANN model and experimental run. The decolorization and degradation of the single dye solution follows the first order kinetics and decolorization of binary mixture of AB113 and AR114 follow the first order kinetics. Total organic carbon (TOC) removal and GC-MS study of all the dyes show the total mineralization.

TiO_2 nanoparticles have been doped and codoped with four different metal ions (Fe, Cu, V and Co) by wet impregnation method with 1 and 2 wt% metal. The doped and codoped TiO_2 has been characterized by standard analytical techniques like XRD, FESEM, TEM, FTIR, UV-Vis DRS and XPS. The powder XRD technique reveals that the modified catalyst contains anatase phase and existence of metal ion in the lattice of TiO_2. FESEM images reveal that average particle size of modified TiO_2 lies between 18 to 24 nm due to asymmetric shape of nano-crystallite TiO_2. From TEM images it is clear that the doping and codoping of metal ions do not leave any change in the shape of the nanoparticles. FTIR patterns show the stretching and vibration patterns of hydroxyl radicals present in nanoparticles. UV-Vis used to find out the energy band gap of modified nanoparticles (2.38, 2.45 and 2.53 eV for $TFe_{1.0}Cu_{1.0}$, $TFe_{1.0}V_{1.0}$ and $TFe_{1.0}Co_{1.0}$ respectively). X-ray Photoelectron Spectroscopy (XPS) showed the elemental surface composition and oxidation state of elements. The photocatalytic activity of the modified nanoparticles (Fe, Cu, V and Co doped and codoped TiO_2) has been studied by photo-decolorization of three textile dyes (Reactive Black 5, Acid Red 114 and Acid Blue 113) under 250 W low pressure halogen lamp. Photocatalytic study shows that the two metal ions codoped TiO_2 retained enhanced rate in comparison to doped and un-doped TiO_2 for the decolorization of all the three textile dyes. The reaction kinetics show the highest rate for the photocatalytic decolorization using codoping of two metal ions for the three dyes.

Further TiO_2 has been immobilized on cement beads using dip coating method. The stability of immobilized beads has been checked in batch reactor and found that the immobilization of TiO_2 is stable for more than 25 cycles. Baffled fixed bed reactor has been used for this study in continuous mode, and it was found that all the three dyes have been degraded up to 90% using baffled fixed bed reactor. Reaction kinetic results show that decolorization of all the three dyes follows the first order reaction kinetics.

Table of Contents

List of Symbols

Symbol	Description	Units
Abs_x	Absorbance at x nanometer wavelength	-
C_i	Concentration of intermediate i	mg l^{-1}
C	Dye concentration at any time t	mg l^{-1}
C_o	Dye concentration at t = 0	mg l^{-1}
e^-	Electron	-
h^+ vb	Hole in valance band	-
•OH	Hydroxyl radical	-
k’	Pseudo-first-order rate constant	min^{-1}
k	First-order rate constant	min^{-1}
t	Time of reaction	min
$[RB5]_o$	Initial concentration of RB5	mg l^{-1}
$[AB113]_o$	Initial concentration of AB113	mg l^{-1}
$[AR114]_o$	Initial concentration of AR114	mg l^{-1}
A/V ratio	Area to volume ratio	cm^{-1}
E_g	Energy band gap	eV
$[TiO_2]$	TiO_2 dose	g l^{-1}
λ	Wavelength	nm

List of Abbreviations

Abbreviation	Description
AB113	Acid Blue 113
ANN	Artificial neural network
ANOVA	Analysis of variance
AOP	Advanced oxidation process
AR114	Acid Red 114
BBD	Box-Behnken Design
BET	Branauer-Emmett-Teller
CB	Conduction band
CCD	Central composite design
DF	Degree of freedom
DOE	Design of experiment
FESEM-EDS	Field-emission scanning electron microscope-energy dispersive spectroscopy
FTIR	Fourier transform infrared spectroscopy
MLF	Multi layered feed forward
MSE	Mean square error
pH_{pzc}	Point of zero charge pH
RB5	Reactive Black 5
RSM	Response surface methodology
SEM	Scanning electron microscope
TEM	transmission electron microscopy
TOC	Total organic carbon
UV	Ultraviolet
UV-DRS	UV-visible diffuse reflectance spectroscopy
VB	Valance band
Vis	Visible
XPS	X-ray photoelectron spectroscopy
XRD	X-ray diffraction

List of Figures

List of Tables

Chapter 1 INTRODUCTION

1.1 Water: The Environmental Problem

Environmental safety and the improvement of environmental issues are the main concern for an actual development of life and for a sustainable development. Water has been utilized in various human deeds for a lot of purposes such as agriculture, industry, domestic and energy production. Globally, domestic use only represents 15% of the total water consumption, while 25% is used in industrial activities and 60% in agriculture. Associated to each of these activities are distinct types of pollution and pollutant compounds. The industrial wastewater streams are posing serious threat to human life, plants and animals and also to ecosystems of receiving water bodies. One of the major sources of ground water and surface water pollution is industrial effluents from textile, pulp and paper, pharmaceutical and other chemical industries [1, 2].

1.2 Dyes and Environmental Concern

It has been predicted that approximately 15 % of the dye is discharged as wastewater from dyeing industry [3]. The color is typically the first pollutant to be identified in the wastewater, which is produced by using synthetic dyes in the industries. Considering both effluent compositions and volumes discharged, the wastewater produced by the textile industry is appraised as one of the most polluting among all industry sectors. Given the large diversity of fibers, dyes, process aids and finishing products in use, the textile industry produced wastewater of great chemical complexity, diversity and volume [4]. Because of increasing demands in textiles, synthetic organic dyes are extensively used in dyeing process for textile fiber like polyester and cotton [5]. Besides the textile industry, the use of synthetic dyes is increasing day by day for coloring of materials such as leather, paper, plastics, petroleum and food products [6]. The dyes are used to color the products and the residuals are discharged into the environment, particularly aquatic environment. Synthetic dyes are difficult to biodegrade because of their complex aromatic nature. Thus, the removal of color from wastewater becomes a challenging problem. The release of the dye wastewater into the ecosystem, million cubic

meters discharged per year to waste water treatment systems, is a remarkable source of aesthetic pollution, eutrophication, perturbation in aquatic life as well as human life disorders. The wastewater containing textile dyes are toxic and carcinogenic. Synthetic dyes such as azo dyes (present one or more azo bonds) have been used more than 50 % of the dyeing in the textile industry and are major source of pollutants in the wastewater. Unfortunately, the dyes, mostly azo dyes with aromatic structures, are recalcitrant in nature. The azo dyes are difficult to degrade by aerobic digestion and steady in oxidizing agents [7]. Wastewater from the dyeing processes is at high temperature and different pH, holding a high amount of the color elements. These concerns have been directed to new and/or stringent rules regarding wastewater discharge from dyeing industry and requires more efficient treatment methods.

Also, most of the treatment studies have been done based on single dye solution. However, industrial effluents discharge a mixture of several dyes and limited information is available on multi-component dye degradation. The simultaneous analysis of multi-component dye mixtures is very complex problem in analytical chemistry due to the spectral interferences, which results in widely overlapped absorption bands. [8].

1.3 Methods for Removal of Dyes and Other Organic Compounds from Wastewater

A wide range of methods have been established over last two decades to remove color from dye contaminated wastewaters in order to reach ecological and environmental guidelines as well as economic constraints. The conventional technologies currently used to degrade the color of the dye-contaminated water include microbiological decomposition (aerobic and anaerobic), enzymatic decomposition, chemical precipitation, adsorption on organic supports (bentonite [9], biogas waste slurry, orange peel, waste banana pith etc.), inorganic supports (carbon, coal, fly ash, china clay, silica, alumina, red mud etc.), flocculation, physiochemical methods (adsorptive bubble separation, electrocoagulation, coagulation etc.) and chemical processes (chlorination, ozonation). However, the complete degradation of these recalcitrant organic compounds present in wastewater is not possible by these well-established techniques. Some of the advantages and disadvantages of these techniques are listed in Table 1.1.

Most of the techniques do not reduce contaminants but they transfer pollutants from one stage to other stage. Some techniques will be selective but slow to moderate in degradation

rate. Other alternative methods produce more harmful intermediates and some methods require more treatment time [10]. The incapability of traditional wastewater treatment techniques to effectively destroy a lot of bio-recalcitrant contaminants leads to discover the new effective treatment systems, which are effective for the complete degradation and mineralization of these contaminants. The advanced oxidation processes (AOPs) have appeared as one of the most auspicious technologies for the degradation of the contaminants/pollutants/toxicants [11].

Table 1.1 Advantages and disadvantages of current methods for dye removal from industrial effluents [12]

Physical/Chemical methods	**Advantages**	**Disadvantages**
Fenton reagent	Effective decoloration of soluble and insoluble dyes	Sludge generation
Ozonation	Applied in gaseous state, no alteration of volume	Short half-life (20 min)
Sodium hypochlorite	Initiates and accelerates azo-bond cleavage	Release of aromatic amines
Electrochemical destruction	Break-down products are non-hazardous	High electricity consumption
Activated carbon	Good removal of a wide variety of dyes	Very expensive
Peat	Good adsorbent due to cellular structure	Specific surface areas for adsorption are lower than activated carbon
Wood chips	Good sorption capacity for acid dyes	Requires long retention times
Silica gel	Effective for basic dye removal	Side reactions prevent commercial application
Membrane filtration	Removal of all dye types	Concentrated sludge production
Ion exchange	No adsorbent loss due to regeneration	Not effective for all dyes
Irradiation	Effective oxidation at laboratory scale	Requires high concentrations of dissolved oxygen
Electro coagulation	Economically feasible	High sludge production

1.4 Advanced Oxidation Processes

The water purification research has been rising mainly from the last few decades. Special consideration made to the environment by political, social, and legislative international authorities, has caused a rigorous research for novel and more competent degradation techniques for pollutants in the wastewater. The AOPs are attractive substitute for the treatment of polluted surface and ground wastewater covering hardly biodegradable anthropogenic

materials and for the cleansing and decontamination of drinking water [13-20]. US-EPA (United State Environmental Protection Agency) has permitted the use of advanced oxidation processes (AOPs) as a best accessible technique to achieve the standard and requirement that deliver safe and sufficient pollution control of industrial processes and remediation of polluted sites. More than 800 organic molecules as well as organic dyes can be destroyed by AOPs [21]. Extremely reactive hydroxyl radicals (•OH) are conventionally believed to be the dynamic species responsible for destroying the contaminants [17, 20, 22, 23]. Hydroxyl radical has a high standard redox potential of 2.8 V in acidic media (Table 1.2) [24].

Table 1.2 Standard reduction potentials of some oxidants in acidic media [24]

Oxidant	Standard reduction potential (V)	Oxidant	Standard reduction potential (V)
Fluorine (F_2)	3.03	Hypobromous acid (HBrO)	1.59
Hydroxyl radical (•OH)	2.80	Chlorine dioxide (ClO_2)	1.50
Atomic oxygen (O)	2.42	Hypochlorous acid (HClO)	1.49
Ozone (O_3)	2.07	Chlorine (Cl_2)	1.36
Hydrogen peroxide (H_2O_2)	1.77	Bromine (Br_2)	1.09
Perhydroxyl radical (O-OH)	1.70	Iodine (I_2)	0.54
Potassium permanganate ($KMnO_4$)	1.67		

These radicals are able to oxidize almost all organic compounds to carbon dioxide and water. The formation of carbon dioxide is of great significance in wastewater treatment, as it is the explicit indication for the total destruction of organic compounds in water. Advanced oxidation processes can be generally classified into homogeneous and heterogeneous processes.

1.4.1 Homogeneous Photocatalysis

The application of homogeneous photocatalysis (single-phase system) to treat polluted surface water, concerns the use of UV/H_2O_2 and UV/ozone [25, 26]. The use of UV light for photo-degradation of contaminants can be classified into two principal areas. Direct

photodegradation, which proceeds following direct excitation of the contaminants by UV light and photo-oxidation, where light drives the oxidation processes principally initiated by hydroxyl radicals. The later process includes the use of an oxidant to produce radicals, which attack the organic contaminants to initiate oxidation. The major oxidants used are: ozone (UV/O_3), hydrogen peroxide and ozone ($UV/O_3/H_2O_2$), hydrogen peroxide (UV/H_2O_2), and photo-Fenton system (Fe^{3+}/H_2O_2).

1.4.2 Heterogeneous Photocatalysis

The definition of photocatalysis is principally the speeding up the photoreaction in the presence of a catalyst. Further in deep, the method would contain a catalyst, which may speed up the photoreaction by interaction with the reactants in its ground or excited state and/or with a primary photo product, depending upon the mechanism of the photoreaction. The method is heterogeneous due to involvement of two active phases, solid (catalyst) and liquid (substrate).

Heterogeneous photocatalytic process employs the near UV irradiation to photo-excite a semiconductor catalyst in the presence of oxygen. Under these conditions, oxidizing species, either bound hydroxyl radicals or free holes, are generated. Using photocatalysis, organic contaminants (textile dyes) can be totally mineralized, reacting with the oxidizers to produce carbon dioxide, water and dilute concentration of simple mineral acids. This process can also be carried out utilizing the near part of solar spectrum ($\lambda < 380$ nm) [1]. The semiconductor based catalyst may be in the form of a powder suspended in the water or fixed on a solid support.

1.4.2.1 Catalysts Used in Heterogeneous Photocatalysis

Several semiconductor oxides are utilized as catalysts for the heterogeneous photocatalytic reactions. The redox potential of the valence band (VB) and the conductance band (CB) for diverse semiconductors differs between + 4.0 and -1.5 V. Consequently, by broad range of the semiconductor photocatalyst, an extensive variety of species could be treated by AOP techniques. Metal oxides and sulphides characterize a huge class of semiconductors, appropriate for photocatalytic processes. It has been shown in Table 1.3 that some of the semiconductors, utilized in photocatalytic processes with the valance band and conductance

band potentials, have the energy band gap and wavelength essential to stimulate the catalyst that generate this gap. The radiation must be of an equivalent or lesser wavelength than that calculated by the Planck's equation (eq. (1.1)).

$$\lambda = \frac{h\,c}{E_{bg}} \tag{1.1}$$

Where E_{bg} is the semiconductor band gap energy, h is the Planck's constant and c is the speed of light.

Table 1.3 Band positions of some common semiconductor photocatalysts

Semiconductor	Valence band (V vs NHE*)	Conductance band (V vs NHE*)	Band gap (eV)	Band gap wavelength (nm)
TiO_2	+ 3.1	- 0.1	3.2	387
SnO_2	+ 4.1	+ 0.3	3.9	318
ZnO	+ 3.0	- 0.2	3.2	387
ZnS	+ 1.4	- 2.3	3.7	335
WO_3	+ 3.0	+ 0.2	2.8	443
CdS	+ 2.1	- 0.4	2.5	496
CdSe	+ 1.6	- 0.1	1.7	729

*NHE is normal hydrogen electrode

Several semiconductor photocatalysts have been discovered for the photocatalytic redox reactions, for example WO_3, TiO_2, ZnO, and Fe_2O_3 (with wide band gap energies). Others like CdS, ZnS, V_2O_5, ZrO_2, SnO_2, CeO_2 and Sb_2O_4 have also been established to show photocatalytic activity, but only as compared to titania or ZnO. Among the possible semiconductors that can be used in heterogeneous photocatalysis, titanium dioxide, (E_{bg} = 3.2 eV) is most extensively used. ZnO also appears to be an appropriate photocatalyst, but it is soluble in acidic medium and so, cannot be utilized for low pH contaminants. Further, semiconductors like CdS absorb higher portions of the sun light as comparison to TiO_2. These semiconductors also form chemically stimulated surface bond byproducts, but inappropriately, these catalysts are treated through the frequent catalytic repetitions typically included in heterogeneous photocatalysis [27]. Therefore, TiO_2 is still the most appropriate photocatalyst for extensive environmental applications. Among several semiconductor materials, titanium

dioxide (TiO_2) has been demonstrated to be the most active photocatalyst for the degradation of organic compounds with similar conditions [28].

1.4.2.2 Photosensitization of the Catalyst

TiO_2 has some limitations too. It uses only about 4-6 % of the solar energy reaching the earth's surface which is in the UV region. This limitation is overcome by its modification. It has been modified by doping and codoping of metal ions and photosensitization by various colored inorganic and organic compounds, in order to spread the photo response of large bandgap semiconductors into the visible region to utilize them for the degradation of colored organic pollutants and other organic contaminants. The metal ions added into polycrystalline TiO_2 or photo-deposited metals increase the absorption of radiation. Therefore, research on catalyst improvement has been done so far on the following points:

i. Physical and chemical modification of TiO_2 to improve the catalyst performance.
ii. Dye sensitization to increase the useful wavelength range of the solar radiation.

A diversity of colored compounds has been considered to act as photosensitizers. In recent researches, it has been recommended that photosensitized degradation on semiconductor surfaces can have significant applications for treating a specific class of colored contaminants like textile dyes.

1.4.2.3 Advantages and Limitations of Heterogeneous Photocatalysis

Heterogeneous photocatalysis along with other AOPs differs from the other treatment processes in the aspect that the compounds present in wastewater are degraded rather than transferred or concentrated into another phase. Because secondary waste materials are not produced, there is no need to dispose off or regenerate materials [29]. A large number of organic compounds dissolved or dispersed in water can be completely mineralized. The rate of reaction is relatively high, if large surface area of the catalyst can be used. UV lamps releasing photons in the spectral region, essential to initiate the photocatalytic oxidation are well known

and are produced in various sizes. Absorption cross-section of photocatalysts can be improved by surface modifications, for example by transition metal ion doping.

One of the limitations of the particulate excitation of the semiconductors is the high degree of recombination between the photo-generated charge carriers. As a consequence of this electron-hole recombination, the effectiveness of the semiconductors reduces thereby, decreasing the quantum yield of the redox processes. Another drawback of this process is that the liquid-solid separation is expensive, because of the formation of milky dispersions after mixing the powder catalyst in water. It is also required to study the photocatalysis under continuous mode. This drawback can be overcome when the TiO_2 can be supported on the inert substrate.

1.5 Titanium Dioxide as a Photocatalyst

Among the various semiconductors employed, the anatase phase of TiO_2 is known to be a good photocatalyst for the degradation of several pollutants due to its high photosensitivity and large bandgap. The bandgap of TiO_2 (3.2 eV) is too large to generate many charge carriers by thermal excitation, charge carriers are generated by absorption of photon with energy equal to or greater than 3.2 eV, which corresponds to UV light of wavelength < 380 nm. The three polymorphic crystalline structures of TiO_2 are anatase (tetragonal), rutile (tetragonal) and brookite (orthogonal). Brookite is not photoactive. Anatase is generally accepted to be more photoactive than rutile, although it may not be true for all conditions or reactions [30]. This is believed to be true due to the bandgap of anatase being wider than that of rutile by about 0.2 eV and higher degree of surface hydroxylation in anatase.

When TiO_2 is illuminated with light of wavelength < 380 nm, upon absorption of a photon by TiO_2 particle, an electron is excited from the valence band to the conduction band leaving behind a hole in the valence band. On the TiO_2 surface, electrons and holes participate in redox reactions. The holes can oxidize water or hydroxide ions into hydroxyl radicals. The excited electrons reduce molecular oxygen to produce superoxide radicals. Both these hydroxyl (•OH) and superoxide radicals ($O_2^{\bullet-}$) are strong oxidizing agents for the decomposition of

organic pollutants such as textile dyes. The application of TiO_2 photocatalyst under visible light is limited due to its wide band gap. So there is a requirement to develop a catalyst of narrow band gap, which can be active under visible light.

1.5.1 Surface Modification of Semiconductor by Metal/Metal ion

Despite the positive attributes of various photocatalysts, there are some drawbacks associated with their use: (i) charge carrier recombination occurs within nano seconds [31, 32] and (ii) the band edge absorption threshold does not allow the utilization of visible light [33]. To overcome these limitations, a number of strategies have been proposed to improve the light absorption features and lengthen the carrier life time characteristics of the catalyst. The long wavelength absorption can be achieved by dye sensitization [34], external surface modification [35] or bandgap tailoring. Dye sensitization of TiO_2 with a number of organic dyes extends the sensitivity of TiO_2 into the visible region by injection of electrons from an excited level of the dye into the semiconductor conduction band. Bandgap tailoring by doping is the most efficient and frequently used approach. Doping, with certain limits, serves to prolong the lifetime of charge carriers if the dopants have energy levels just below the conduction band or just above the valence band of TiO_2 to realize shallow charge carrier trapping. Bandgap narrowing also becomes possible if the electronic coupling effect between dopant and semiconductor is strong enough to change the band structure. The bandgap narrowing can cause a small reduction of the photoredox potential energy of TiO_2 but the increased photon absorption efficiency or generation rate of charge carriers can compensate for this negative effect and largely enhance the overall photoreactivity as long as the redox potential of $H_2O/•OH$ couple (~ -2.8 V) lies within the bandgap. Doping with various metal and non-metal ions have been attempted to improve the photocatalytic activity and optical absorption of TiO_2. Another main approach to increase the efficiency of charge separation involves the coupling of semiconductor particle with another semiconductor.

The doping of a range of transition metal ions in to TiO_2 could shift its optical absorption edge from UV to visible light range, but a major change in TiO_2 band gap has not

been observed [36]. Also, the transition metal ion doped TiO_2 has some severe drawbacks, such as low quantum efficiency of photo induced charge carriers and thermal instability. Further improvement in photocatalytic properties was reported when TiO_2 was codoped with suitable amount of more than one type of metals [37]. Few studies [38, 39] also showed that the codoping with two transition metals or metal ions could successfully modify the electronic structures of TiO_2 and shift its absorption edge to a lower energy [40]. Recently, research work on metal codoping of TiO_2 has been reported [41-43]. This configuration has a number of advantages, including the improvement of charge separation, the increase in the lifetime of the charge carrier and enrichment of the interfacial charge transfer to the adsorbed substrate. Different types of codoped TiO_2 have been reported by several researchers. However, there is still a need to develop new effective codoped photocatalyst for the treatment of dyes present in textile wastewater.

1.5.2 Immobilization of TiO_2 on Solid Supports

Immobilized TiO_2 is an alternative solution to suspended TiO_2 systems mainly because of the convenience of not requiring additional post-treatment recovery of catalyst after the reaction process. Such photo reactors have photocatalysts immobilized or coated on porous and non-porous support substrates. The support materials vary largely depending on reactor design, requirements and applications. Some researchers have designed immobilized photo reactors with catalyst coated on the reactor walls [44-47]. However, when the photocatalyst is immobilized, one has to sacrifice substantial amount of active surface area available for reaction since the catalyst has to be adhered onto a support substrate. Inadequate mixing and interaction between the photocatalyst and aqueous matrix in the reaction solution may also impede and reduce photocatalytic efficiency. Moreover, undesirable introduction of foreign ionic species from the supporting substrate can compromise catalyst purity and contribute to recombination of charges within the photocatalyst, leading to its deactivation [48].

1.6 Modeling and Optimization

Photocatalytic degradation of organic dyes depends on agitation, catalyst loading, initial dye concentration, pH, geometry of reactor, flow behavior, radiation flux etc. Due to complexity of the processes, they are difficult to be modeled using conventional mathematical modeling. Artificial neural network (ANN) is used in many areas of science and engineering as a promising tool because of its simplicity in prediction and modeling of process performance [49]. One of the characteristics of modeling based on ANN is that it does not require the mathematical description of the phenomena involved in the process, and therefore might prove useful in simulating and upsizing complex photochemical systems [50]. ANN and response surface methodology (RSM) are the techniques that can be used for modeling and optimization of the photocatalytic treatment processes of water and wastewater.

1.6.1 Artificial Neural Network (ANN)

The ANN is an artificial intelligence technique that mimics the human brain's biological neural network in the problem solving processes. As humans solve a new problem based on the past experience, a neural network takes previously solved examples, looks for patterns in these examples, learn these patterns and develops the ability to correctly classify new patters. In addition, the neural network has the ability to resemble human characteristics in problem solving that is difficult to simulate using logical, analytical techniques of expert system and standard software technologies [51]. A neural network is defined as a system by a set of weights. The neuron is a processing element that takes a number as inputs, weights them, sums them up, adds a bias and uses the outcome as the argument for single-valued function (transfer function) which results in the neuron's output [52].

1.6.2 Response Surface Methodology (RSM)

Response surface methodology (RSM) is a collection of mathematical techniques that are useful for the optimizing of process variables in which a response of interest is influenced by several variables and the objective is to optimize this response. It is a sequential

experimentation strategy for optimization. This methodology not only estimates linear interaction, and quadratic effects of the factors on the response, but also provides a prediction model for the response at the range of the variables studied and the optimum conditions to achieve the highest performance. By conducting experiments and applying regression analysis, a model of the response to some independent input variables can be obtained. Based on the model of the response, a near optimal point can then be deduced.

Chapter 2 LITERATURE REVIEW

In this chapter, a comprehensive literature review of the fundamentals of semiconductor photocatalysis along with the modification of TiO_2 has been presented. The mechanism, applications, drawbacks, and the operational parameters affecting TiO_2 photocatalysis have also been described. Methods for enhancing the efficiency of TiO_2 photocatalysts along with the need of its immobilization have been dealt with. Later on modeling and optimization of photocatalytic degradation of textile wastewater have been discussed.

2.1 Fundamentals of Semiconductor Photocatalysis

Semiconductors have been characterized by an intermediate electronic behavior i.e., a semiconductor is a solid, whose electrical resistivity (or conductivity) lies in between insulator and conductor [53]. The electronic structure of a solid can be explained well with the help of the band gap theory. According to this theory, two bands for a crystalline solid are proposed namely, the valence band (VB), which is the highest occupied molecular orbital (HOMO) comprising of bonding orbitals, and the conduction band (CB), which is the lowest unoccupied molecular orbital (LUMO), comprising of anti-bonding orbitals. The two bands are detached by a prohibited zone known as the band gap or energy gap (E_g). In the case of metallic conductors, there is superficially an absence of band gap between the VB and the CB due to the overlapping of the molecular orbitals. Whereas, in insulators, a large band gap separates the VB and the CB. A relatively intermediate band gap is present between the VB and the CB in case of semiconductors [54].

The term “photocatalysis” is a composite word that is made of two words “photo” and “catalysis.” “Photo” means light and “catalysis” is described as a process in which a substance, known as catalyst, modifies the rate of a chemical reaction without itself being affected [55]. The catalyst increases the rate of reaction by lowering the activation energy. Thus, photocatalysis is defined as a reaction that utilizes light radiation to activate a substance - the photocatalyst, which absorbs light and initiates a chemical reaction or modifies its rate without

itself being involved [56]. The main difference between a photocatalytic reaction and a traditional catalytic reaction is that the catalyst has been activated by light in the former case and by heat (major catalytic reactions) in the latter. On the basis of difference in the phase of reacting species and the catalyst, the photocatalytic processes can be categorized as homogeneous and heterogeneous. In homogeneous photocatalysis, the substrates and the photocatalysts should be in the same phase. The best commonly used homogeneous photocatalysts include ozone and photo-Fenton systems. In the case of heterogeneous photocatalysis, the photocatalysts and the reactants are present in different phases [57]. Heterogeneous photocatalysis using semiconductor as a photocatalyst has been an active area of research since 1972, when Fujishima and Honda published their novel finding in 'Nature' that ultraviolet (UV) irradiated TiO_2 electrode could split water into hydrogen and oxygen [58]. This discovery has since been regarded as a stepping-stone for the numerous other studies carried out on photocatalysis till date. As a common rule, a good photocatalyst for photocatalytic oxidation is characterized by the following attributes [55, 59]:

- Photoactivity,
- Inexpensive and ready availability,
- Non-toxicity,
- Chemically and biologically inert,
- Ability to absorb visible and/or near UV light,
- Photostability, and
- Capability to adsorb reactants under efficient photonic activation.

In other words, an efficient photocatalyst should have a combination of good photoelectronic and chemisorptive properties so that it possesses the features as able to efficiently absorb photons; has ability to generate electron-hole (e^- - h^+) pairs, and is able to separate them so as to have a minimum rate of recombination. The semiconductors that are most commonly used as photocatalysts are oxides or sulfides of the transition metals. The inorganic semiconductors have been identified as the most successful photocatalysts that are finding use in various kinds of applications. Some examples of significant semiconductors

being used in the field of environmental heterogeneous photocatalysis are titanium dioxide (TiO_2), zinc oxide (ZnO), zinc sulfide (ZnS), cadmium sulfide (CdS), tungsten oxide (WO_3), tin oxide (SnO_2), cadmium telluride (CdTe), iron(III) oxide (α-Fe_2O_3), silver niobium trioxide ($AgNbO_3$) and strontium titanate ($SrTiO_3$) [53]. Figure 2.1 summarizes the band gap energies of some commonly used semiconductor photocatalysts at pH = 0. Although these metal oxide semiconductors have been tested for various environmental remediation, their use for large-scale applications is restricted because of one or more of the following reasons:

i. Instability in aqueous medium that leads to the decomposition of the photocatalyst,
ii. Large band gap that often necessitates the use of UV light, and
iii. High electron (e^-) - hole (h^+) recombination rates.

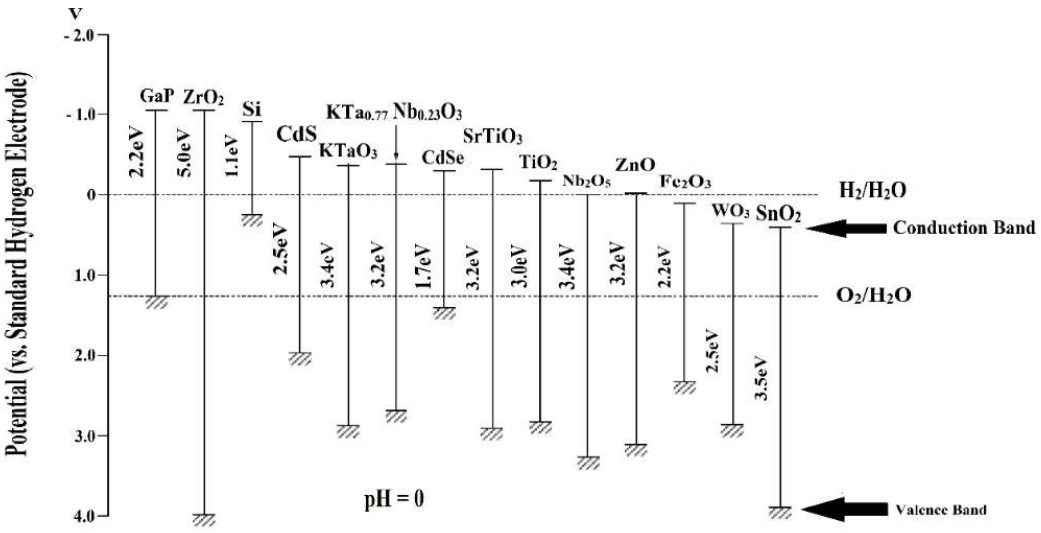

Figure 2.1 Energy band gap of some commonly used semiconductor photocatalysts [60]

For example, the relatively shorter band gap of CdS makes it a prospective photocatalyst for solar cells and photocatalysis as it can absorb most part of the visible light. However, it is not very stable under photocatalytic reaction conditions. It undergoes photocorrosion and releases toxic Cd^{2+} ions in aqueous medium [53, 61, 62]. Similarly, ZnO shows several important features such as piezoelectric properties and extended spectral absorption but its tendency for photo-dissolution is a problem that affects its efficiency as a photocatalyst [62, 63]. On the other hand, SnO_2 has a wider band gap (3.5-4.2 eV; 350–300 a nm) thus utilizing lesser fraction

of UV light, and therefore exhibits a relatively lower photoactivity [64]. Although both WO_3 and hematite (α-Fe_2O_3) can be activated in the visible light yet their use is restricted owing to a relatively lesser photocatalytic activity [65-67].

2.1.1 Heterogeneous Photocatalysis

Heterogeneous photocatalysis is a discipline that includes a large variety of reactions like mild or total oxidation, dehydrogenation, hydrogen transfer, metal deposition, gaseous pollutant removal, bactericidal action, and water detoxification etc. [68]. Heterogeneously dispersed semiconductor surface provides both a fixed environment to influence the chemical reactivity of a large range of adsorbates and a means to initiate light induced redox reactivity in these weakly associated molecules [69]. The photo-excitation process results in simultaneous oxidation and reduction reactions. Figure 2.2 shows various reactions occurring over the TiO_2 semiconductor [68].

A number of excellent reviews are available in literature regarding heterogeneous photocatalysis with comprehensive discussions on all relevant aspects [30, 55, 70-73]. A review by Herrmann suggests that the photocatalytic process can be divided in to five independent steps [68].

1. Mass transfer (diffusion) of the reactant(s) from the bulk fluid to the external surface of the catalyst
2. Adsorption of reactant onto the catalytic surface
3. Reaction on the surface of the catalyst
4. Desorption of the products from the surface
5. Mass transfer of the products from the external surface to the bulk fluid

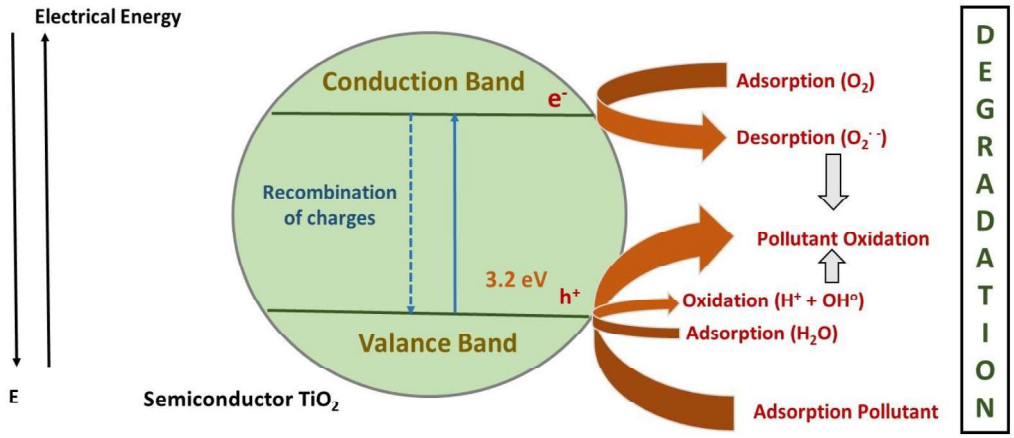

Figure 2.2 Photocatalysis process on TiO_2 surface [68]

Steps 1, 2, 4 and 5 of photocatalysis are common to conventional catalytic reactions. However, the step 3 contains all the photo-electronic processes and can be subdivided in to following steps.

a) Absorption of a photon by solid and not by reactant. There is no photochemistry in adsorbed phase.

b) Creation of electron hole pairs which dissociate in to photoelectron and positive holes

c) Electron transfer reactions such as ionosorption, charge neutralization, surface reactions, etc.

When TiO_2 surface is irradiated with UV radiation, the valance band electrons of TiO_2 are excited and jump to conduction band. This results in generation of an electron-hole pair. Minimum energy required for generation of an electron-hole pair is 3.2 eV. This electron-hole pair results in different oxidation and reduction reactions unless recombination of electron-hole pair occurs. Major reaction during photocatalytic degradation of dyes can be expressed as follows [74]:

$$TiO_2 + h\nu(UV) \leftrightarrow TiO_2(e_{CB}^- + h_{VB}^+) \quad (2.1)$$

$$TiO_2(h_{VB}^+) + H_2O \rightarrow TiO_2 + H^+ + \cdot OH \quad (2.2)$$

$$TiO_2(h_{VB}^+) + OH^- \rightarrow TiO_2 + \cdot OH \quad (2.3)$$

$$TiO_2(e_{CB}^-) + O_2 \rightarrow TiO_2 + O_2^{\cdot -} \quad (2.4)$$

$$O_2^{\cdot -} + H^+ \rightarrow HO_2^{\cdot} \quad (2.5)$$

$$Dye + \cdot OH \rightarrow degradation\ products \quad (2.6)$$

$$Dye + h_{VB}^{+} \rightarrow oxidation\ products \quad (2.7)$$

$$Dye + e_{CB}^{-} \rightarrow reduction\ products \quad (2.8)$$

In the above equations, OH^- $\bullet OH$, and $O_2^{\cdot-}$ represent hydroxyl ion, hydroxyl radical and superoxide anion respectively. Various AOPs depend upon application of hydroxyl radical for oxidizing the pollutant. In case of TiO_2 based photocatalytic degradation, oxidation and reduction reactions based upon eq. (2.7) and (2.8) are important, since cationic dyes get adsorbed over catalyst surface in acidic pH conditions.

There are certain reactions in which adsorbed phase plays a role by taking part in photoelectronic processes during photocatalysis. The adsorbed phase in certain cases of dyes receives energy from photon in visible range of wavelength. Excitation of an electron in the dye molecule happens to either the singlet or triplet excited state of the molecule (eq. (2.9)). If the oxidative energy level of the excited state of the dye molecule with respect to the conduction band energy level of the semiconductor is favorable (i.e. more negative), the dye molecule can transfer the electron to the conduction band of the semiconductor (eq. (2.10)). The surface acts as a quencher accepting an electron from the excited dye molecule. The electron in turn can be transferred to reduce an adsorbed organic acceptor molecule or adsorbed oxygen on the surface (eq. (2.11)) whereas the dye is converted to the cationic dye radicals (Dye•+) that undergoes degradation (eq. (2.12)). This is called surface sensitization. Surface sensitization of a wide bandgap semiconductor photocatalyst (TiO_2) via chemisorbed or physisorbed dyes can increase the efficiency of the excitation process. Thus photosensitization process can also expand the wavelength range of excitation for the photocatalyst through excitation of the sensitizer followed by charge transfer to the semiconductor [75].

$$Dye + h\nu(vis) \rightarrow Dye^{*} \quad (2.9)$$

$$Dye^{*} + TiO_2 \rightarrow Dye + TiO_2(e_{CB}^{*}) \quad (2.10)$$

$$TiO_2(e_{CB}^{*}) + O_2 \rightarrow O_2^{\cdot-}TiO_2 \quad (2.11)$$

$$Dye^{+} \rightarrow degradation\ products \quad (2.12)$$

Solar radiation can be utilized as source of energy. Additionally, this technology is emerging due to lack of restrictions in mass transfer, the capability to be accepted at the ambient conditions, and its ability to completely mineralize the pollutants [76]. Heterogeneous photocatalysis consists of employing the near UV radiation to photo-excite a semiconductor catalyst in the presence of oxygen. Under these conditions oxidizing species, either bound hydroxyl radicals or free holes, are generated as shown in Figure 2.2. Using photocatalytic process, organic contaminants can be totally destroyed reacting with the oxidizers to form carbon dioxide, water and dilute concentration of modest mineral acids. This process can also be carried out utilizing the part of solar spectrum ($\lambda < 380$ nm) which transforms it into a good option to be used [77]. TiO_2/ UV process holds several advantages [78]:

1. A wide number of organic complexes dissolved or dispersed in water can be totally destroyed.
2. The rate of reaction is comparatively high, if large surface area of the catalyst can be used.
3. TiO_2 is available at a relatively low price and can be recycled on a technical scale.
4. UV lamps emitting in the spectral region required to initiate the photocatalytic oxidation are well-known and are produced in various sizes.
5. Absorption cross-section of TiO_2 can be improved by its surface modifications, e.g. by transition metal ion doping and codoping.

TiO_2 has been reported as the most efficient photocatalyst that is being used for the removal of aqueous contaminants till date. This is attributed to its unique properties, such as being cheap, non-toxic, readily available in the market, high turnover rate, photolytically and chemically stable, and exhibiting a relatively higher photocatalytic activity in the UV light [79].

2.1.1.1 Titanium Dioxide as a Photocatalyst

TiO_2, C.I. 77891, also known as titanium (IV) oxide or titania was discovered in the year 1821, and is reported to be one amongst the top twenty inorganic chemicals of industrial importance [80]. It is widely used as a pigment in paints, coatings, sunscreens, ointments, and toothpastes because of its brightness and a very high refractive index. TiO_2 is generally sourced

from a variety of ores such as ilmenite, rutile and anatase. The two most common crystalline forms of TiO_2 namely, anatase and rutile, are produced from titanium mineral concentrates either by the older sulphate or a newer chloride process [81]. The first industrial production of TiO_2 started in the year 1918 [82]. Although the studies on semiconductors being used as photocatalysts for the oxidation of substances can roughly be traced to the early twentieth century, yet to find out where it exactly originated seems difficult to answer [83]. It was found for the first time in 1921 that TiO_2 and some other oxides when irradiated in the presence of a suitable organic acceptor, formed dark reduction products. The utilization of TiO_2 for the photodiscoloration of dye was investigated in 1938 whereas the oxidation of organic solvents by TiO_2 was studied in 1956 [53]. It was not used until 1972 when Fujishima and Honda [58] reported the discovery of photocatalytic splitting of water on n-type rutile TiO_2 electrode that TiO_2-mediated heterogeneous photocatalysis came into the limelight, and has since remained an active and extensively studied research area. In fact, dedicated efforts using this technology are being put for the complete destruction of undesirable organic pollutants both in aqueous and gaseous phases with the help of either artificial UV light or solar light [84].

Commercially available Degussa P25 based TiO_2 photocatalyst has been extensively studied from last few years. The total effectiveness of pure TiO_2 is very poor due to recombination rate of photo induced electron-hole pairs. Also, the major limitation of pure TiO_2 (Degussa P25) anatase phase is due to its wide band gap ~ 3.2 eV, which needs excitation wavelength of $\lambda < 400$ nm. So, pure TiO_2 cannot be used under visible light. Thus, immense efforts were made to dope various metal and non-metal elements on TiO_2 surface to enhance the photoactive wavelength region to visible light. The presence of metal ion dopants in the TiO_2 persuade the photo-reactivity by changing charge carrier recombination rates, and interfacial electron transfer rates by shifting the band gap of the photo-catalysts in to visible region. This would extend the lifetime of the generated charge carriers and enhance the photo-catalytic activity.

2.1.1.1.1 Doping

For improving the photocatalytic efficiency of titania, there has been a growing pursuit to go beyond the threshold wavelength of TiO_2. For this, different strategies have been adopted. The main focus of these approaches is to suppress e^- - h^+ recombination and to improve the photo-sensitivity of titania for effective large-scale applications. The major strategies can be summarized as either chemical modifications by doping, surface sensitization, metal coating or morphological changes, such as increasing surface area and porosity. The main aim of these activities include the following:

i. Combination of energy levels into the band gap of TiO_2,
ii. Changing the life time of photogenerated charge carriers,
iii. Swap of the Ti^{4+} with cation of the identical size, and
iv. Shifting the VB and/or the CB in order to enable the process of photo-excitation at lesser energies; achievement of which depends on the method of preparation [85-87].

In order to alter the optical response of TiO_2 photocatalysts, doping of titania is an effective method in altering the band gap energy. The main objective of doping is to decrease the band gap of TiO_2, i.e., to induce a bathochromic shift and thus extend its wavelength range response to the visible region [59]. Many attempts have been made to sensitize TiO_2 to the whole visible region by doping with transition metals [36, 88-98], transition metal ions [99-104], nonmetal atoms [36, 105, 106], and organic materials [107, 108]. When metal ions such as Fe^{3+}, Co^{3+}, Ni^{2+}, Cu^{2+}, etc. are doped into TiO_2, the change of semiconductor property from an n-type to a p-type was reported [109].

2.1.1.1.1.1 Non-metal doping

Various studies have been devoted for achieving desired band gap narrowing of titania by using non-metals such as nitrogen (N), phosphorous (P), sulfur (S), fluorine (F), and carbon (C) [110-116]. N has been reported to be the most promising dopant as it can easily substitute oxygen (O) in the TiO_2 lattice owing to its atomic size comparable with that of O, small ionization energy and high stability. Non-metal dopants P and S have also been reported to

show optimistic outcomes for visible light activity in titania photocatalysts [117, 118]. For the non-metal-doped titania photocatalysts, the mixing of N, S or C (2p) O (2p) states shifts the VB edge upwards, resulting in a decrease of the band gap of the N-doped TiO_2 and thereby the photocatalyst can be energetic under visible light irradiation.

2.1.1.1.1.2 Transition/Noble metal doping

The doping of a range of transition metal ions in to TiO_2 could shift its optical absorption edge from UV to visible light range [36]. Various transition metals such as chromium, cobalt, vanadium, molybdenum, iron, and copper have been used to modify titania photocatalysts and are found to not only enhance the photocatalytic activity of TiO_2 but also extend its spectral response into the visible region [118]. The incorporation of transition metals such as iron, copper, cobalt, molybdenum, chromium, vanadium, manganese, nickel, niobium and tungsten in the crystal lattice of TiO_2 may constitute in the development of new energy levels between VB and CB, tempting a shift of light absorption towards the visible light region. The enhancement in the photocatalytic activity typically depends on the quantity of dopant. At a high dopant concentration, the metal ions can behave as recombination centers for the photoinduced charge carriers thereby, depressing the quantum efficiency [118, 119].

Further, it has been reported that there is an optimum dopant concentration for the greatest photocatalytic performance of a specific improved TiO_2. For instance, titania nanocatalyst doped with 1 atomic % copper showed the best performance in the decolorization as well as mineralization of Acid Orange 7 [120]. A higher dopant concentration (>1 atomic % Cu) led to a reduction in the photocatalytic activities due to the recombination of e^- - h^+ pairs. Moreover, it was quite possible that the higher concentration of dopant also blocked TiO_2 from absorbing the incident photons. Addition of noble metals such as platinum (Pt), silver (Ag), gold (Au), palladium (Pd), and rhodium (Rh) is another approach for the modifying titania and enhancing its photocatalytic activity [121-125]. The fermi levels of these noble metals are lower than that of titania. Therefore, the photogenerated electrons can be transferred from the CB of titania to the metal particles deposited on the TiO_2 surface, whereas the photogenerated

holes in the VB remain on TiO_2. Thus, the probability of e^- - h^+ recombination is greatly reduced, which further results in efficient charge separation and hence a higher photocatalytic activity [119]. For instance, Pt [126], Au [127, 128] and Ag [129] deposited on or doped in titania served as electron traps, endorsing interfacial charge transfer and therefore suspending recombination of the charge carriers. This in turn, enhanced the quantum efficiency and the oxidation of dyes as contaminants. Along with enhancing the photocatalytic activity, the modification through noble metals enables titania nanoparticles to be active in the visible light range. Also, it has been reported that noble metal modified TiO_2 exhibited excellent stability as well as reproducibility. For example, silver ion (Ag^+) modified titania on reuse, degraded mixed dyes (crystal violet and methyl red) with 90 % efficiency [130]. The dosage level is an important parameter that affects the enhancement effect produced by the noble metals. At or below an optimum dosage level, these metals act as charge separation centers and enhance the photocatalytic efficiency of the modified titania. However, at dopant level higher than the optimum dosage, noble metals can act as e^- - h^+ recombination centers and thus have detrimental effect on the activity of the photocatalyst. However, the extensive acceptance for TiO_2 modification with noble metals for experimental remediation is limited due to the expensive nature of noble metals [131].

Choi et al. [132] studied the effects of various types of metal ions doping on the titanium dioxide and found that the Fe^{3+} dopant has better photocatalytic activity. Transition metals, like Fe^{3+} simply combined into the crystal lattice of TiO_2 because of their alike ionic radii (the ionic radii of Fe^{3+} = 0.69 Å are fairly alike to that of Ti^{4+} = 0.75 Å ions). Iron is frequently employed due to its unique half-filled electronic configuration, which might narrow the energy gap through the formation of new intermediate energy levels [133, 134]. Vanadium [36, 135], copper [136, 137] and cobalt [96] doping on TiO_2 offers a possibly promising strategy to enhance the characteristics of photocatalytic species and found active under visible light.

2.1.2.1.1.3 Co-doping

An effective method to improve the charge separation and hence the catalytic activity of titania is the co-doping of the photocatalyst. Further improvement in photocatalytic properties was reported when TiO_2 was codoped with suitable amounts of more than one type of metals [37]. This configuration has several advantages, including the improvement of charge separation, increase in the lifetime of the charge carrier and enhancement of the interfacial charge transfer to the adsorbed substrate [138]. The co-doped titania holds the benefits of iron doping which is important charge separation. In fact, synergistic effects of the co-doping have been reported. Similarly, an enhanced photocatalytic activity was reported for TiO_2 co-doped with optimal concentrations of europium ion (Eu^{3+}) and ferric ion (Fe^{3+}) compared with the bare titania. The Eu^{3+} ion acted as an electron trap while the Fe^{3+} ion as a hole trap, thereby improving interfacial charge transfer and the photocatalytic activity [139]. Various other co-doped TiO_2 photocatalysts with dopants (Cu, N), (N, Ce), (Cu, Ni) and (Cu, Ag) have also been studied [119, 140]. However, the only drawback in using the nanosize catalyst particles is that the liquid-solid separation is costly, because of production of milky suspended solution after mixing the powdered catalyst in water. To solve this separation problem, fixed TiO_2 was prepared by immobilizing TiO_2 on an inert support. However, in general, the adherence of TiO_2 to support is not by a chemical bond and the heavier catalyst can be worn off easily.

2.1.1.1.2 Immobilization of TiO_2

In the literature, the most widely used photocatalytic process is carried out in a batch slurry photo-reactor operating with titanium dioxide suspensions [141-143]. However, slurry reactors have a number of practical and economical disadvantages, which have been mentioned in various previous works [141, 144]. The main problem related to slurry photoreactor is the separation of TiO_2 nanoparticles after treatment, which imposes high filtration costs. In addition, the depth of penetration of UV light in the suspended photocatalyst systems is limited because of the strong light absorption by TiO_2 particles. In order to solve these problems, supported photocatalysts have been developed. The most important properties of a suitable

support are to be chemically inert, to have a high specific surface area and to be transparent to UV radiation [81].

2.2 Photocatalytic Treatment of Textile Dye

Photodegradation of various classes of dyes has been a subject of research and is reported by several researchers. Reactive dyes have emerged to be the most important class of dyes which are causing environmental pollution as only small amount of it is fixed and rest remains unfixed [145]. Some studies of degradation of dyes by photocatalysis have been reported [146-149]. Parameters affecting the photodegradation process of aqueous solution have been studied such as initial dye concentration, photocatalyst dose, initial pH, light irradiation and reaction time [150-153]. Very few researchers have worked on the application of semiconductors in the photocatalytic degradation of photo-stable dyes [154]. With the aim of elucidating the potential application of the photodegradation processes, the kinetic and mechanistic aspects of degradation of dye have been explored and reported in literature [155-157].

TiO_2-mediated photocatalytic degradation of various dyes was studied in aqueous suspension of TiO_2 under a selection of process variables by observing the change in initial dye concentration using UV spectroscopic analysis and reduction in total organic carbon content as a function of irradiation time [158, 159]. The photocatalytic degradation processes of two azo dyes was investigated by Khalil et al. [160] at TiO_2/H_2O interface under visible and UV irradiation with different experimental techniques. Vinodgopal and Kamat [161] employed thin film semiconductor to enhance the rate of azo dye photocatalytic degradation. Neppolian et al. [162] investigated the photocatalytic degradation of three commercial textile dyes with different structures using TiO_2 (Degussa P25) photocatalyst in aqueous solution under solar irradiation. Several studies have been reported in the literature for the degradation of the reactive dyes [163-166]. Photocatalytic degradation of textile dye, Reactive Red M5B has been carried out on TiO_2 and ZnO semiconductor particles by Neppolian et al. [167]. Many researches [38, 151, 153, 168] reported that RB5 can be efficiently degraded under UV light

with Degussa P25 photocatalyst. Nikazar et al. [169], Pawar et al. [170] and Lee et al. [171] reported that AR114 can be efficiently degraded by photo-Fenton process. Researchers reported that organic dyes can also be degraded under visible light with metal ion doped Degussa P25 catalyst.

The photodegradation of a triphenyl methane dye (Crystal Violet) in aqueous solutions was examined with Ag^{+} ion doped titanium dioxide with UV light irradiation and simulated solar light by Sahoo et al. [172] and observed 88% degradation after 10 h irradiation for 20 mg l^{-1} dye concentration. The kinetics of degradation was well fitted to Langmuir–Hinshelwood rate law. Ghasemi et al. [136], Liu et al. [38] and Zhou et al. [93] used Fe metal ion and Nguyen et al. [173] used Zn metal ion to doped TiO_2 and find up to 90% degradation of organic dyes such as Acid Blue 92, RB5, Methylene Blue etc. Behnajady and Eskandarloo [140] used silver and copper co-impregnated onto TiO_2-P25 nanoparticles for the photodegradation of Acid Orange 7 (AO7). They concluded that the photodegradation of AO7 follows the pseudo first reaction kinetics and the maximum degradation was found with 1 and 0.03 wt% Ag and Cu codoped TiO_2.

Many researchers reported that immobilized TiO_2 can work efficiently in degradation of organic dyes. Various methods have been reported for immobilization of TiO_2 on different supports. Lu et al. [174], Virkutyte et al. [175], Uddin et al. [176] used cellulose as support for TiO_2 and found up to 90% degradation of textile dye. Bouna et al. [177] used palygorskite clay mineral as support for TiO_2 and found 0.37 g l^{-1} catalysts loading for 96% degradation of Orange G dye. The advantage of immobilized catalyst and the possibility to use these systems under flow conditions, avoiding the catalyst recovery step have also been discussed [178]. Behnajady et al. [179] studied the photocatalytic degradation of an anionic monoazo dye (C.I. Acid Red 27), in a tubular continuous-flow photoreactor with immobilized TiO_2 on glass plates with irradiation of UV light and found that a linear relation exists between pseudo-first order reaction rate constant and reciprocal of volumetric flow rate. Sakthivel et al. [180] used glass and alumina beads to support TiO_2 and investigated their photocatalytic activities by photo-oxidation of commercial Acid Brown 14 and leather dye in aqueous solution under solar light.

The efficiency of a photocatalytic reaction depends on a number of factors, which govern the performance of photocatalysis. The initial concentration of pollutant, photocatalyst concentration, pH, volume of solution, radiantion flux and agitation, irradiation time, light intensity, irradiation wavelength, temperature, geometrical parameters of the experimental setup and multiple degradation pathways are the parameters that can be studied for the photocatalytic degradation [181].

2.2.1 Effect of Catalyst Loading

Some studies [182, 183] have shown that the photocatalytic rate initially increased with catalyst loading but levelled off at high values due to light-scattering effects. Pareek and Adesina [184] have also suggested that the tendency toward agglomeration at high catalyst concentration might lead to reduced photoreaction rate due to a reduction in available surface area for light harvesting.

2.2.2 Effect of Initial Concentration

The concentration of dye also plays an important role in the degradation rate by photocatalysis. It is generally noted that the degradation rates increase with increase in dye concentration from very low values. However, the rate of degradation starts decreasing beyond a certain value of dye concentration. The degradation rates are affected by summation of the probability of •OH formation and further the probability of effective reactions resulting from theses radicals on dye and other dye degradation intermediates. The degradation rates are the result of series process of •OH formation and its subsequent effective utilization. So the initial trend of increasing rate might be due to enhanced probability of •OH formation as required adsorption upon catalyst surface is attained with increasing dye concentration. The importance of initial adsorption of dye upon catalyst surface has been confirmed by number of studies. It has been reported that dye degradation follows the Langmuir-Hinshewood (LH) kinetics [185-188] which implies that degradation steps are influenced by adsorbed species on catalyst surface.

At higher concentrations of dyes, the dye screening effect also comes in to play. Dye screening refers to the absorption of UV radiation by dye molecules rather than getting used effectively in generation of electron hole pair [189, 190]. The screening by dye reduces the intensity and shields the catalyst.

2.2.3 Effect of Solution pH

This parameter is one of the most critical parameter in determining the efficiency of photocatalytic degradation. Understanding the effect of pH in determining photocatalytic degradation is very difficult task due to its multiple roles [74]. It is also difficult to generalize in most of the cases. The most important role played in many cases by the ionization state of surface is as per following reactions [191].

$$TiOH + H^+ \leftrightarrow TiOH_2^+ \quad (2.13)$$

$$TiOH + OH^- \leftrightarrow TiO^- + H_2O \quad (2.14)$$

The ionization state of reactant dyes, other chemicals and intermediates generated during degradation is also equally important. Adsorption which is an important step in photocatalytic degradation is thus influenced due to surface charge interaction and dye and chemical to be degraded. The effect of acid base properties of metal oxide surfaces on photocatalytic properties has been well reviewed [74, 192]. The point of zero charge pH (pH_{pzc}) for Degussa P25 TiO_2 have been found to be 6.8 [148]. Thus, TiO_2 surface is positively charged in acidic medium (pH < 6.8) and is negatively charged in alkaline conditions (pH > 6.8).

It has been reported that degradation rate of azo dyes increases with decrease in pH [193]. At lower values of pH (i.e. pH < pH_{pzc}), the negatively charged dye can easily get adsorbed over catalyst surface. However, under alkaline condition similar charges exist over catalyst surface and dye. Thus there is hardly any adsorption [194, 195]. Another factor is formation of hydroxide ions and hydroxyl radical. Both of these are involved in degradation reactions. Hydroxyl radicals can be formed by reaction between hydroxide ion and positive

holes. The positive holes are considered as major oxidation species in acidic conditions while hydroxyl radicals are considered to be dominant species in case of alkaline or neutral conditions [196]. It has been reported that in alkaline condition the hydroxyl ions can be easily generated as more hydroxide ions are available on TiO_2 surface [197].

2.2.4 Effect of Wavelength and Light Intensity

Radiation source (lamp or sunlight) provides the photon energy required for electron excitation from valence to conduction band, and therefore it must have wavelengths shorter than the critical wavelength, which is dependent on the semiconductor band-gap. In addition, the total energy input to the photocatalytic process is dependent upon the light intensity. Reaction rates for several reactions involving gases, organic liquids, or aqueous solutions, are found to be proportional to light radiation flux. Okamoto et al. [198] and Ollis et al. [182] reported that at low intensities the photodegradation rate increased linearly, however, at medium light intensities the rate became dependent on the square root of light intensity and independent at high intensities. The penetration length of light in the solid-liquid medium is another important parameter, which is a function of particle size and catalyst charge or slurry concentration. In the case of artificial light, the intermediates generated are also affected by the wavelength as well as intensity of the light [199].

Although most of the authors considered the effect of various parameters like dye concentration, TiO_2 dose, pH, and reaction time on the treatment efficiency, there is also a need to study the other reaction parameters such as light intensity and geometrical parameters of experimental setup.

2.3 Modeling and Optimization

The wastewater treatment depends on several variables like catalyst dose, pH, initial dye concentration, and time, etc. It is a very complex task to develop a model based on many variables [200]. It is obvious that these complex quandaries cannot be solved by multivariate correlation [201]. Artificial neural networks (ANNs) are a computer based tool for solving nonlinear systems, especially when there is interaction of more than one process parameters.

ANN is capable to solve the system without requiring previous information of the interactions of process variables [202]. Also, the response surface methodology (RSM) in systematic optimization is the most suitable technique. RSM is based on statistical design of experiments [203]. In the recent studies, RSM based central composite design (CCD) and Box-Behnken design (BBD) were used in various wastewater treatment techniques including AOPs.

2.3.1 Artificial Neural Network (ANN)

The phenomenological treatment of a photochemical system is, in general, quite complex. This is caused by the complexity of solving the equations that involve the radiant energy balance, the spatial distribution of the absorbed radiation, mass transfer, and mechanisms of a photochemical photocatalytic degradation involving radical species. Due to these reasons, the modeling of the degradation process via artificial neural network (ANN) techniques is quite appropriate [204-206].

Neural network analysis of the experimental data does not require the use of any kinetic or phenomenological equations and allows the simulation and the prediction of the pollutant degradation as a function of irradiation time, as well as prediction of reaction rate, under varying conditions within the experimental region. Kasiri et al. [207] applied ANN for the degradation of Acid Red 14 dye by photo-Fenton process and found that the initial concentration of the dye and initial pH to be more influential parameters in the degradation process. Khataee [208] applied ANN for the degradation of Basic Red 46 by heterogeneous photocatalysis and found that the reaction time, pH, initial dye concentration and UV light intensity have the importance of 26.75, 27.03, 30.75 and 15.47 % respectively. Khataee and Zarei [181] and Zarei et al. [209] have developed an ANN model with feed forward back propagation for the photodegradation of Direct Yellow 12 and Basic Red 46 dyes using photoelectron-Fenton process and found a reasonable predictive performance.

2.3.2 Response Surface Methodology (RSM)

In most of thet studies, only traditional one-factor-at-a-time experiments were tested for evaluating the influence of operating factors on the photocatalytic process efficiency. This technique is not only time and work demanding, but also completely lacks representation of the effect of interaction between different factors. Due to the complexity and variety of influencing factors, into photocatalytic degradation it is difficult to evaluate the relative significance of several affecting factors by conventional optimization techniques, especially in the presence of complex interactions. RSM is a statistical technique for designing experiments, evaluating the effects of various parameters, and for identifying optimum conditions for desirable responses [210, 211]. It makes possible to estimate linear interaction and quadratic effects of the input parameters and to establish a mathematical model for prediction of the response. RSM has been used to optimize process parameters for a number of processes [212-215]. Cho and Zoh [216], Khataee et al. [217] and Khataee et al. [218] have also applied RSM methodology to model and optimize UV/TiO_2, photo-Fenton and visible light/TiO_2 processes.

2.4 Scope and Objectives of the Present Study

The photocatalytic processes are widely recognized for wastewater treatment. The literature reveals the following gaps:

- Although doping on TiO_2 catalysts have been extensively studied, the development of effective metal doped and codoped TiO_2 photocatalysts are still of great interest for the treatment of textile wastewater.
- The preparation of Fe-V, Fe-Co codoped TiO_2 has not been reported. Also, the photocatalytic activity of Fe-V, Fe-Co and Fe-Cu codoped TiO_2 has not been examined under the visible light irradiation for the treatment of textile wastewater.
- Most of the work in the literature has been reported on slurry pond reactor; there is a need to research on immobilized catalyst in the continuous type reactor for the treatment of textile dye wastewater.

- The phenomenological treatment of a photochemical system is, in general, quite complex. Due to this reason, the modeling of the degradation process is very difficult.
- Very little work has been done on the modeling and optimization of photocatalytic treatment of textile waste water.

The proposed study was undertaken with the following objectives:

- Preparation and characterization of doped (such as Fe, Cu, V and Co) and immobilized (such as on cement beads) TiO_2 photocatalysts.
- Degradation of azo dyes (such as Reactive Black 5, Acid Red 114, Acid Blue 113) by photocatalytic process using TiO_2 and doped TiO_2 and optimizing the parameters like pH, catalyst loading, initial concentration of dye etc.
- Modeling and optimization of the process parameters by artificial neural network and response surface methodology.

Chapter 3 MATERIALS, METHODS AND CHARACTERIZATION

This chapter describes the materials used, methods adopted and different characterization techniques used for synthesized photocatalyst, which is used for the photocatalytic degradation of the dye.

3.1 Materials

3.1.1 Dyes

Three dyes namely Reactive Black 5, Acid Red 114 and Acid Blue 113 were procured from Sigma Aldrich (Germany) and used without any processing, as model dyes for aqueous solution. The structure and physico-chemical data of dyes have been shown in Figure 3.1 and Table 3.1 respectively.

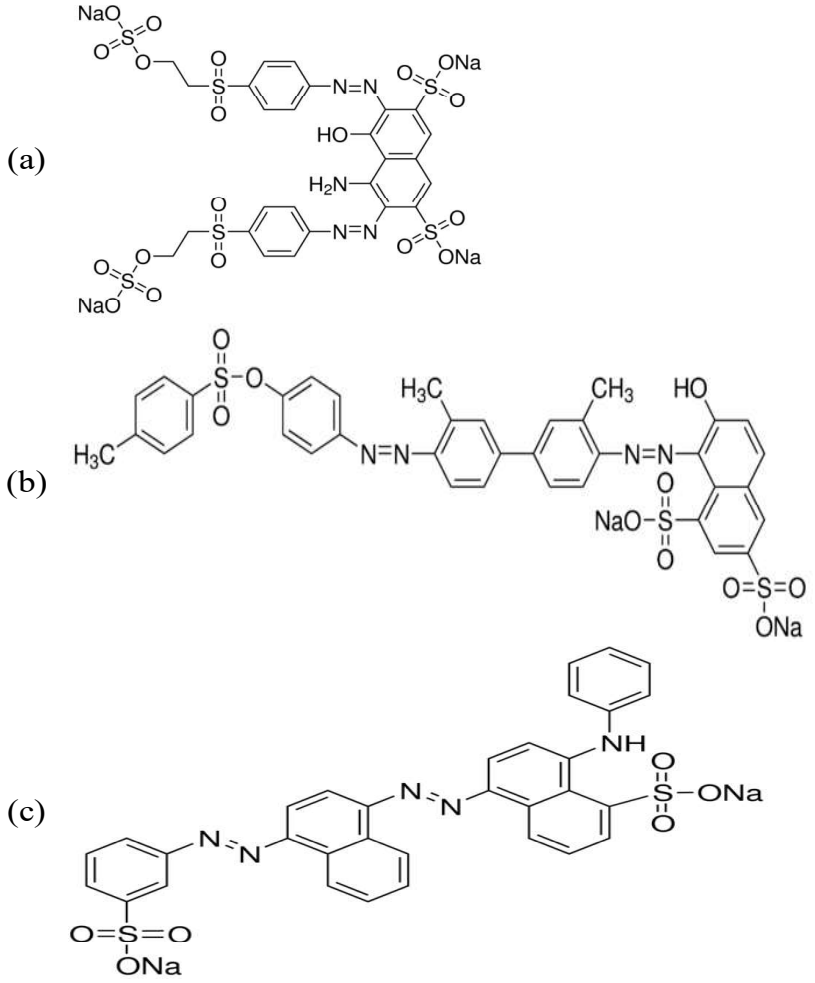

Figure 3.1 Molecular structure of (a) Reactive Black 5 (b) Acid Red 114 and (c) Acid Blue 113 dyes

Table 3.1 Physico-chemical data of dyes

Properties	Typical value		
	Reactive Black 5	**Acid Red 114**	**Acid Blue 113**
Molecular formula	$C_{26}H_{21}N_5Na_4O_{19}S_6$	$C_{37}H_{28}N_4Na_2O_{10}S_3$	$C_{32}H_{21}N_5Na_2O_6S_2$
Molecular weight (g mol^{-1})	991.82	830.81	681.65
Appearance	Dark black powder	Red powder	Navy blue powder
Dye content (%)	55	45	50
λ_{max} for UV absorption	597 nm	522 nm	566 nm
Application	Dyeing of silk, wool, nylon, leather and paper	Dyeing of wool, silk and their blended fabric	Dyeing of wool, polyamide fiber, and silk

3.1.2 Catalyst

AEROXIDE® TiO_2 P25 was kindly provided by Evonik Degussa Corporation, Germany. Its physico-chemical data are given in Table 3.2:

Table 3.2 Physico-chemical data of TiO_2 P25

Properties	Units	Typical value
Appearance		Fluffy white powder
Specific surface area (BET)	$m^2 g^{-1}$	50±15
Average particle size	nm	30
Behaviour towards H_2O		Hydrophilic
Crystalline polymorphs		70% anatase and 30% rutile
Tamped density	g l^{-1}	130
pH in 4% dispersion		3.5-4.5
Titanium dioxide content	wt %	≥ 99.5
HCl Content	wt %	≤ 0.3
Al_2O_3 content	wt %	≤ 0.3
Fe_2O_3 content	wt %	≤ 0.01
SiO_2 content	wt %	≤ 0.2
Application		Photocatalytic reaction, raw material, adsorption and thermal stability

3.1.3 Reagents and Chemicals

Hydrochloric acid and sodium hydroxide (S. D. Fine Chemicals Limited, India) were used to adjust the pH. Ferric nitrate nonahydrate ($Fe_2(NO_3)_3.10H_2O$), ammonium metavanadate (NH_4VO_3), cobalt (II) nitrate hexahydrate ($Co(NO_3)_2.6H_2O$), copper (II) nitrate hexahydrate ($Cu(NO_3)_2.6H_2O$) have been procured from SD Fine-Chemical Limited, India and used without further treatment as dopant and codopant on TiO_2. All chemicals were used as received. In all the experiments, distilled water was used for preparing the solutions.

3.2 Experimental Setup

3.2.1 UV Chamber and Shallow Pond Reactor

The photocatalytic degradation studies were conducted using shallow pond slurry reactor (Figure 3.2). A batch type bench scale photocatalytic reactor system was fabricated for conducting the experiments. The set up consisted of a batch reactor placed on a platform under UV light (8 UV black tubes of 40 W each). A Borosil glass vessel of 500 ml capacity was used as the shallow pond reactor and was irradiated with UV rays. This reactor is placed on a magnetic stirrer to keep the contents in the reactor well mixed, so that the TiO_2 remains suspended and the concentration of the pollutant within the reactor could be assumed to be constant at any time.

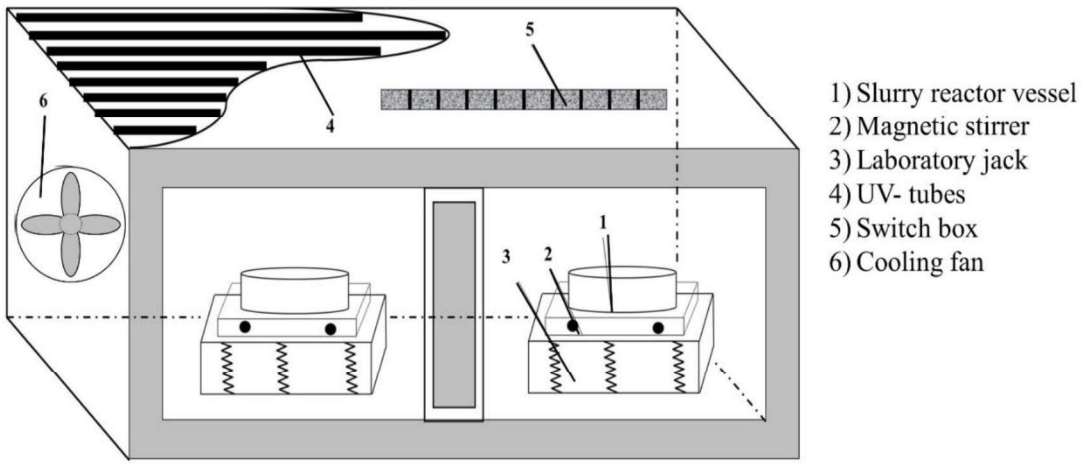

Figure 3.2 Experimental setup consisting of UV chamber, magnetic stirrer and slurry pond reactor

3.2.2 Visible Light Chamber and Shallow Pond Reactor

A schematic diagram of lab scale set up for slurry pond reactor with visible light source has been shown in Figure 3.3. The photocatalytic degradation studies were conducted using shallow pond slurry reactor. The set up consisted of a batch reactor placed on a platform under visible light (250 W low voltage halogen lamp). A Borosil glass vessel of 50 ml capacity was used as the shallow pond reactor and visible light was irradiated on the glass vessel. The reactor is placed on a magnetic stirrer to keep the contents in the reactor well mixed so that the photocatalyst remains suspended.

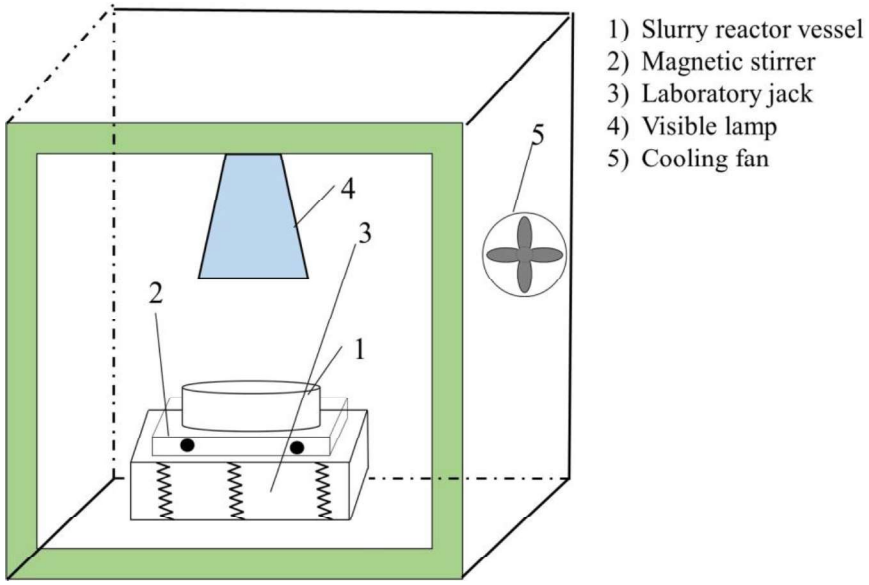

Figure 3.3 Experimental setup consisting of visible light, magnetic stirrer and slurry pond reactor

3.2.3 UV Chamber and Continuous Baffled Reactor

A schematic diagram of lab scale baffled reactor set up has been shown in Figure 3.4. It consists of a rectangular baffled reactor in which immobilized cement beads have been placed. Peristaltic pump has been used to maintain the flow of dye solution.

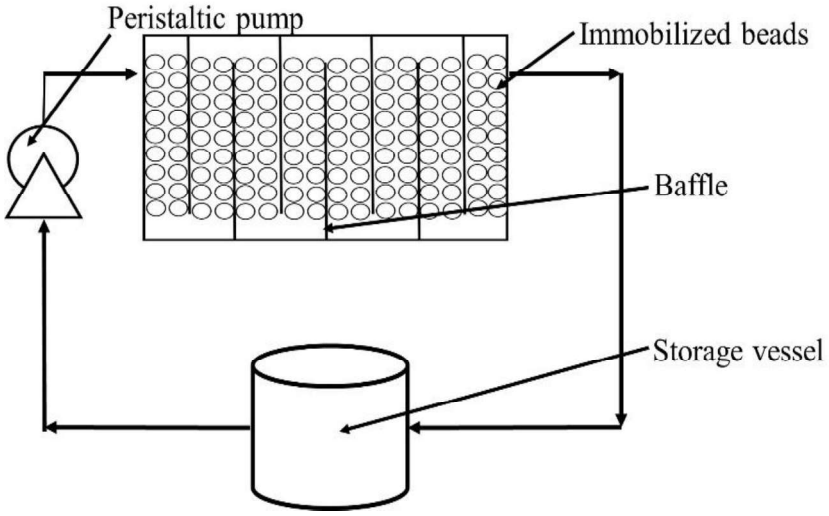

Figure 3.4 Experimental setup consisting of baffled reactor

3.3 Equipment and Instruments

3.3.1 Radiometer

The UV light intensity was measured by using an Eppley radiometer (model no. 33013). Its sensitivity is 150 $\mu V/Wm^{-2}$ and response time is milli seconds.

3.3.2 Centrifuge

After the photocatalytic treatment of the dye sample, the suspended TiO_2 particles have to be separated from the dye sample before measuring its absorbance. The TiO_2 particles were separated by using high speed micro centrifuge (Hitachi, model no: CF15RXII). A centrifuge is a piece of equipment, driven by a motor, which spins liquid samples at high speed (15,000 rpm). The centrifuge works using the sedimentation principle, where the centripetal acceleration is used to separate substances of greater and lesser density.

3.3.3 UV-Vis Spectrophotometer

For determining the concentration of various dyes, we first measured the absorbance of the dye sample at λ_{max} using UV-Vis spectrophotometer. Then we use calibration curve (concentration versus absorption curve) to determine the concentration of the dye sample. The

concentration of the dye was indirectly determined by measuring absorbance. For measuring absorbance of the dye samples, Perkin Elmer Lambda 35 UV-Vis spectrophotometer was used.

3.4 Experimental Procedures

3.4.1 Procedure for Photocatalytic Experiments using Shallow Pond Slurry Reactor

The general procedure for all the photocatalysis experiments is as follows:

1. The stock solution of three dyes (RB5, AB113 and AR114) was prepared in distilled water for all the experiments.
2. Fixed volume of dye solution was withdrawn from the stock solution in the shallow pond reactor.
3. HCl and NaOH solutions were used to maintain the pH of the solution and pH was measured using pH meter (Hach USA HQ30d with pH gel probe).
4. Desired amount of TiO_2 was added in the shallow pond reactor.
5. The reactor is placed on the magnetic stirrer and magnetic bead is put in the dye solution for proper stirring.
6. The adsorption of dye on the catalyst is done for 30 min in dark condition. An aliquot of 5 ml was taken from the reactor with the help of a syringe.
7. After 30 min, UV lights are switched on. The door of the UV chamber is closed so that no UV rays come out.
8. At particular time interval (30 min), 5 ml sample was withdrawn from the reactor with the help of syringe and 1:1 dilution is done each time.
9. The photocatalysis is done for next 180 min.
10. To filter the suspended TiO_2 particles from the dye sample, centrifugation is done, making sure that the level of sample in each centrifuge tube is same. The centrifuge tubes are spun at the high speed of 15,000 rpm for 10 min. The TiO_2 particles get settled at the bottom of the tube.
11. A computer based UV-Vis spectrophotometer was used for determination of concentration of samples as per detailed below:

a. The system is switched on and warmed up.

b. Thoroughly cleaned quartz cuvettes are taken.

c. Both cuvettes are filled with distilled water and absorbance at λ_{max} (of dye) is checked. Auto zero is done.

d. After auto zeroing, one cuvette is filled with the reference sample (distilled water) and the other one with the sample whose absorbance has to be measured at λ_{max}.

e. To get the relationship between concentration and absorbance of the compound, a calibration curve is prepared. Calibration solutions are prepared from standard solutions of known concentration. The absorbance is plotted against known concentration of the calibration samples. These calibration curves are stored in the system itself and the concentration of the unknown sample can be calculated directly from the absorbance.

12. The conversion percent of each dye can be obtained in different intervals. The decolorization and degradation (X) is given by eq. (3.1)

$$X = \frac{C_o - C_t}{C_o} \tag{3.1}$$

Where C_o is the initial concentration of dye and C_t is the concentration of dye at time t.

For decolorization and degradation of dye with the above mentioned setup, the various experiments were conducted for optimizing the parameters like initial concentration, pH and catalyst loading, UV light intensity, area to volume ratio and time.

3.4.2 Preparation, Characterization and Photocatalytic Experiments of Synthesized Catalyst

3.4.2.1 Preparation of Metal Ion Doped and Codoped TiO_2

The surface of TiO_2 photocatalyst has been modified (doping and codoping) by wet impregnation method. In the wet impregnation method ferric, vanadium, cobalt and copper ions doped and codoped TiO_2 photocatalysts were prepared according to the following steps:

First, 3 g of TiO_2 was added to 100 ml distilled water. Then molal solution of the $Fe_2(NO_3)_3.10H_2O$, NH_4VO_3, $Co(NO_3)_2.6H_2O$ and $Cu(NO_3)_2.6H_2O$ were prepared. The required amounts of these solutions for doping and codoping were added to TiO_2 suspension. The slurry was stirred well and allowed to rest for 24 h and then it was washed two times with distilled water to remove undoped metal ions and dried in an air oven at 100° C for 12 h. The dried solids were ground in an agate mortar and calcined at 500° C for 6 h in a muffle furnace. The doped and codoped TiO_2 photocatalysts prepared with dopant and codopant concentrations of 0.5, 1 and 2 wt% are denoted by TFe_x, TCu_x, TV_x, TCo_x (x = 1, 2) and TFe_yCu_y, TFe_yV_y, TFe_yCo_y (y = 0.5, 1), where x and y are the wt % of Fe, Cu, V and Co.

3.4.2.2 Characterization of Metal Ion Doped and Codoped TiO_2

The structural, physical and chemical characteristics of catalysts are essential for deriving correlation between physico-chemical properties and catalytic activities of the materials. Different methods were employed to characterize the synthesized catalysts. The metal ion doped and codoped photocatalyst samples were characterized by different techniques like X-ray diffraction (XRD), Fourier transform infrared (FTIR) spectroscopy, UV-visible diffuse reflectance spectroscopy (UV-DRS), field-emission scanning electron microscope-energy dispersive spectroscopy (FESEM-EDS), transmission electron microscopy (TEM) and X-ray photoelectron spectroscopy (XPS).

3.4.2.2.1 X-ray diffraction (XRD)

X-ray diffraction is an analytical technique to know about phases, crystallinity, crystal grain size, lattice parameters, phase composition, lattice defects etc of samples. In the present study, the powder X-ray diffraction of the samples was performed using a Panalytical's X'Pert Pro diffractometer with Cu Kα radiation (λ = 0.154060 nm) at working voltage and current of 40 kV, 40 mA at angular range of 20° to 80°.

3.4.2.2.2 Fourier transform infrared spectroscopy (FTIR)

Fourier transform infrared (FT-IR) spectroscopy is a multidisciplinary analytical tool, which gives information pertaining to the structural details of a material. IR spectra of as-synthesized and calcined samples were recorded on a FTIR spectrometer (PerkinElmer Spectrum RX I) using KBr pellet technique. About 10 mg of the sample was ground with about 70 mg of spectral grade KBr to form a mixture, which was then made into a pellet using hydraulic press. This pellet was scanned 50 times at 4 cm^{-1} resolutions, and it was used to record the infrared spectra in the range 4000-400 cm^{-1}.

3.4.2.2.3 UV-visible diffuse reflectance spectroscopy (DRS)

Diffuse reflectance spectroscopy is a sensitive technique which uses the interaction of light, absorption and scattering to produce characteristic spectrum. It is used to study the electronic transitions between orbitals or bands in the case of atoms, ions and molecules in gas, liquid or solid state. In present study, UV-visible diffuse reflectance spectroscopy (DRS) of samples were performed using a UV-Vis spectrophotometer (Hitachi U-3900H). Reflectance patterns were determined at 240-780 nm wavelength.

3.4.2.2.4 Field emission scanning electron microscopy (FESEM)

Field emission scanning electron microscopy (FESEM) provides topographical and elemental information at magnifications of 10x to 300,000x, with virtually unlimited depth of field. Compared with convention scanning electron microscopy (SEM), field emission SEM (FESEM) produces clearer, less electrostatically distorted images with spatial resolution down to 1-1/2 nanometers – three to six times better. The size and morphology of powder samples have been carried out by field-emission scanning electron microscope-energy dispersive spectroscopy (FESEM-EDS) (Zeiss Ultra 55 FE-SEM with Oxford EDX system) in the present work.

3.4.2.2.5 Transmission electron microscopy (TEM)

Transmission electron microscopy is a powerful tool that provides information about the morphology, crystallography and elemental composition for advanced materials. The morphology and size of nanoparticles are characterized using transmission electron microscope (Hitachi, H-7500) operated at an accelerating voltage of 120 kV. The prepared samples are dissolved in ethanol and drop of colloids is put on the copper grid for TEM measurement.

3.4.2.2.6 Energy dispersive X-ray analysis (EDX)

Energy Dispersive X-Ray Spectroscopy (EDS or EDX) is a chemical microanalysis technique used in conjunction with FESEM. The EDS technique detects x-rays emitted from the sample during bombardment by an electron beam to characterize the elemental composition of the analyzed volume. Features or phases as small as 1 μm or less can be analyzed. EDX type X-ray spectrometer is commonly associated with FESEM and TEM. Compositional information about the sample was analyzed by EDX using Zeiss Ultra FE-SEM with Oxford EDS system.

3.4.2.2.7 X-ray photoelectron spectroscopy (XPS)

XPS determines the qualitative and quantitative identification of chemical elements by detecting X-rays characteristic that are emitted from atoms irradiated by a high-energy beam. XPS is purely based on photoelectric effect where kinetic energy of the ejected electron is measured and reported in terms of binding energy. In photoelectron spectroscopy, intensity is measured as a function of kinetic energy of the electrons [219]. Surface composition and electronic structures were analyzed by X-ray photoelectron spectroscopy using an ULVAC-PHI (model: PHI5000VersaProbeII) XPS system with a monochromatic Al Kα radiation ($h\upsilon$ = 1486.6 eV) of source voltage and emission current for X-ray 15 kV, 3 mA, ion gun 8 V, 7mA and E-neutralization 30 V, 20 μA. All scans were carried out at ultrahigh vacuum of 1.5×10^{-6} Pa. The obtained XPS spectra were deconvoluted using Casa XPS programme (Casa Software Ltd, UK), in which the background was simulated using the Shirley function and the peaks

were fitted using a Gaussian Lorentzian function. All binding energies were referenced to C1s for calibration.

3.4.3 Preparation of immobilized TiO_2 and photocatalytic experiments

3.4.3.1 Preparation of Immobilized TiO_2

TiO_2 nanoparticles have been immobilized on cement beads (average diameter ranging from 1.0 to 2.5 cm) by dispersing the cement beads in the TiO_2 slurry until uniform deposition was achieved as reported by Verma et al. [220]. To remove the excess water, the beads were exposed to 110 ^{0}C in hot air oven. For the complete immobilization of the TiO_2, cement beads were further calcined at 400 ^{0}C in muffle furnace for 2 h. The above cycle has been repeated for two times for attaining uniform and stable layer of the TiO_2. The coated beads were washed with distilled water after each cycle to remove the loosely bound TiO_2 particles.

3.4.3.2 Photocatalytic Experiments using Baffled Reactor

The lab scale set-up consisted of a baffled reactor 30 cm X 30 cm made up of glass with four baffles at equal distance (Figure 3.4). The TiO_2 immobilized cement beads were placed in baffled reactor in such a way that they are effectively submerged in the solution. The flow rate of the dye solution was maintained by peristaltic pump for getting the required retention time.

3.5 Modeling and Optimization

3.5.1 Modeling by Artificial Neural Network

An artificial neuron is a computational model instigated from normal neurons. The ANNs involve artificial neurons, which are grouped in a layer and have parallel relation with each other. Multi layered feed forward (MLF) was found the best widespread neural network and it could be trained by a back-propagation learning algorithm [221]. MLFs are useful to a widespread divergence of chemical engineering and other related problems. However, universal approximation theory suggests that a neural network with a single hidden layer of a sufficiently large number of neurons can build any input-output configuration of ANN [206,

222]. So, in the present study, single layer of hidden-neurons was used. The number of neurons in the hidden layer is resolute by the desired precision in the neural prophecies. Also, it is measured as a parameter for the ANN design.

All ANN calculations were carried out using MATLAB 2010b mathematical software with ANN toolbox for Windows running on a personal computer (Core 2 Duo processor 2.40 GHz). A three-layer network with a tan-sigmoid transfer function with back-propagation algorithm was designed for this study.

3.5.2 Multi Response Optimization by Response Surface Methodology

RSM comprises a number of statistical techniques including Box-Behnken design (BBD) and central composite design (CCD) for model building and model exploitation. BBD and CCD are used extensively for the design of experiments and estimation of optimum operating conditions. It permits identification of interactive effects of various parameters and their values. RSM is able to optimize the number of experimental and/or simulation runs required to be carried out and to determine the possible inter-parametric effects on photocatalytic decolorization and degradation of dyes. To examine a process or system including a response Y, where Y depends on the input factors x_1, x_2 . . . x_k, the relationship between the response and the input process parameters is described as:

$$Y = h\left(x_1, x_2, \ldots\ldots, x_k\right) \pm \varepsilon \tag{3.4}$$

Where h is the unknown but real response function and its format is unknown, and ε is the residual error. A second-order polynomial, eq. (3.5), was used through nonlinear regression to fit the experimental/simulated data and to recognize the relevant model terms. Considering all the linear terms, square terms, and linear-by-linear interaction terms, the quadratic response model can be described as [223]:

$$Y = s_0 + \sum_{i=1}^{k} s_i x_i + \sum_{i=1}^{k} s_{ii} x_i^2 + \sum\sum_{i<j} s_{ij} x_i x_j + \varepsilon \tag{3.5}$$

Where s_0 is the constant, s_i is the slope or linear effect of the input factor x_i, s_{ij} is the linear-by-linear interaction effect among the input factors x_i and x_j, and s_{ii} is the quadratic effect of input factor x_i [210].

These designs are generally used for fitting the second order model. It is important to be noted that the second order model provides good prediction throughout the region of interest. Box and Hunter [210] suggested that the second order response surface design should be rotatable. Rotatability is a reasonable basis for the selection of response surface design. Because the purpose of RSM is the optimization of the location of the optimum that is unknown prior to running the experiment or simulation. It makes sense to use design that provides equal precisions of estimation in all directions. The cubic model is found to be aliased and is inappropriate for further investigations. For an aliased model the numbers of simulation or experimental runs are not enough for independent estimation of all the terms for that model. If the number of independent points in the design is less than the number of terms in the model, then some of the parameters cannot be estimated independently.

The sequential F-test and other adequacy measures are generally used for selecting the best model [224]. An F-test is any statistical test in which the test statistics has an F-distribution under the null hypothesis. It is most often used when comparing statistical models that have been fit to a data set, in order to identify the model that best fits the population from which the data were sampled. The least squares method is used to estimate the parameters in approximating the polynomials. The response surface analysis is then performed using the fitted surface. If the fitted surface is an adequate approximation of the true response function, then analysis of the fitted surface will be approximately equivalent to analysis of the actual system.

There are two responses in this study. Therefore, multi-response process optimization with desirability function approach was used for the optimization of the photocatalytic process parameters. The desirability, d_i, lies between 0 and 1, representing the closeness of a response to its ideal value [223]. The individual desirability functions are combined in order to obtain the overall desirability, D_e, as follows:

$$D_e = \left(d_1 \times d_2\right)^{\frac{1}{2}} \quad (3.6)$$

Where d_1 and d_2 are the indiviual desirability of the first and second responce, respectively and $0 \leq D_e \leq 1$.

RSM (BBD and CCD) was applied to the simulated data using the Design-Expert software version 6.0.6 (STAT-EASE Inc., Minneapolis, US). The simulated data were analyzed by regression analysis to fit the equations developed and also for the evaluation of the statistical significance of the equations.

Chapter 4 RESULTS AND DISCUSSION

This chapter deals with the studies on decolorization and degradation of three textile dyes (Reactive Black 5, Acid Blue 113 and Acid Red 114) and binary dye mixture of Acid Blue 113 and Acid Red 114 by heterogeneous photocatalytic process. ANN and RSM have been used for modeling and optimization of photodegradation of textile dyes. An attempt has been made to modify the photocatalyst by doping and codoping of metal ions. Later on immobilization of TiO_2 on cement beads has been discussed.

4.1 Photocatalytic Activity of RB5, AB113 and AR114 Dyes under UV/TiO_2

4.1.1 Determination of Wavelength of Maximum Absorbance

The absorbance data of aqueous solutions of RB5, AB113 and AR114 (concentration = 10 mg l^{-1}) were recorded over the entire wavelength range of UV-Vis spectrophotometer (200-700 nm). The data obtained were plotted to visualize the highest absorbance and the corresponding wavelength was designated as the wavelength of maximum absorbance (λ_{max}). The UV-Vis spectra of RB5, AB113 and AR114 show two peaks of each dye absorption spectra (Figure 4.1). The first absorption peak observed in UV region (i.e. 312, 273 and 278 nm for RB5, AB113 and AR114 respectively) represents the aromatic rings of the dyes. The second absorption peak observed in the visible region (i.e. 597, 566 and 522 nm for RB5, AB113 and AR114 respectively) represents the -N=N- (azo) bond. The reduction in the absorption peak of the UV region indicates the degradation of the dye, whereas the reduction in absorption peak of visible region indicates the decolorization of the dye solution.

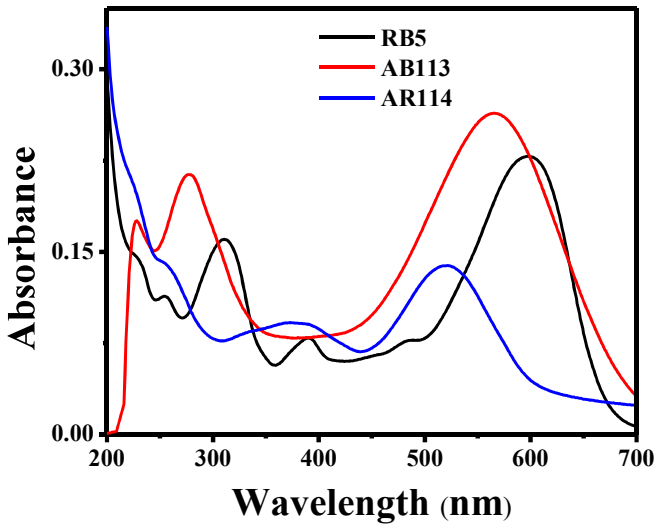

Figure 4.1 UV-Vis spectra of RB5, AB113, and AR114 dyes

4.1.2 Artificial Neural Network Model Development

In the current study, a tan-sigmoid transfer function with three-layered feed forward back propagation ANN network (6:10:2) has been used for the modeling of photocatalytic decolorization and degradation of RB5, AB113 and AR114. This network contains three layers, as shown in Figure 4.2: (1) independent variables (input layer) (2) number of neurons (hidden layers) and (3) dependent variables (output layer). The number of neurons in input and output layers depends on the type of the problem. In the current study, the input and output process variables and their ranges to the feed forward neural network are shown in Table 4.1.

Optimization of ANN topology is the most important step in the development of a model. To optimize the number of hidden nodes in a layer, a series of topologies were used, in which the numbers of nodes were changed from 2 to 12. Each topology has been repeated two times to remove arbitrary connection due to arbitrary initialization. Mean square error (MSE) was taken as error variable. From Figure 4.3, it is clear that, the MSE is minimum with eight, ten and ten neurons for RB5, AB113 and AR114 respectively for both (decolorization and degradation efficiency) cases.

In the present work, the training-and-test method was used to weigh the ANN with the trainscg (scaled conjugate gradient) training function. From the number of experimental data points, 125 data sets were used to feed the ANN structure. The data sets were divided into training, validation and test subsets, each of them confined to 89, 18 and 18 sets, respectively.

The validation and test sets were arbitrarily selected from the experimental data. Figure 4.2 shows the schematic diagram of ANN architecture, in which, the input layer has six neurons (TiO_2 dose, dye concentration, pH, area to volume ratio, UV light intensity and time) and output layer has two neurons (decolorization and degradation efficiency).

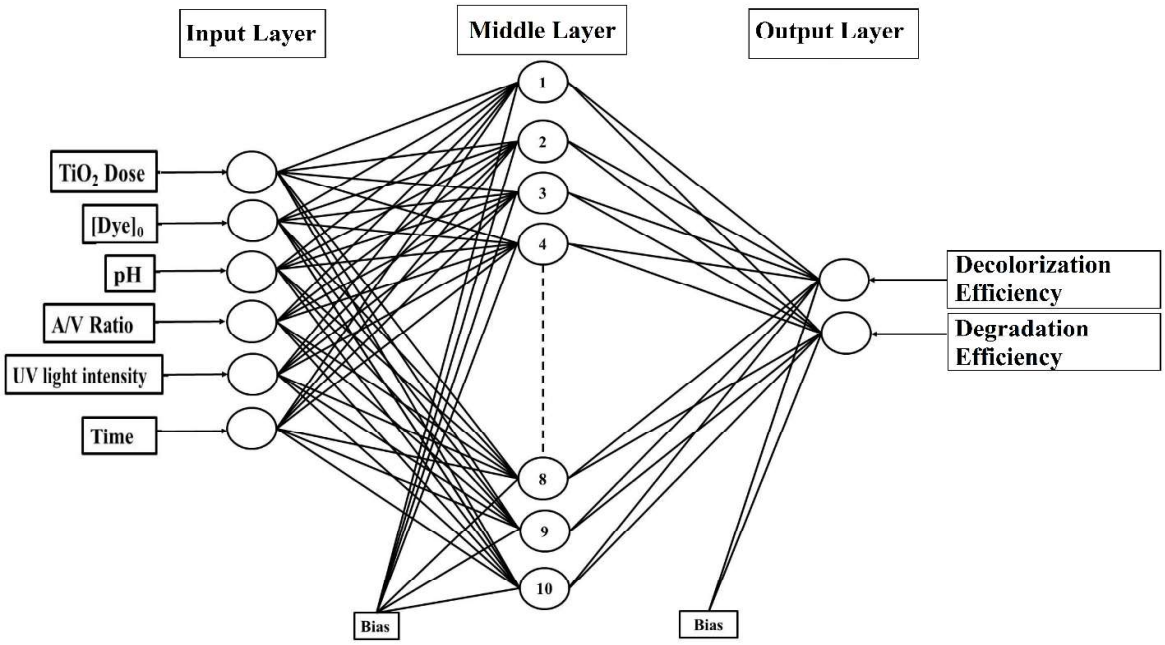

Figure 4.2 Schematic view of the developed ANN

Table 4.1 Model variables and their ranges

Variable	**Range**
Input layer	
TiO_2 dose (g l^{-1})	1.0 - 2.25
Dye concentration (mg l^{-1})	25 - 150
pH	2 - 10
A/V ratio (cm^{-1})	0.112 - 0.262
UV light intensity (Wm^{-2})	9.4 – 12.4
Time (min)	0 - 180
Output layer	
Decolorization efficiency	0 - 1
Degradation efficiency	0 - 1

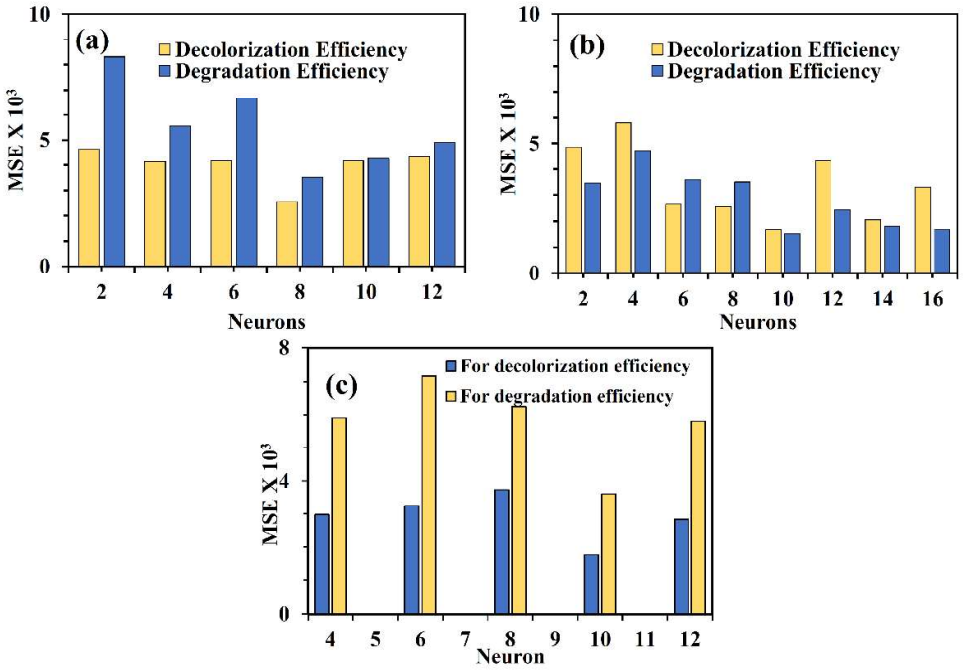

Figure 4.3 Effect of the number of neurons in hidden layer (a) RB5 (b) AB113 and (c) AR114

Figure 4.4 shows a comparison between simulated and experimental values of the output variables for data set by using neural network model. The correlation coefficients for decolorization and degradation efficiency are 0.9864 and 0.983 for RB5, 0.9827 and 0.9745 for AB113 and 0.9809 and 0.984 for AR114, respectively. It indicates the reliability of the model and confirms that the neural network model reproduces both the output responses, decolorization and degradation efficiency for this system, within experimental ranges adopted for fitting the model.

4.1.3 Statistical Analysis with BBD

A three-level BBD was applied to investigate the photocatalysis process parameters affecting decolorization and degradation efficiency. A range of values of the TiO_2 amount, initial dye concentration, pH of the dye solution, area to volume ratio, light intensity and time were used as the variable input parameters for the optimization. The input parameters used in the present work are given in Table 4.1. The factor levels were coded as -1 (low), 0 (central point or middle), and 1 (high) [225]. The simulated data were analyzed by regression analysis to fit the equations developed and also for the evaluation of the statistical significance of the equations. The results of the decolorization and degradation efficiency (responses) for

photocatalytic degradation of RB5, AB113 and AR114 were analysed according to the design matrix as suggested by BBD.

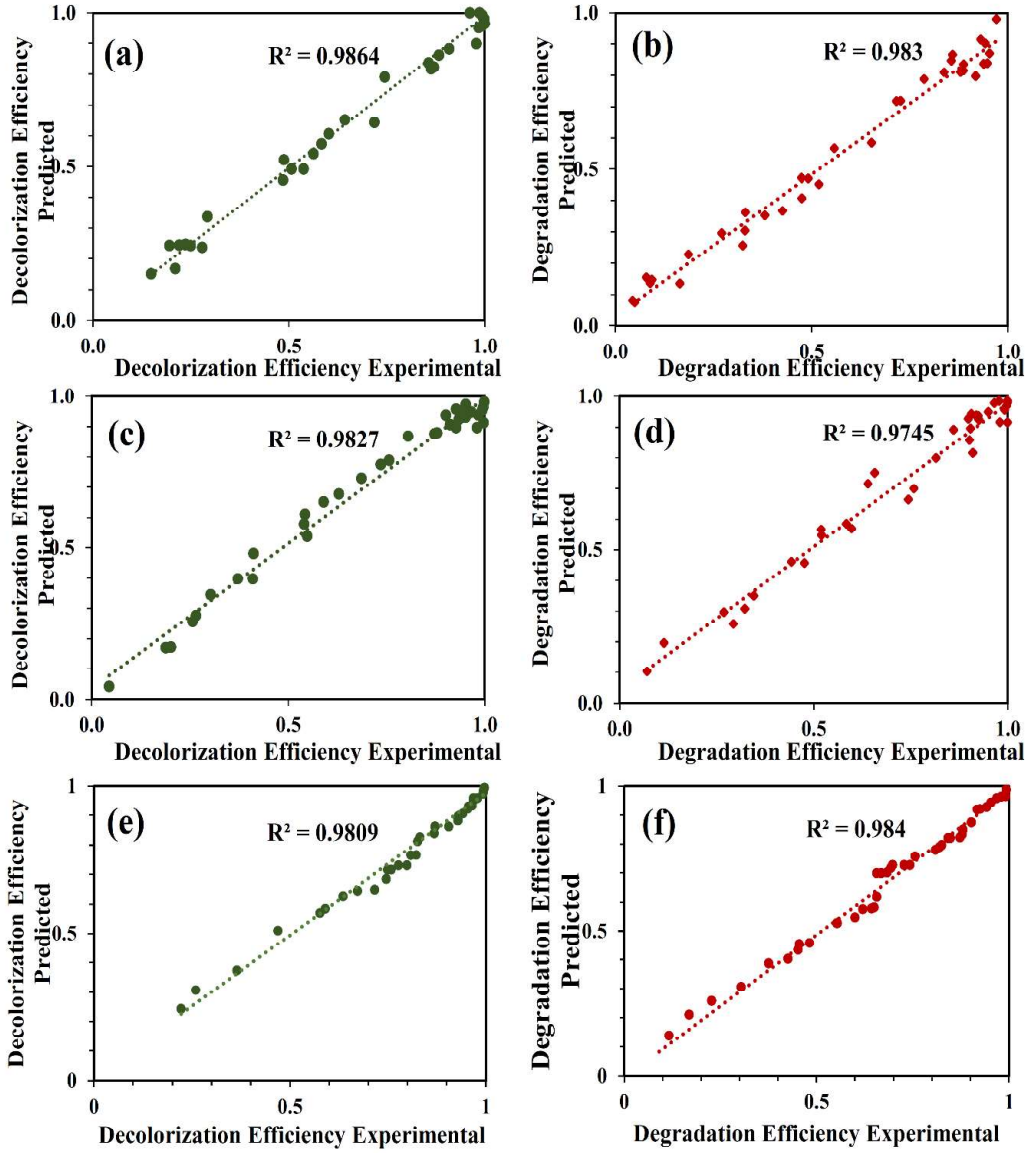

Figure 4.4 Comparison of the experimental results with those calculated via neural network modeling for the test set for decolorization efficiency (a) RB5 (c) AB113 and, (e) AR114 and for degradation efficiency of (b) RB5 (d) AB113 and, (f) AR114

The sequential F-test and other adequacy measures are generally used for selecting the best model. A manual regression method was used to fit the second order polynomial eq. (3.5) to the simulated data and to identify the relevant model terms. The model summary statistics are shown in Table 4.2. An adequate precision ratio above 4 indicates adequate model efficacy

and that the model can be used to navigate the design space [226]. Table 4.3, Table 4.4 and Table 4.5 show the analysis of variance (ANOVA) results for the decolorization and degradation efficiency, with a model F- value of 17.03 and 14.29, 15.28 and 16.17, and 12.89 and 11.53 for decolorization and degradation efficiency of RB5, AB113 and AR114 respectively implying that the model is significant. By eliminating the insignificant model terms, the resulting ANOVA for the reduced quadratic model summarizes the results for each response and shows the significant model terms. TiO_2 concentration, initial dye concentration, pH and time are the highly significant parameters for both decolorization and degradation of RB5, AB113 and AR114. Sahoo and Gupta [227] also reported that initial dye concentration and pH were the most significant parameters for the photocatalytic degradation of methylene blue.

Table 4.2 The model summary statistics

	Regression Coefficient (R^2)		**Precision Ratio**	
	Decolorization Efficiency	Degradation Efficiency	Decolorization Efficiency	Degradation Efficiency
RB5	0.9465	0.9369	18.43	17.99
AB113	0.9407	0.9438	15.29	16.18
AR114	0.9305	0.9229	12.90	11.53

The data points on normal probability plot and a dot diagram of these residuals lie reasonably close to a straight line. This means that the assumptions used in the analysis are satisfied. Therefore, the developed models can be considered to be adequate because the residuals for the prediction of each response are minimum. The three-dimensional response surface plots of two independent variables, while keeping the other constant, can give information about the individual and interaction effects of the independent variables on the responses. Figure 4.5, Figure 4.6 and Figure 4.7 show the 3D response surface plots for photocatalytic decolorization and degradation of RB5, AB113 and AR114 respectively.

Table 4.3 ANOVA model for RB5 decolorization and degradation efficiency

	Decolorization Efficiency					Degradation Efficiency				
Source	**Sum of Squares**	**DF**	**Mean Square**	**F Value**	**Prob> F**	**Sum of Squares**	**DF**	**Mean Square**	**F Value**	**Prob> F**
Model	6.09	27	0.22	17.03	< 0.0001	5.57	27	0.20	14.29	< 0.0001
$[TiO_2]$	0.20	1	0.20	15.49	0.0006	0.11	1	0.11	8.03	0.0087
C_o	2.71	1	2.71	204.8	< 0.0001	2.58	1	2.58	178.92	< 0.0001
pH	0.31	1	0.31	23.47	< 0.0001	0.33	1	0.33	23.29	< 0.0001
A/V Ratio	0.032	1	0.032	2.427	0.1313	0.10	1	0.10	7.33	0.0118
Light Intensity	0.00	1	0.00	0.05	0.8212	0.01	1	0.01	1.31	0.2620
Time	2.06	1	2.06	156.03	< 0.0001	1.55	1	1.55	107.27	< 0.0001
Model	0.00	1	0.00	0.05	0.8174	0.00	1	0.00	0.03	0.8434
$[TiO_2]$	0.00	1	0.00	0.47	0.4959	0.14	1	0.14	9.80	0.0043
C_o	0.00	1	0.00	0.35	0.5541	0.00	1	0.00	0.12	0.7273
pH	0.00	1	0.00	0.00	0.9628	0.00	1	0.00	0.52	0.4749
A/V Ratio	0.00	1	0.00	0.05	0.8203	0.00	1	0.00	0.21	0.6480
Light Intensity	0.08	1	0.08	6.78	0.0150	0.07	1	0.07	4.91	0.0356
Time	0.00	1	0.00	0.00	0.9657	0.00	1	0.00	0.40	0.5308
$([TiO_2])^2$	0.00	1	0.00	0.34	0.5599	0.00	1	0.00	0.21	0.6456
$(C_o)^2$	0.04	1	0.04	3.22	0.0843	0.01	1	0.01	1.07	0.3104
$(pH)^2$	0.00	1	0.00	0.68	0.4148	0.00	1	0.00	0.10	0.7437
$(A/V\ Ratio)^2$	0.01	1	0.01	1.49	0.2321	0.03	1	0.03	2.75	0.1092
$(Light\ Intensity)^2$	0.02	1	0.02	1.65	0.2090	0.01	1	0.01	1.00	0.3247
$(Time)^2$	0.00	1	0.00	0.44	0.5112	0.00	1	0.00	0.23	0.6328
$[TiO_2]* C_o$	0.06	1	0.06	5.22	0.0306	0.02	1	0.02	1.88	0.1817
$([TiO_2] * pH)$	0.08	1	0.08	6.27	0.0189	0.12	1	0.12	8.49	0.0072
$([TiO_2] * A/V\ Ratio)$	0.00	1	0.00	0.02	0.8646	0.00	1	0.00	0.01	0.9026
$([TiO_2] * Light\ Intensity)$	0.01	1	0.01	1.35	0.2558	0.00	1	0.00	0.57	0.4545
$([TiO_2] *Time)$	0.23	1	0.23	17.755	0.0003	0.23	1	0.23	15.92	0.0005
$(C_o *pH)$	0.00	1	0.00	0.03	0.8577	0.00	1	0.00	0.00	0.9877
$(C_o * A/V\ Ratio)$	0.00	1	0.00	0.50	0.4857	0.01	1	0.01	1.11	0.3012
$(C_o * Light\ Intensity)$	0.08	1	0.08	6.62	0.0161	0.08	1	0.08	5.65	0.0251
$(C_o *Time)$	0.34	26	0.01			0.37	26	0.01		
(pH* A/V Ratio)	0.34	21	0.01			0.37	21	0.01		
(pH* Light Intensity)	0	5	0			0	5	0		
(pH*Time)	6.43	53				5.95	53			

Table 4.4 ANOVE model for AB113 decolorization and degradation efficiency

	Decolorization Efficiency					Degradation Efficiency				
Source	**Sum of Squares**	**DF**	**Mean Square**	**F Value**	**Prob> F**	**Sum of Squares**	**DF**	**Mean Square**	**F Value**	**Prob> F**
Model	5.48	27	0.208	15.28	< 0.0001	5.40	27	0.20	16.17	< 0.0001
$[TiO_2]$	0.06	1	0.062	4.69	0.039	0.007	1	0.007	0.59	0.4471
C_o	0.26	1	0.262	19.72	0.0001	0.375	1	0.375	30.36	< 0.0001
pH	0.72	1	0.716	53.93	< 0.0001	0.44339	1	0.4433	35.82	< 0.0001
A/V Ratio	0.06	1	0.057	4.35	0.0469	0.0065	1	0.0065	0.52	0.4746
Light Intensity	0.03	1	0.027	2.07	0.1615	0.237	1	0.2378	19.22	0.0002
Time	3.29	1	3.28	247.4	< 0.0001	3.477	1	3.47	281.0	< 0.0001
$([TiO_2])^2$	0.03	1	0.033	2.55	0.1221	8.73E-06	1	8.73E-06	0.00	0.9790
$(C_o)^2$	0.11	1	0.115	8.69	0.0066	0.067	1	0.067	5.42	0.0279
$(pH)^2$	0.017	1	0.017	1.35	0.2552	0.009	1	0.0097	0.787	0.3831
$(A/V\ Ratio)^2$	2.07E-05	1	2.07E-05	0.001	0.9688	0.013	1	0.013	1.126	0.2982
$(Light\ Intensity)^2$	0.062	1	0.062	4.67	0.0400	0.029	1	0.029	2.389	0.1342
$(Time)^2$	0.287	1	0.287	21.62	< 0.0001	0.239	1	0.239	19.34	0.0002
$[TiO_2]* C_o$	0.017	1	0.017	1.29	0.2660	0.055	1	0.055	4.444	0.0448
$([TiO_2] * pH)$	0.008	1	0.008	0.64	0.4305	2.63E-05	1	2.63E-05	0.002	0.9636
$([TiO_2] * A/V$ Ratio)	0.0008	1	0.00	0.06	0.8024	0.01967	1	0.019	1.589	0.2186
$([TiO_2] *$ Light Intensity)	0.0172	1	0.0172	1.29	0.2649	0.0002	1	0.0002	0.020	0.8870
$([TiO_2] *$Time)	0.009	1	0.009	0.68	0.4150	0.0004	1	0.0004	0.035	0.8522
$(C_o *$pH)	0.0007	1	0.0007	0.05	0.8121	0.00062	1	0.0006	0.050	0.8246
$(C_o *$ A/V Ratio)	0.022	1	0.0224	1.68	0.2056	0.0008	1	0.0008	0.065	0.8004
$(C_o *$ Light Intensity)	0.018	1	0.018	1.38	0.2499	0.011	1	0.011	0.947	0.3393
$(C_o *$Time)	0.108	1	0.108	8.13	0.0084	0.122	1	0.122	9.874	0.0042
(pH* A/V Ratio)	0.001	1	0.001	0.13	0.7211	0.0012	1	0.001	0.100	0.7537
(pH* Light Intensity)	0.002	1	0.002	0.20	0.6512	6.64E-06	1	6.64E-06	0.000	0.9817
(pH*Time)	0.249	1	0.249	18.74	0.0002	0.158	1	0.158	12.78	0.0014
(A/V Ratio *Light Intensity)	0.112	1	0.11	8.48	0.0073	0.071	1	0.071	5.759	0.0239
(A/V Ratio *Time)	0.002	1	0.002	0.22	0.6402	0.002	1	0.002	0.196	0.6612
(Light Intensity*Time)	0.000	1	0.000	0.02	0.8709	0.0064	1	0.006	0.519	0.4776
Residual	0.345	26	0.013			0.3217	26	0.012		
Lack of Fit	0.345	21	0.016			0.321	21	0.015		
Pure Error	0	5	0			0	5	0		
Cor Total	5.83	53				5.726	53			

Table 4.5 ANOVA model for AR114 decolorization and degradation efficiency

	Decolorization Efficiency					Degradation Efficiency				
Source	**Sum of Squares**	**DF**	**Mean Square**	**F Value**	**Prob> F**	**Sum of Squares**	**DF**	**Mean Square**	**F Value**	**Prob> F**
Model	7.099	27	0.263	12.895	< 0.0001	6.318	27	0.234	11.531	< 0.0001
$[TiO_2]$	0.003	1	0.003	0.171	0.6827	0.033	1	0.033	1.616	0.2149
C_o	0.341	1	0.341	16.720	0.0004	0.462	1	0.462	22.753	< 0.0001
pH	0.315	1	0.315	15.431	0.0006	0.234	1	0.234	11.514	0.0022
A/V Ratio	0.014	1	0.014	0.681	0.4169	0.066	1	0.066	3.265	0.0823
Light Intensity	0.000	1	0.000	0.003	0.9596	0.000	1	0.000	0.000	0.9848
Time	4.175	1	4.175	204.74	< 0.0001	3.744	1	3.744	184.53	< 0.0001
$([TiO_2])^2$	0.106	1	0.106	5.184	0.0313	0.123	1	0.123	6.082	0.0206
$(C_o)^2$	0.055	1	0.055	2.700	0.1124	0.037	1	0.037	1.815	0.1895
$(pH)^2$	0.016	1	0.016	0.763	0.3904	0.010	1	0.010	0.477	0.4961
$(A/V\ Ratio)^2$	0.000	1	0.000	0.022	0.8820	0.003	1	0.003	0.146	0.7056
$(Light\ Intensity)^2$	0.024	1	0.024	1.178	0.2876	0.029	1	0.029	1.428	0.2428
$(Time)^2$	1.461	1	1.461	71.640	< 0.0001	1.142	1	1.142	56.264	< 0.0001
$([TiO_2]* C_o$	0.000	1	0.000	0.004	0.9520	0.013	1	0.013	0.645	0.4292
$([TiO_2]$ * pH)	0.001	1	0.001	0.050	0.8245	0.005	1	0.005	0.234	0.6325
$([TiO_2]$ * A/V Ratio)	0.004	1	0.004	0.202	0.6569	0.026	1	0.026	1.283	0.2676
$([TiO_2]$ * Light Intensity)	0.000	1	0.000	0.015	0.9044	0.000	1	0.000	0.018	0.8947
$([TiO_2]$ *Time)	0.000	1	0.000	0.000	0.9916	0.000	1	0.000	0.004	0.9519
(C_o *pH)	0.150	1	0.150	7.375	0.0116	0.111	1	0.111	5.491	0.0270
(C_o * A/V Ratio)	0.015	1	0.015	0.742	0.3970	0.007	1	0.007	0.331	0.5697
(C_o * Light Intensity)	0.000	1	0.000	0.009	0.9233	0.003	1	0.003	0.144	0.7071
(C_o *Time)	0.009	1	0.009	0.430	0.5177	0.018	1	0.018	0.897	0.3524
(pH* A/V Ratio)	0.135	1	0.135	6.627	0.0161	0.098	1	0.098	4.807	0.0375
(pH* Light Intensity)	0.001	1	0.001	0.048	0.8280	0.006	1	0.006	0.291	0.5941
(pH*Time)	0.005	1	0.005	0.251	0.6208	0.002	1	0.002	0.087	0.7700
(A/V Ratio *Light Intensity)	0.003	1	0.003	0.153	0.6992	0.004	1	0.004	0.218	0.6445
(A/V Ratio *Time)	0.127	1	0.127	6.233	0.0192	0.122	1	0.122	5.990	0.0215
(Light Intensity*Time)	0.000	1	0.000	0.000	0.9963	0.000	1	0.000	0.023	0.8815
Residual	0.530	26	0.020			0.528	26	0.020		
Lack of Fit	0.530	21	0.025			0.528	21	0.025		
Pure Error	0.000	5	0.000			0.000	5	0.000		
Cor Total	7.629	53				6.845	53			

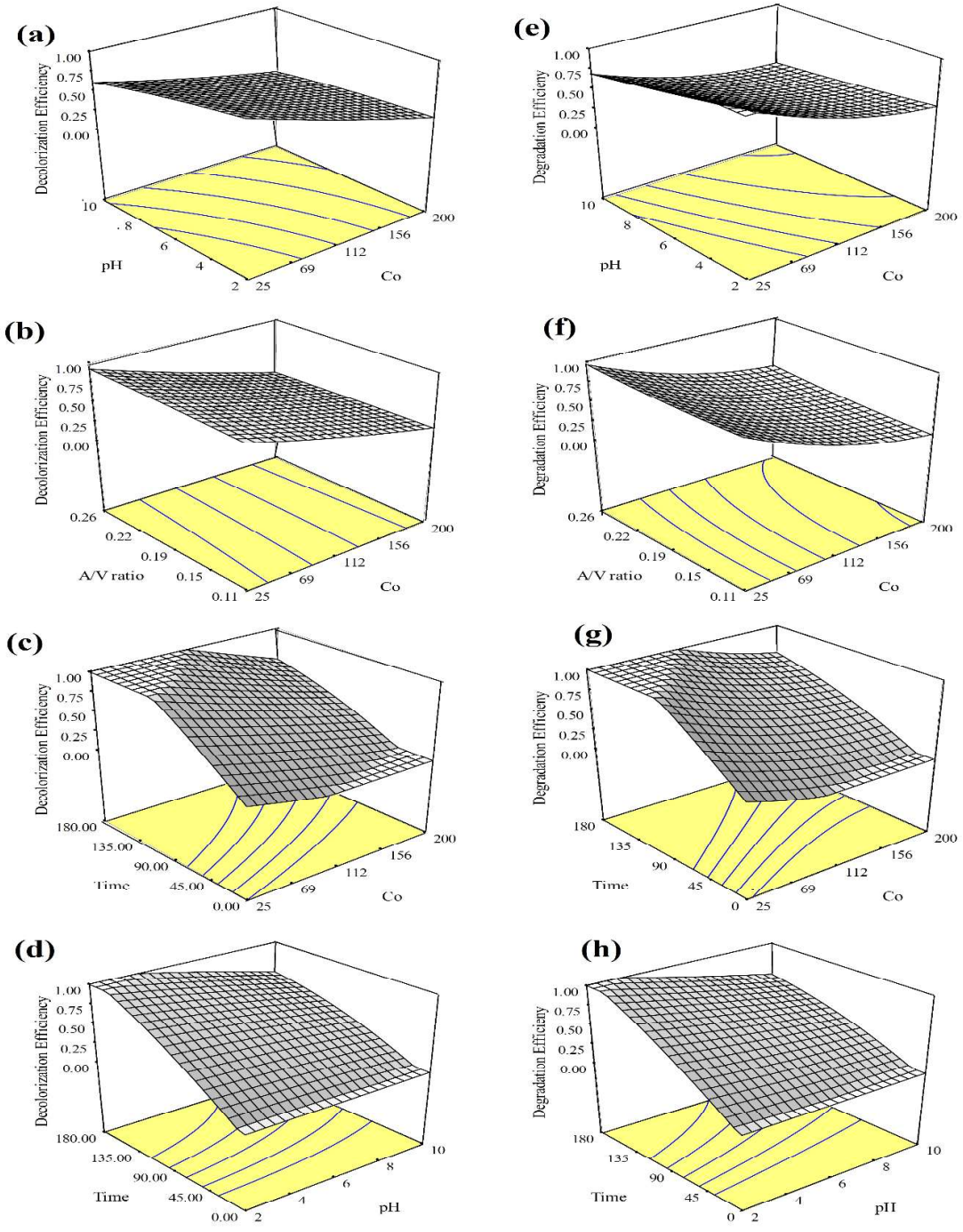

Figure 4.5 3D response surface plots for RB5 (a) pH Vs C_o for the decolorization efficiency, (b) A/V ratio Vs C_o for the decolorization efficiency, (c) time Vs C_o for the decolorization efficiency, (d) time Vs pH for the decolorization efficiency, (e) pH Vs C_o for the degradation efficiency, (f) A/V ratio Vs C_o for the degradation efficiency, (g) time Vs C_o for the degradation efficiency, (h) time Vs pH for the degradation efficiency.

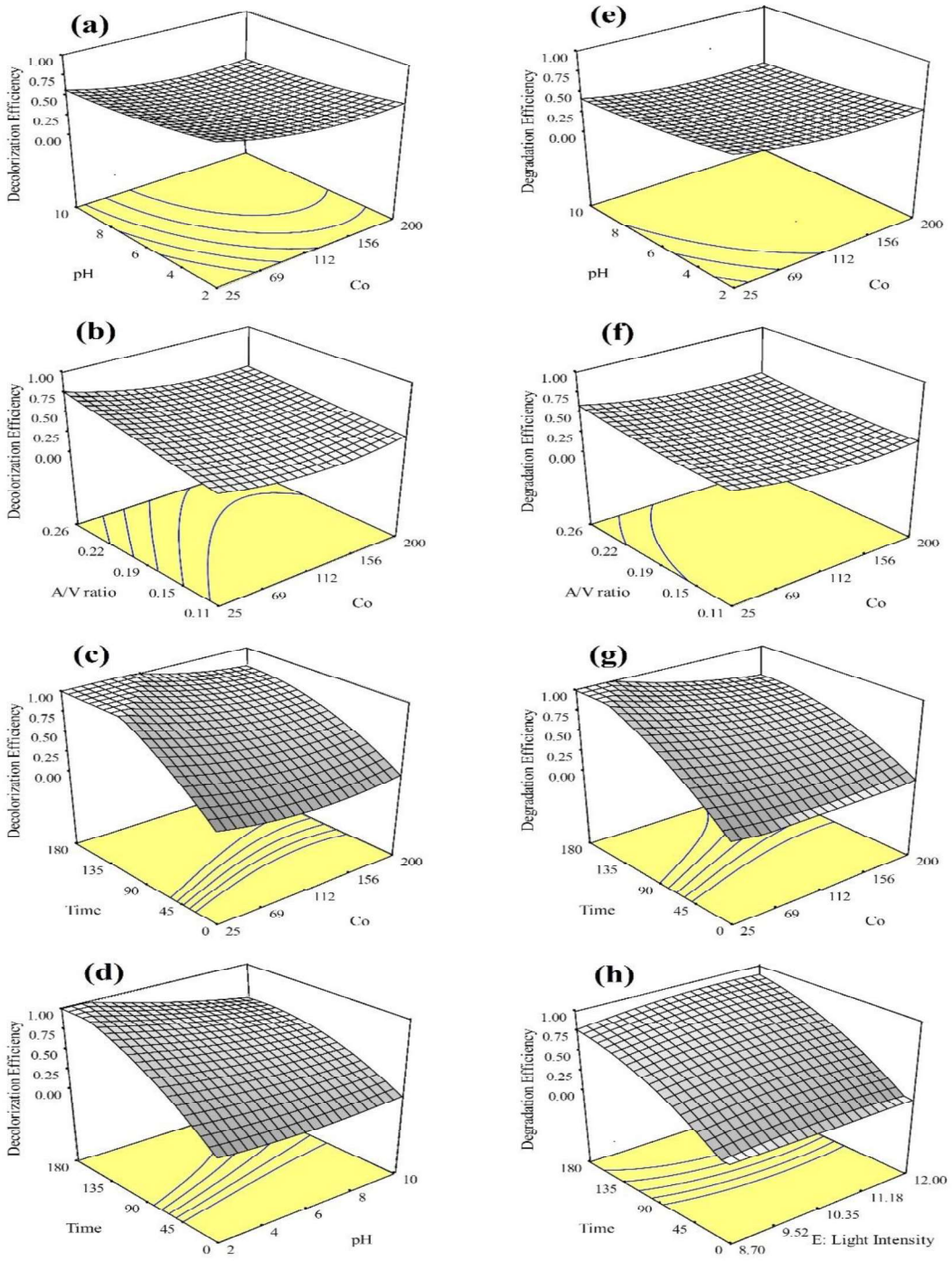

Figure 4.6 3D response surface plots for AB113 (a) pH Vs C_o for the decolorization efficiency, (b) A/V ratio Vs C_o for the decolorization efficiency, (c) time Vs C_o for the decolorization efficiency, (d) time Vs pH for the decolorization efficiency, (e) pH Vs C_o for the degradation efficiency, (f) A/V ratio Vs C_o for the degradation efficiency, (g) time Vs C_o for the degradation efficiency, (h) time Vs pH for the degradation efficiency.

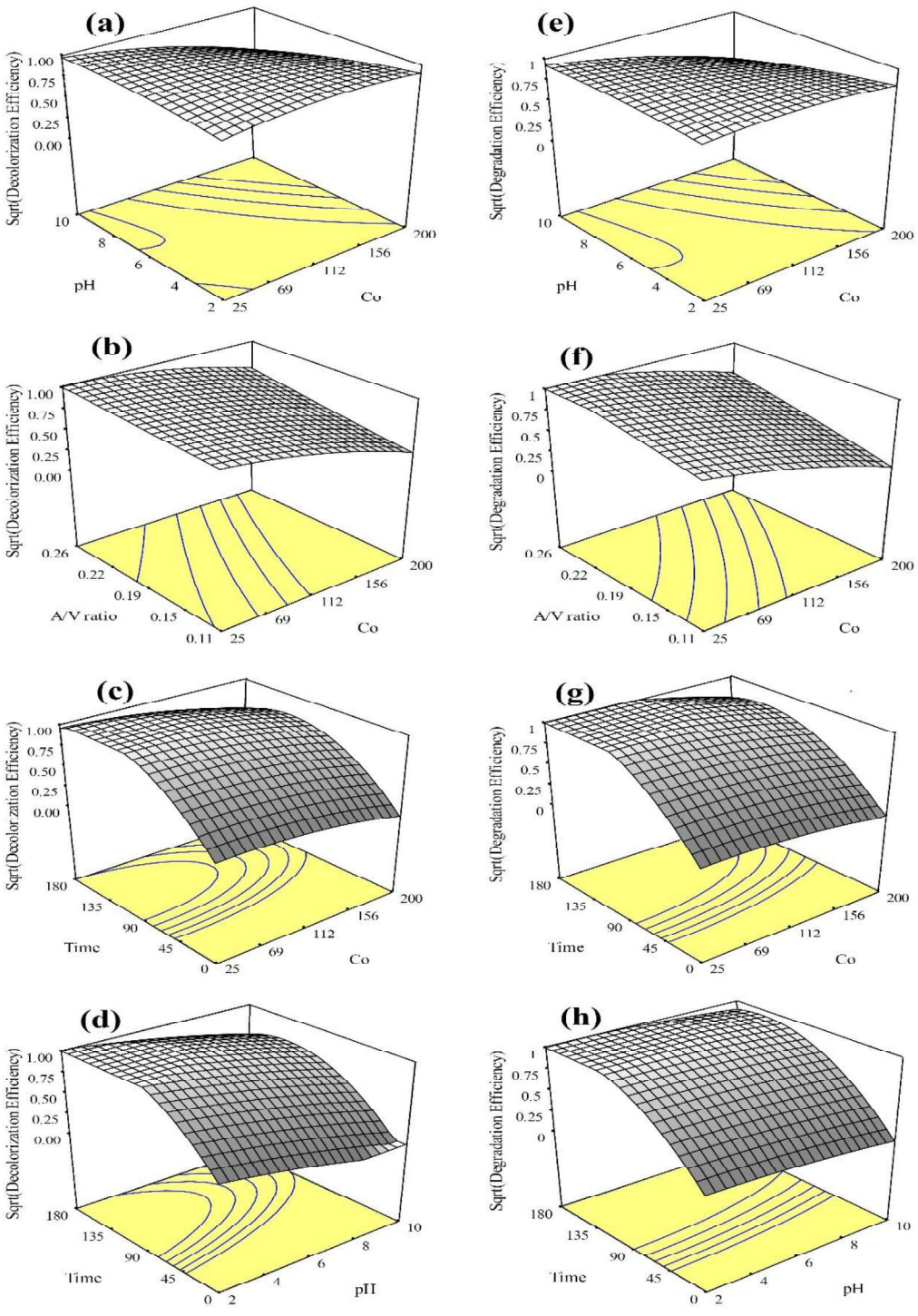

Figure 4.7 3D response surface plots for AR114 (a) pH Vs C_o for the decolorization efficiency, (b) A/V ratio Vs C_o for the decolorization efficiency, (c) time Vs C_o for the decolorization efficiency, (d) time Vs pH for the decolorization efficiency, (e) pH Vs C_o for the degradation efficiency, (f) A/V ratio Vs C_o for the degradation efficiency, (g) time Vs C_o for the degradation efficiency, (h) time Vs pH for the degradation efficiency.

From Figure 4.5a and e, Figure 4.6a and e and Figure 4.7a and e, it is clear that the maximum decolorization and degradation was in the pH range of 2-4. Also, the decolorization rate and degradation rate increase rapidly with irradiation time. Similar observations were reported by Sahoo and Gupta [227] for the photocatalytic degradation of methylene blue dye. The decolorization and degradation efficiency increases with increase in A/V ratio of the reactor (Figure 4.5b and f, Figure 4.6b and f and Figure 4.7b and f). There is rapid increase in decolorization and degradation efficiency up to 135 min, irrespective of the initial dye concentration (Figure 4.5c and g, Figure 4.6c and g and Figure 4.7c and g), after that there is little increase in decolorization and degradation efficiency. Also, the maximum decolorization and degradation was achieved in the concentration range of 25-100 mg l^{-1}.

The point prediction option in the software was used for the optimization of the process parameters. The adequacy of the developed models was verified by carrying out the confirmatory simulation runs using test conditions within the simulation ranges defined earlier. The optimized process parameters at an initial dye concentration of 100 mg l^{-1} are given in Table 4.6. Table 4.7 shows the comparisons of decolorization and degradation efficiency obtained by BBD, ANN model and experimental run at optimum process parameters. From Table 4.7, it is clear that the optimization of process parameters for the photocatalytic decolorization and degradation of RB5, AB113 and AR114 can be carried out easily and satisfactorily by using this method. This method also reduces the number of simulation runs significantly in comparison to other methods reported in literature.

Table 4.6 Optimized parameters suggested by BBD

	Optimized Results		
Process Parameters	**RB5**	**AB113**	**AR114**
Input			
TiO_2 Amount (gl^{-1})	2.0	1.5	1.5
Initial Dye Conc (mgl^{-1})	100	80	100
pH	4	4	4
Area to Volume Ratio (cm^{-1})	0.26	0.24	0.2
Light Intensity (Wm^{-2})	12	9.1	12
Time (min)	90	60	90

Table 4.7 Comparisons of decolorization and degradation efficiency between results obtained by BBD, ANN model and experimental run at optimum process parameters

	Decolorization Efficiency			**Degradation Efficiency**		
	RB5	**AB113**	**AR114**	**RB5**	**AB113**	**AR114**
Response from BBD	1	1	1	1	1	1
Response from ANN	0.98	0.978	0.99	0.984	0.983	0.985
Response from Experiments	0.99	0.989	0.988	0.965	0.974	0.968

4.1.4 Kinetic Studies

The decolorization and degradation could be related by a simple power law kinetic model. The first order kinetics in terms of decolorization and degradation can be written as:

$$\frac{-d[C]}{dt} = k'[C] \tag{4.1}$$

where k′ is the first order rate constant.

On integration, (with the limit of C = C_o at t = 0) with C_o being the equilibrium concentration of the bulk solution, ln C_o/C = k′t, where, C_o is the equilibrium concentration of dye and C is the concentration at time t. A plot of ln C_o/C versus *t* for photodecolorization and degradation is shown in Figure 4.8. A linear relationship between dye concentration and irradiation time has been observed. The kinetic constants are shown in Table 4.8. Barka et al. [228] also found the first order kinetics for photocatalytic degradation of Reactive Yellow 84.

Table 4.8 First order reaction rate constants

	Reaction Rate Constants (min^{-1})	
	Decolorization Efficiency	Degradation Efficiency
RB5	0.0515	0.0246
AB113	0.0470	0.0205
AR114	0.0542	0.0253

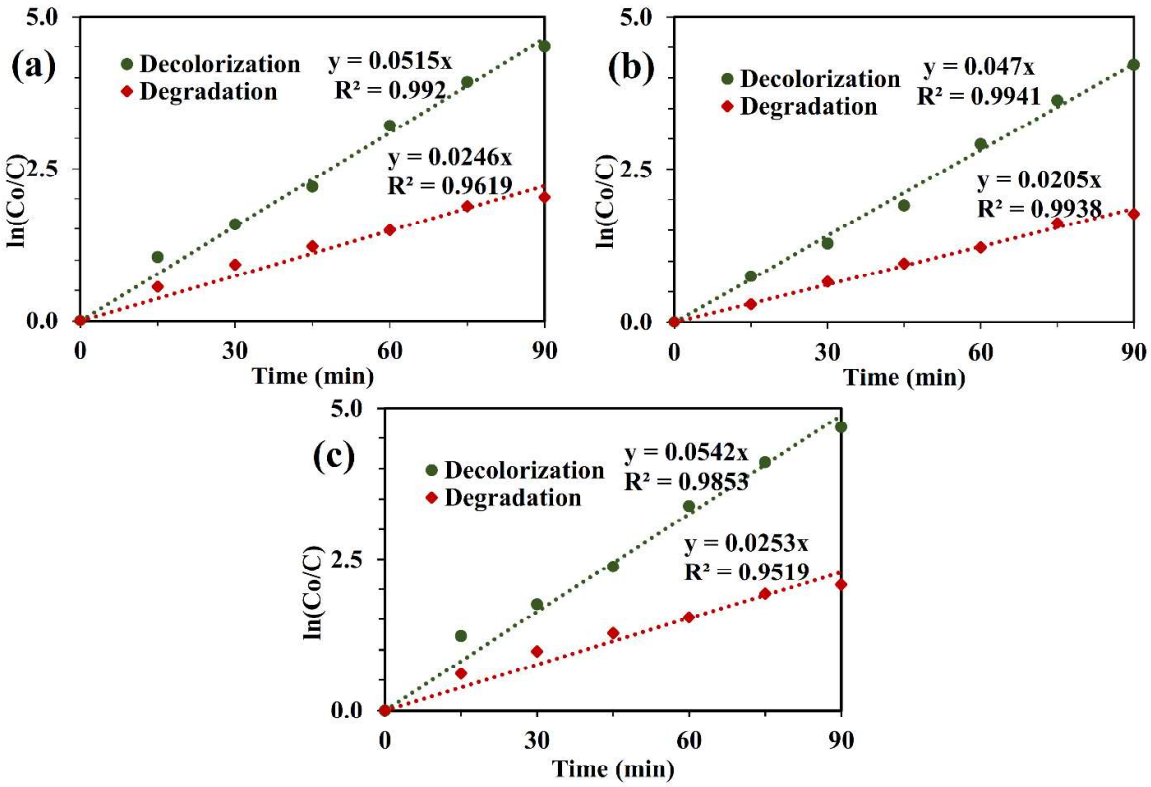

Figure 4.8 Reaction kinetics of (a) RB5, (b) AB113 and (c) AR114 at optimized conditions

4.1.5 TOC Removal versus Decolorization and Degradation

In order to determine the total degradation during photocatalysis, the TOC, decolorization and degradation efficiency of RB5, AB113 and AR114 at optimized conditions have been determined and plotted as shown in Figure 4.9. The RB5, AB113 and AR114 dyes under optimized conditions show high decolorization and degradation efficiency and almost completely degradation after 150 min. But TOC removal is slower with respect to degradation efficiency. This will be due to formation of intermediates and later on these intermediates have been degraded and almost mineralized after 150 min.

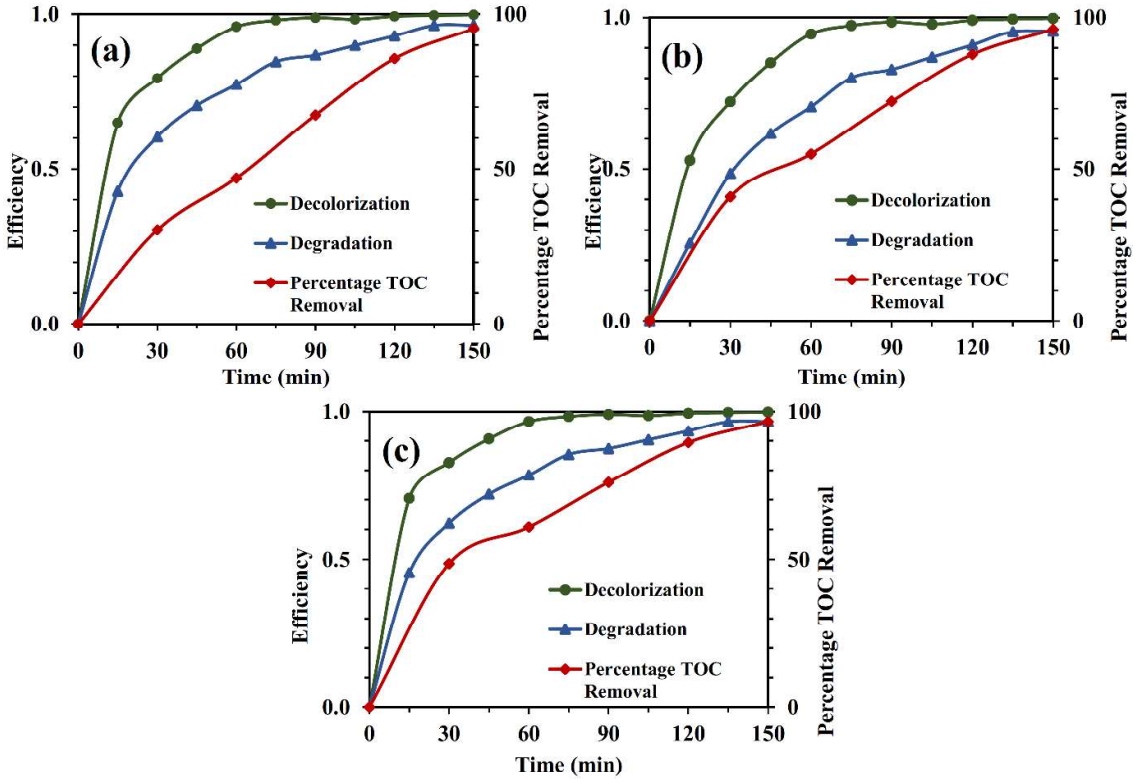

Figure 4.9 Dye decolorization, degradation and TOC removal versus time at optimized conditions for (a) RB5, (b) AB113 and (c) AR114 dyes

4.1.6 Determination of Dye Degradation Products/Intermediates in UV/TiO_2 Process

GC-MS analysis was carried out to recognize probable organic/aromatic compounds/intermediates formed during the photocatalytic degradation of RB5. The photocatalytic degradation was carried out at optimized conditions and samples have been withdrawn at a fixed interval of 30 min. The chromatograms are shown in Figure 4.10 with respect to samples collected at various time intervals 30, 60 and 90 min of reaction and the chromatogram of original sample (time = 0 min) is also shown. The probable intermediates formed during the photocatalytic degradation of RB5 have been presented in Table 4.9. It is clear from the Table 4.9 that after 90 min of irradiation, only C_6 and C_7 compounds are left in the dye solution.

Table 4.9 Intermediates recognized by GC–MS

Symbol	Compound	Structural formula	Sample time (min)		
			30	60	90
C_0	Reactive Black 5	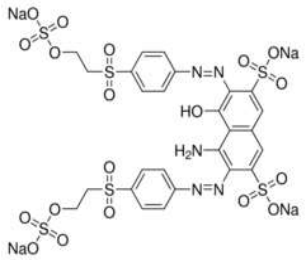			
C_1	Ethyl ethanoate	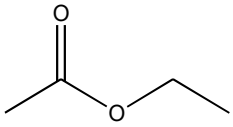	√	X	X
C_2	Urethane	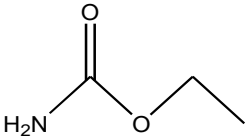	√	X	X
C_3	Hepta-4,6-Diyn-2-Ol	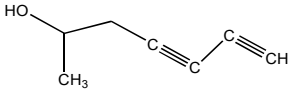	√	X	X
C_4	Butanedioic Acid 2,3-Dihydroxy-Dimethyl Ester	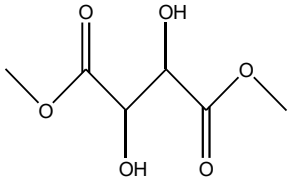	√	√	X
C_5	2-(2-sulfanylpropanoylamino) acetic acid	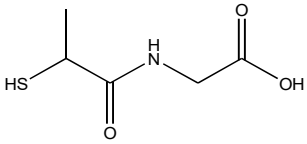	√	√	X
C_6	Propanoic Acid, 2-(Ethylthio)-Ethyl Ester	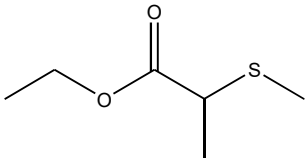	√	√	√
C_7	Tert-Butyl N-Hydroxycarbamate	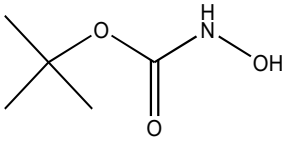	√	√	√

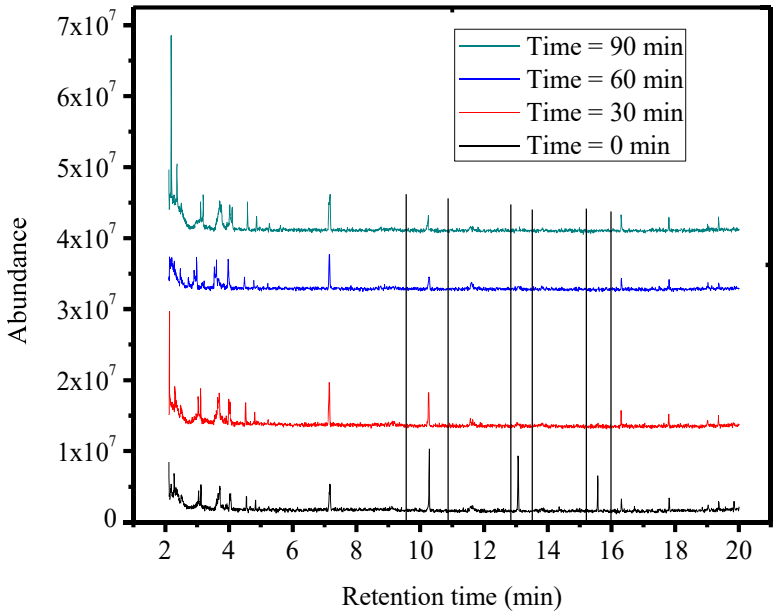

Figure 4.10 GC-MS chromatograms of RB5 samples after photocatalysis

4.2 Photocatalytic Activity of Binary Dye Mixture of AB113 and AR114

4.2.1 Calibration for Quantification of RB5, AB113 and AR114

In analytical chemistry, a calibration curve is used for determining the concentration of a substance in an unknown sample by comparing the unknown sample to a set of standard samples of known concentration.

4.2.1.1 Calibration of Spectrophotometer for Binary Dye Solution

It is a difficult task to calibrate dye in dye mixture due to the interference of one dye on another as shown in Figure 4.11a. The absorption of one dye is interfering the absorption of other as the intensity of their peaks are increasing in dye mixture. Therefore, their analysis is not possible by direct absorbance method. Due to this interference, the traditional spectrophotometric method is not able to analyze the individual dye concentration in binary dye mixture. Here, we have used two different methods to find the concentration of individual dyes in binary dye mixture: (1) first order derivative spectrophotometric technique, and (2) multivariate calibration technique.

4.2.1.1.1 First order derivative spectrophotometric technique

The absorption spectra of individual and binary dye mixture of AB113 and AR114 are show in Figure 4.11a. The first order derivative of absorbance with respect to wavelength are shown in Figure 4.11b. The first derivative will be the change in rate of absorbance with respect to wavelength. The first order derivative intersects at zero baseline at the related wavelength as λ_{max} of the absorbance band by first a positive and then a negative band, with the maximum and minimum at the similar wavelengths as the modulation points in the absorbance band [229].

The derivation of zero order spectrum leads to overlapped signals, reducing the interaction signals and decreasing the consequence of spectral background interferences affected by the other dye in the mixture [230]. Therefore, the concentration of AB113 and AR114 in binary dye mixture is analyzed by computing the absorbance at the first order derivative wavelength. For the binary dye solution of AB113 and AR114 dyes, the concentration of AB113 is determined at 511 nm in the presence of AR114, at this wavelength the absorbance of AR114 is found to be zero. Also, the concentration of AR114 is determined at 563 nm in presence of AB113, at this wavelength the absorbance of AB113 is found to be zero (Figure 4.11b).

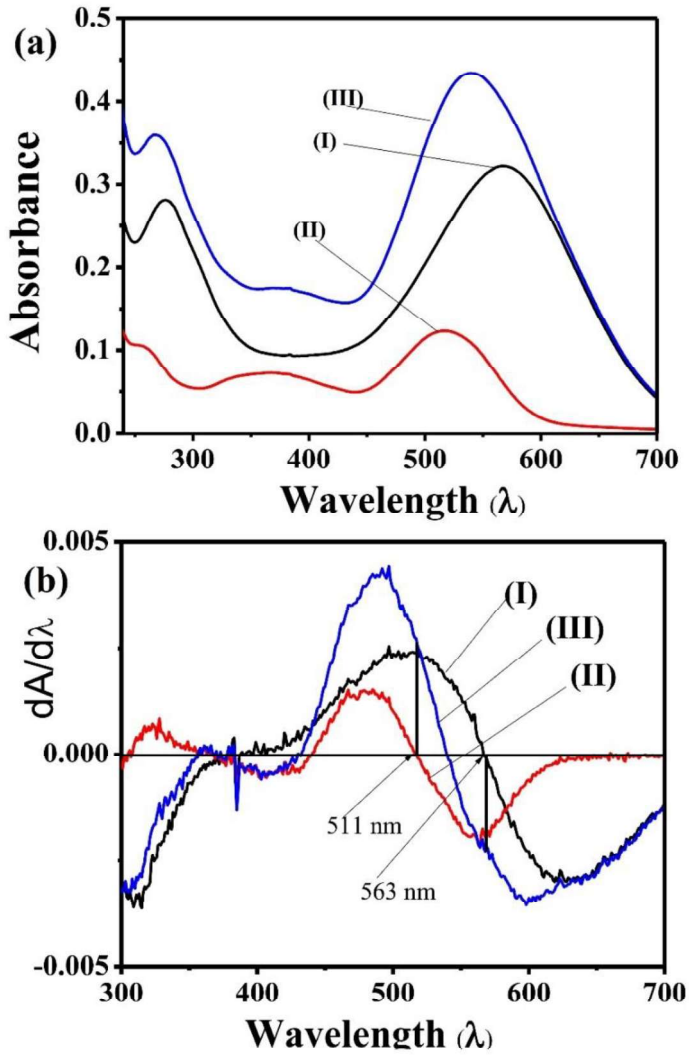

Figure 4.11 (a) The UV-Vis absorption spectra and (b) the first order derivative of absorption spectra of (I) $[AB113]_o$ = 10 mg l^{-1}, (II) $[AR114]_o$ = 10 mg l^{-1} and (III) mixture of 10 mg l^{-1} each

4.2.1.1.2 Multivariate calibration method

Multivariate or multiple regression method can also be exploited for the calibration of dyes in the binary dye mixture [231]. Various mixtures with varying dye ratios of AB113 and AR114 were used for calibration purpose. From Figure 4.11a maximum absorbance for AB113 and AR114 was found at 566 and 522 nm respectively. From multiple regressions, the equations to calculate individual dye concentration in binary dye mixture are as follows:

$$[AB113]\,(mg\,l^{-1}) = -2.657 + 44.165 \times (abs)_{566} - 14.872 \times (abs)_{522} \quad (4.2)$$

$$[AR114]\,(mg\,l^{-1}) = 2.582 + 129.06 \times (abs)_{522} - 107.01 \times (abs)_{566} \quad (4.3)$$

where $(abs)_{566}$ and $(abs)_{522}$ are the absorption at 566 and 522 nm, respectively of individual dyes. It may be observed that negative terms in the eq. (4.2) and (4.3) indicate the interference from other dyes in proportion to their concentration. The values of R^2 to above multivariate calibration methods are > 0.99 for both the dyes (Table 4.10), which indicate a good fit of the model to data. The comparison between first order derivative spectrophotometric and multivariate calibration methods have been presented in Table 4.11. It has been shown that both methods are suitable to quantify individual dye concentration in binary dye mixture. So, we can follow any of the methods for calibration of the individual dye in binary dye mixture.

Table 4.10 Statistical constraints related to calibration of dyes in binary dye mixture

	AB113	AR114
No. of points	8	8
Degree of freedom	2	2
Residual sum of squares	0.081	0.025
Adjusted R square	0.99867	0.99756

Table 4.11 Comparison between first order derivatives spectrophotometric and multivariate calibration methods

Sample		**First Order Derivatives Spectrophotometric Method**		**Multivariate Calibration Method**	
$[AB113]_o$ (mg l^{-1})	**$[AR114]_o$ (mg l^{-1})**	**$[AB113]_o$ (mg l^{-1})**	**$[AR114]_o$ (mg l^{-1})**	**$[AB113]_o$ (mg l^{-1})**	**$[AR114]_o$ (mg l^{-1})**
5	25	4.97	24.91	4.96	24.99
10	20	9.94	19.89	9.98	19.87
15	15	14.91	14.96	14.97	14.92
20	10	19.98	9.98	19.91	9.91
25	5	24.89	4.99	24.99	4.93

4.2.2 Equilibrium Adsorption

Equilibrium adsorption study has been carried out in dark room for different doses of TiO_2 and binary mixture at different doses of TiO_2 (50-250 mg l^{-1}). The results are shown in Figure 4.12.

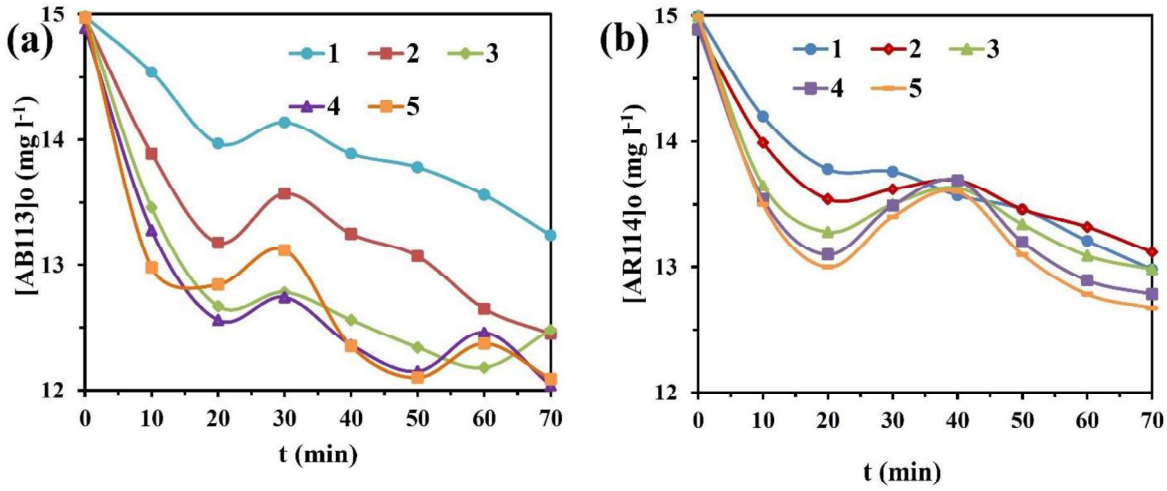

Figure 4.12 Equilibrium adsorption of (a) AB113 and (b) AR114 in binary dye mixture each 15 mg l^{-1} and TiO_2 dose (1) 50 mg l^{-1} (2) 100 mg l^{-1} (3) 150 mg l^{-1} (4) 200 mg l^{-1} and (5) 250 mg l^{-1}

The adsorption study shows a significant change till 20 min and then desorption starts. After 20 min, the patterns of adsorption and/or desorption were found depending on the amount of TiO_2. But, for all TiO_2 doses the first desorption started after 20 min. Initially, the concentration in solution goes down due to adsorption on the catalyst surface. It takes around 20 min. After that the desorption starts but complete desorption does not take place. Some dyes remain adsorbed. Therefore, the concentrations in the solution do not come back to original values (15 mg l^{-1}). In fact, adsorption & desorption both are taking place (unsteady state) and finally some sort of equilibrium is reached (adsorption & desorption) when a part of initial dye remains adsorbed on the catalyst surface. As far as the temperature is concerned, no appreciable change in the temperature was observed. There may be only small variation in temperature mainly due to heat of adsorption and desorption. So, 20 min was found to be equilibrium adsorption time.

4.2.3 The ANNs Model Training

The ANN structure implemented was the feed-forward back propagation type, containing three layers (input, hidden and output layers) (Figure 4.13).

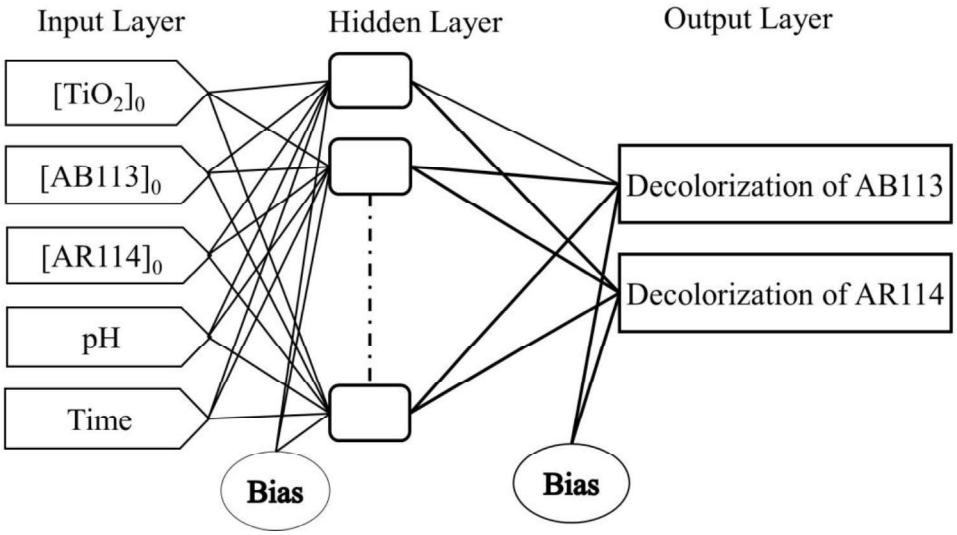

Figure 4.13 Schematic view of the developed ANN

Five input variables to the neural network were selected: (1) $[TiO_2]_o$, (2) $[AB113]_o$, (3) $[AR114]_o$, (4) $[pH]_o$ and (5) Time. The input and output layer variables with their ranges have been shown in Table **4.12**. In the current study, decolorization of AB113 and AR114 are the output variables. Hence, there are two neurons in the output layer of the ANN network. Out of the numerous data points produced, 160 experimental data sets were exploited to develop the ANN model. The experimental samples were separated into training, validation and test subsections that each of them having 112, 24 and 24 samples, respectively. The test and validation sets were arbitrarily selected from the experimental samples for the assessment of the validation and modeling.

Table 4.12 The ranges of input and output model parameters

Variable	Range
Input layer	
TiO_2 dose (mg l^{-1})	50-300
$[AB113]_o$ (mg l^{-1})	5-25
$[AR114]_o$ (mg l^{-1})	5-25
pH	3-9
Time (min)	30-240
Output layer	
Decolorization of AB113	0 - 1
Decolorization of AR114	0 - 1

The optimization of ANN topology is very significant stage for the development of ANN model. A sequence of topologies was used to improve the number of neurons in hidden layer, in which number of neurons was varied from 4 to 14 (Figure 4.14). Each topology was reiterated three times to evade random connections. Root mean square error (RMSE) has been taken as error variable. The RMSE is a frequently used term for the differences between experimental and predicted model values. It is clear from Figure 4.14 that the optimized neurons for the photocatalytic decolorization of the mixture of AB113 and AR114 dyes are ten.

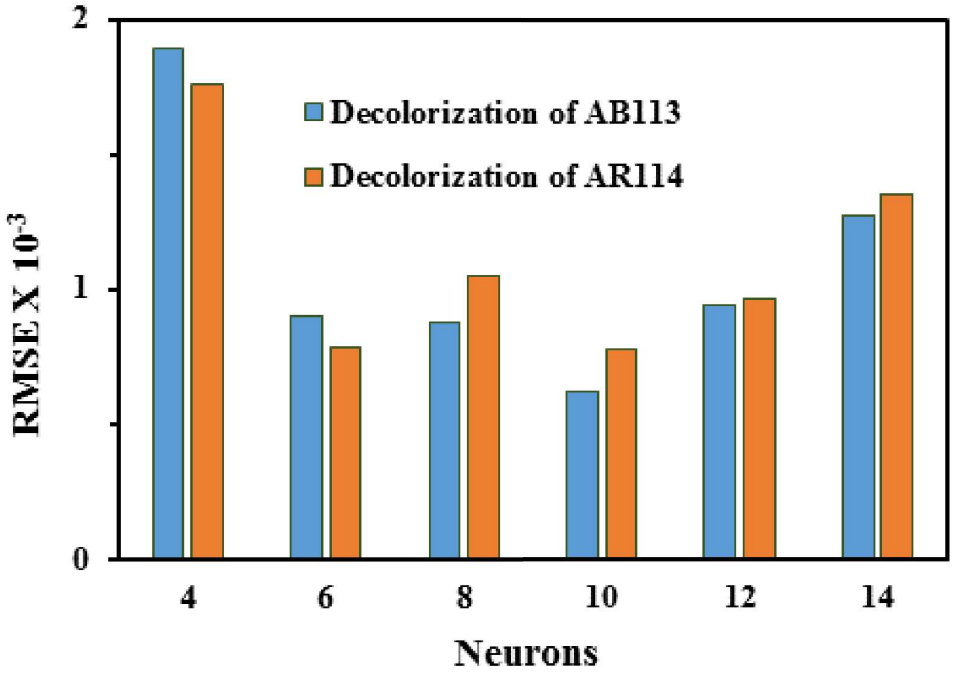

Figure 4.14 Effect of the number of neurons in hidden layer

The validation (comparison) for the output variable (decolorization of AB113 and AR114) has been predicted by ANNs and experimental runs. The predicted and experimental values of decolorization of AB113 and AR114 show good correlation coefficients, i.e., 0.9907 for decolorization of AB113 and 0.9932 for decolorization of AR114 (Figure 4.15). It shows a good consistency of the model and define that the neural network model imitates both the output responses decolorization of AB113 and AR114.

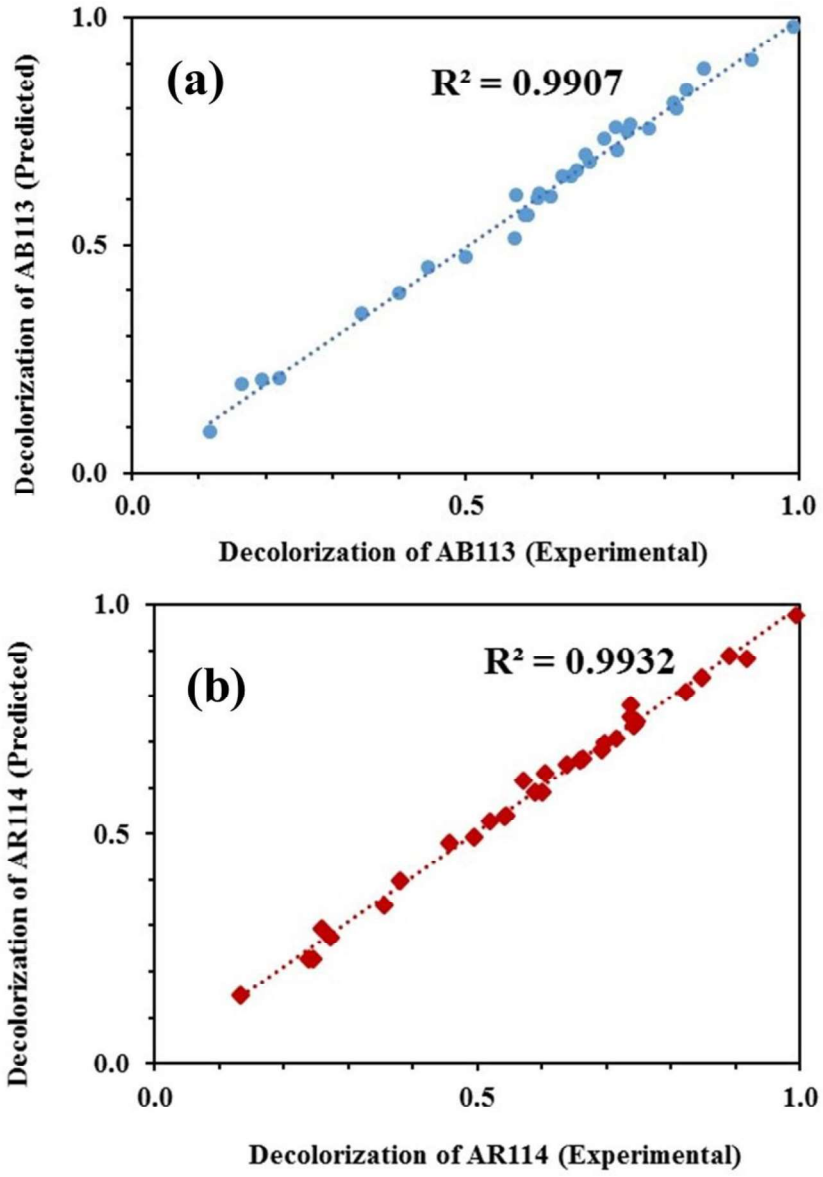

Figure 4.15 Comparison of the experimental results with those predicted via neural network modeling for the test set for the decolorization of (a) AB113 and (b) AR114

4.2.4 Statistical Analysis with CCD

The responses (decolorization of AB113 and AR114) for photocatalytic decolorization of AB113 and AR114 were measured by performing the ANN model simulation by considering input variables TiO_2 dose, initial concentration of AB113, initial concentration of AR114, pH of the binary dye solution and time. The ranges and levels of input variables were coded at five levels between -2 to +2 as shown in Table 4.12.

.

Table 4.13 Simulated design levels of chosen variables

Variables	Range and levels in CCD				
	-2	**-1**	**0**	**+1**	**+2**
TiO_2 Amount (mg l^{-1})	50	100	150	200	250
$[AB113]_o$ (mg l^{-1})	5	10	15	20	25
$[AR114]_o$ (mg l^{-1})	5	10	15	20	25
pH	3	5	7	9	11
Time (min)	0	60	120	180	240

A power law transformation with power two was applied to the simulated data for the decolorization of AB113 and AR114. A manual regression process was used to fit the second order polynomial eq. (3.5) to the simulated data and to recognize the pertinent model terms. The fit quality of quadratic model was evaluated by the coefficient of determination, R^2 and adjusted R^2. To come to a verdict about the competency of the model for the output responses of decolorization of AB113 and AR114, two diverse tests such as the model summary statistics and sequential model sum of squares were done [232]. The sequential model sum of squares showed the quadratic model to be best fitted for both responses (decolorization of AB113 and AR114). The cubic model is found to be aliased and is not suitable for further investigation. For an aliased model, the number of experimental or simulation runs are not enough for independent estimation of all the terms for that model. If the number of independent points in the design is less than the number of terms in the model, then some of the parameters cannot be estimated independently [226].

The regression coefficient (R^2) was found to be 0.9732 and 0.9741 for decolorization of AB113 and AR114 respectively. These values indicate a great relationship between the experiential and predicted values. Model F values predicted by ANOVA were 52.63 and 54.50 for decolorization of AB113 and AR114 respectively (Table 4.14). It indicates that the models are significant. The lack of fit of F-test designates the difference of the data in the region of the fitted model. If the model does not sufficiently fit the data, the lack of fit will be significant [233, 234]. In this study, the lack of fit is insignificant, indicating significant model correlation between the variables and responses.

$[TiO_2]_o$, $[AB113]_o$, $[AR114]_o$, $[pH]_o$, t, $([AB113]_o)^2$, $([pH]_o)^2$, $[TiO_2]_o*[AB113]_o$, $[TiO_2]_o*[pH]_o$, $[TiO_2]_o*t$, $[pH]_o*t$ were found highly significant parameters for decolorization of AB113 and AR114. $[TiO_2]_o*[AR114]_o$ is found highly significant parameter for the decolorization of AR114. Figure 4.16a and c illustrate that the response decolorization of AB113 and AR114 first increases with increasing TiO_2 dose, up to a value of 200 mg l^{-1}, after that no change has been observed in the decolorization of AB113 and AR114. In fact, by increasing the TiO_2 content, the number of active sites increases. On increase in TiO_2 concentration beyond a certain value, photocatalytic decolorization decreases due to enhancement of light reflectance of the catalyst particles and the decrease in light penetration. Agglomeration and sedimentation of TiO_2 can be additional causes for the observed decrease in photocatalytic efficiency at high catalyst concentration [235].

Figure 4.16b and d illustrate that the response decolorization of AB113 and AR114 increases with decreasing the pH. The catalyst behavior can be elucidated by TiO_2 surface charge density. The point of zero charge of the TiO_2 (Degussa P25) is at pH 6.8. In acidic media ($pH \leq 6.8$) the TiO_2 surface is positively charged, whereas under alkaline media ($pH \geq 6.8$) it is negatively charged [236]. Excess positive charge at the TiO_2 surface promotes a strong interaction with SO_3^{2-} groups of the dye. A negative excess charge promotes the repulsion of the dye by the titania surface, diminishing the catalytic activity of TiO_2 semiconductor. These results suggest that the influence of the initial pH of the solution on photocatalytic kinetics is due to the amount of the dye adsorbed on TiO_2 [237, 238].

Table 4.14 ANOVA model for decolorization of AB113 and AR114

	Decolorization of AB113					Decolorization of AR114				
Source	**Sum of Squares**	**DF**	**Mean Square**	**F Value**	**Prob> F**	**Sum of Squares**	**DF**	**Mean Square**	**F Value**	**Prob> F**
Model	2.70	20	0.13	52.63	< 0.0001	2.36	20	0.11	54.50	< 0.0001
$[TiO_2]_o$	0.34	1	0.34	134.58	< 0.0001	0.31	1	0.31	146.16	< 0.0001
$[AB113]_o$	0.32	1	0.32	125.67	< 0.0001	0.16	1	0.16	73.86	< 0.0001
$[AR114]_o$	0.05	1	0.05	22.03	< 0.0001	0.05	1	0.05	23.83	< 0.0001
$[pH]_o$	1.21	1	1.21	474.50	< 0.0001	1.15	1	1.15	533.57	< 0.0001
t	0.50	1	0.50	197.88	< 0.0001	0.43	1	0.43	200.48	< 0.0001
$([TiO_2]_o)^2$	0.00	1	0.00	1.22	0.2783	0.00	1	0.00	0.9769	0.3311
$([AB113]_o)^2$	0.01	1	0.01	5.61	0.0246	0.01	1	0.01	5.83	0.0222
$([AR114]_o)^2$	0.00	1	0.00	0.35	0.5543	0.00	1	0.00	0.43	0.5171
$([pH]_o)^2$	0.06	1	0.06	24.70	< 0.0001	0.06	1	0.06	30.06	< 0.0001
t^2	0.00	1	0.00	0.66	0.4206	0.00	1	0.00	0.54	0.4657
$[TiO_2]_o$* $[AB113]_o$	0.02	1	0.02	10.12	0.0035	0.02	1	0.02	13.42	0.0010
$[TiO_2]_o$* $[AR114]_o$	0.00	1	0.00	3.13	0.0870	0.01	1	0.01	5.05	0.0324
$[TiO_2]_O$*$[pH]_o$	0.05	1	0.05	19.78	0.0001	0.05	1	0.05	24.35	< 0.0001
$[TiO_2]_o$*t	0.04	1	0.04	16.34	0.0004	0.03	1	0.03	15.07	0.0005
$[AB113]_o$* $[AR114]_o$	0.00	1	0.00	0.18	0.6711	0.00	1	0.00	0.78	0.3817
$[AB113]_o$*$[pH]_o$	0.00	1	0.00	0.49	0.4880	0.00	1	0.00	0.03	0.8490
$[AB113]_o$*t	0.00	1	0.00	0.25	0.6186	0.00	1	0.00	0.07	0.7841
$[AR114]_o$*$[pH]_o$	0.00	1	0.00	2.39	0.1329	0.00	1	0.00	3.24	0.0819
$[AR114]_o$*t	0.00	1	0.00	0.31	0.5804	0.00	1	0.00	0.07	0.7826
$[pH]_o$ *t	0.03	1	0.03	12.49	0.0014	0.02	1	0.02	12.20	0.0015
Residual	0.07	29	0.00			0.06	29	0.00		
Lack of Fit	0.07	22	0.00			0.06	22	0.00		
Pure Error	0	7	0			0	7	0		
Cor Total	2.77	49				2.42	49			

The optimization of photocatalytic decolorization process variables has been exercised by point estimation option in the software. The optimized process parameters were found to be TiO_2 dose 200 mg l^{-1}, pH 5 and time 180 min for a dye concentration of 20 mg l^{-1}. The competence of the developed models was confirmed by carrying out the confirmatory experimental and simulation run at optimized conditions.

Table 4.15 shows the comparison between decolorization of AB113 and AR114 found by ANN model, CCD and photocatalytic experimental run at optimum parameters. It is clear form Table 4.15 that the optimization of photocatalytic process parameters for the decolorization of AB113 and AR114 dye mixture are acceptable by means of these methods.

This method also reduces the number of simulation runs appreciably in contrast to other approaches reported in literature.

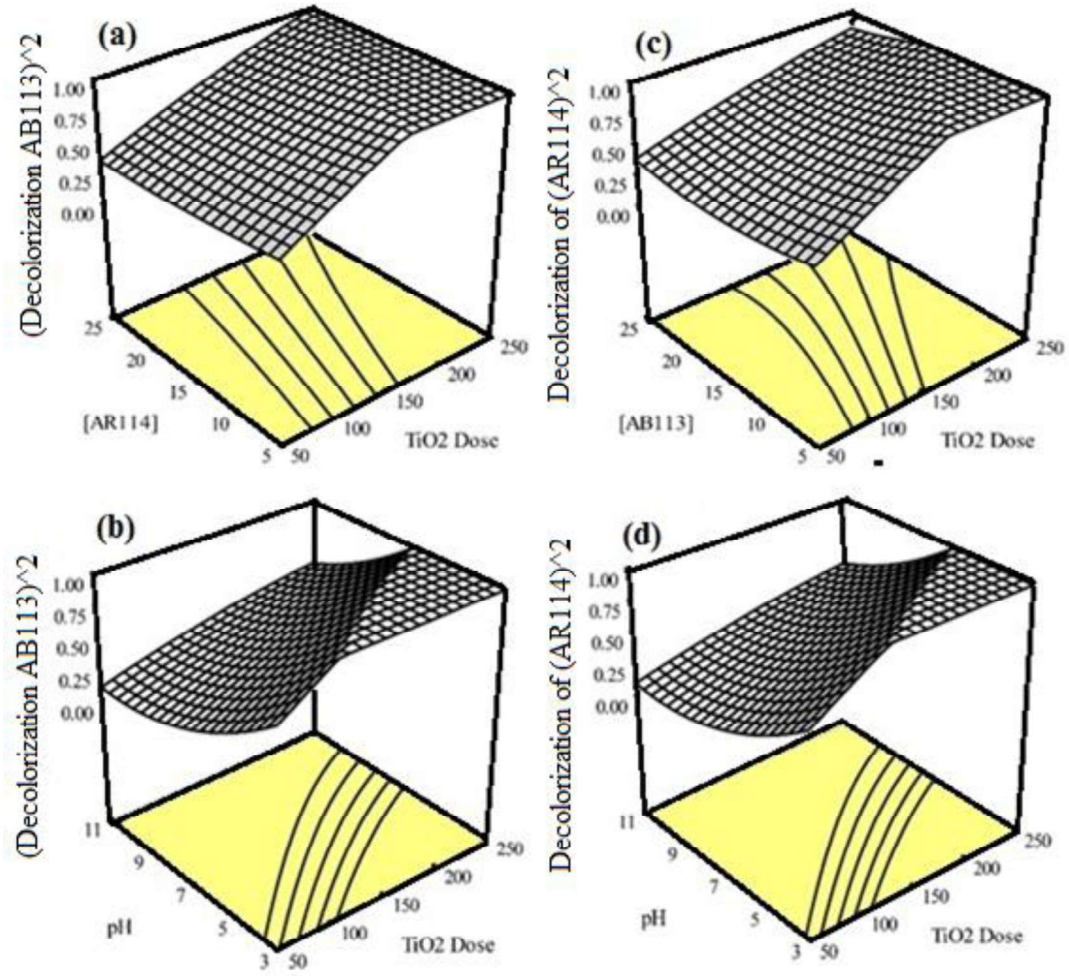

Figure 4.16 3D response surface plots (a) [AR114] Vs TiO_2 dose, and (b) pH Vs TiO_2 dose, for decolorization of AB113 and (c) [AB113] Vs TiO_2 dose, and (d) pH Vs TiO_2 dose, for decolorization of AR114

Table 4.15 Comparison of decolorization efficiency of AB113 and AR114 between results obtained by CCD, ANN model and experimental run at optimum process parameters

	Decolorization Efficiency of AR114	**Decolorization Efficiency of AB113**
Response from CCD	1	1
Response from ANN	0.982	0.984
Response from Experiments	0.984	0.99

4.2.5 Kinetic Study

The decolorization of AB113 and AR114 in a dye mixture can be described by a power law kinetic model. The first order reaction kinetics in relations of decolorization of AB113 and AR114 can be described by eq. (4.1).

A graph of ln C_o/C versus t for photocatalytic decolorization of AB13 and AR114 is presented in Figure 4.17. A linear correlation between ln C_o/C and time was detected. The reaction rate constants were 0.0164 min^{-1} and 0.0228 min^{-1} with the value of R^2 0.9694 and 0.9912 for the decolorization of AB113 and AR114, respectively.

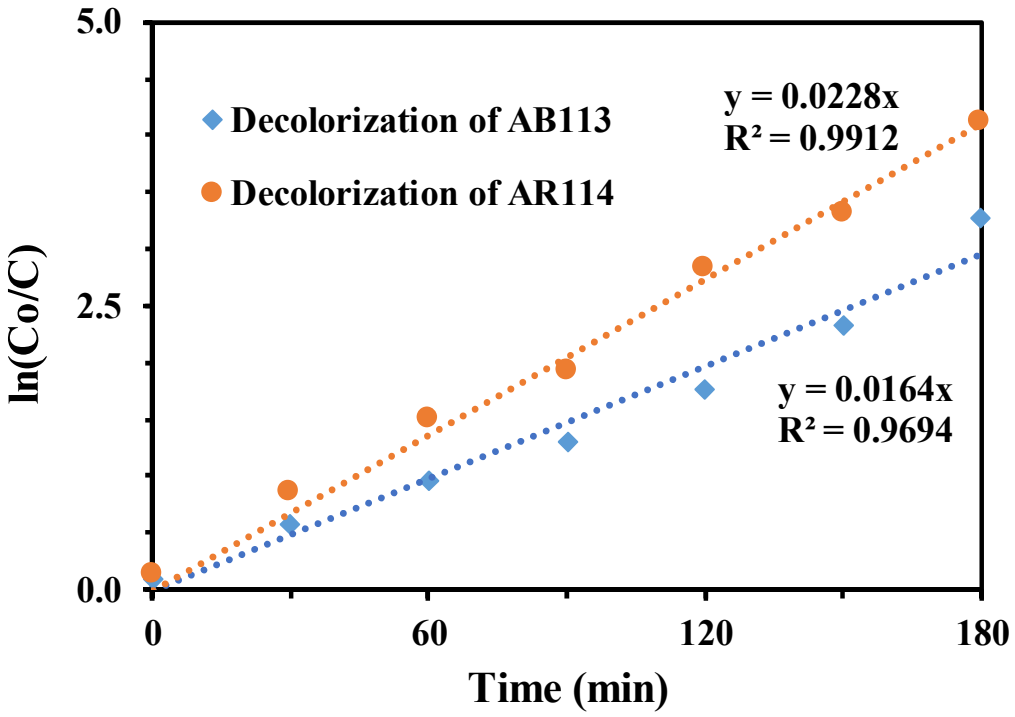

Figure 4.17 Decolorization kinetics of AB113 and AR114 in binary dye mixture

4.2.6 TOC Study versus Photocatalytic Decolorization

In order to delineate the total decolorization throughout the photocatalysis, the TOC removal and decolorization of AB113 and AR114 were determined at optimized conditions and plotted on same graph as shown in Figure 4.18. The mixture of AB113 and AR114 dyes at optimized parameters showed high extent of decolorization and almost entirely decolorized after 180 min. TOC removal was found to be lower than the decolorization of both the dyes.

This will be due to the formation of intermediate compounds which have been mineralized afterwards.

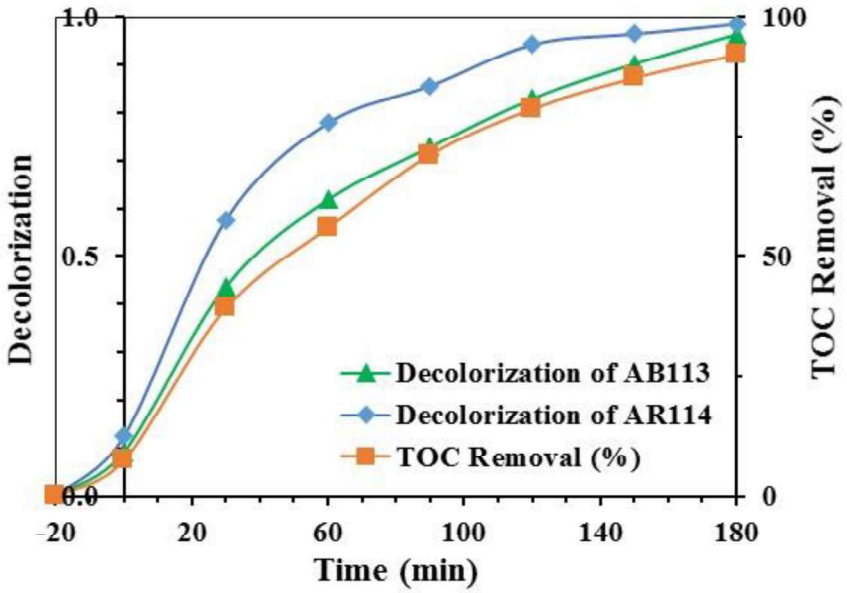

Figure 4.18 Decolorization and TOC removal versus time at optimized conditions for binary mixture of AB113 and AR114 dyes

4.2.7 Determination of Intermediate Products for Photocatalytic Decolorization of Binary Dye Mixture

The intermediate products formed during the photocatalytic decolorization of binary dye mixture was recognized from the GC-MS analysis as shown in Table 4.16. Based on the intermediates found during GC-MS analysis, the possible reaction pathway was identified and shown in Figure 4.19. It was noticed that other chromatographic peaks were also established but could not be positively recognized than the successfully detected compounds, (i.e. the match factor of the spectrum was not significant). It is clear that as the aromatic rings of AB113 and AR114 reduce, extensive variety of cleavage compounds are expected. Inappropriately, these intermediate compounds were not detected because of the restrictions linked with the analytical method employed or these intermediate compounds were not significantly collected in the medium.

The poly-aromatic dyes first experienced azo reduction, to yield aromatic compounds and aniline derivative. The formation of intermediate products such as long chain alkanes, pthalic acid and dibutyl pthalate showed a decolorizationgradation method for the non-nitrogen

compounds in the dye. Further, these intermediate compounds have been treated and converted to long chain hydrocarbons like hexadecane, tetradecane, octadecane etc. These long chain hydrocarbons are then converted to water and carbon dioxide. From the reaction pathway, it is clear that the both poly-aromatic dyes degraded into nontoxic end compounds.

Table 4.16 Intermediate compounds recognized from GC-MS analysis during the photocatalytic decolorization of binary dye mixture of AB113 and AR114

Retention time (min) (180 min sample)	**m/Z**	**Prominent intermediate compound formed**
9.76	226	Hexadecane
11.46	198	Tetradecane
16.27	254	Octadecane
19.86	166	Pthalic acid
21.47	278	Dibutyl Pthalate
22.76	93	Benzenamine
24.11	156	Undecane
23.278	268	Nonadecane
24.92	142	Decane

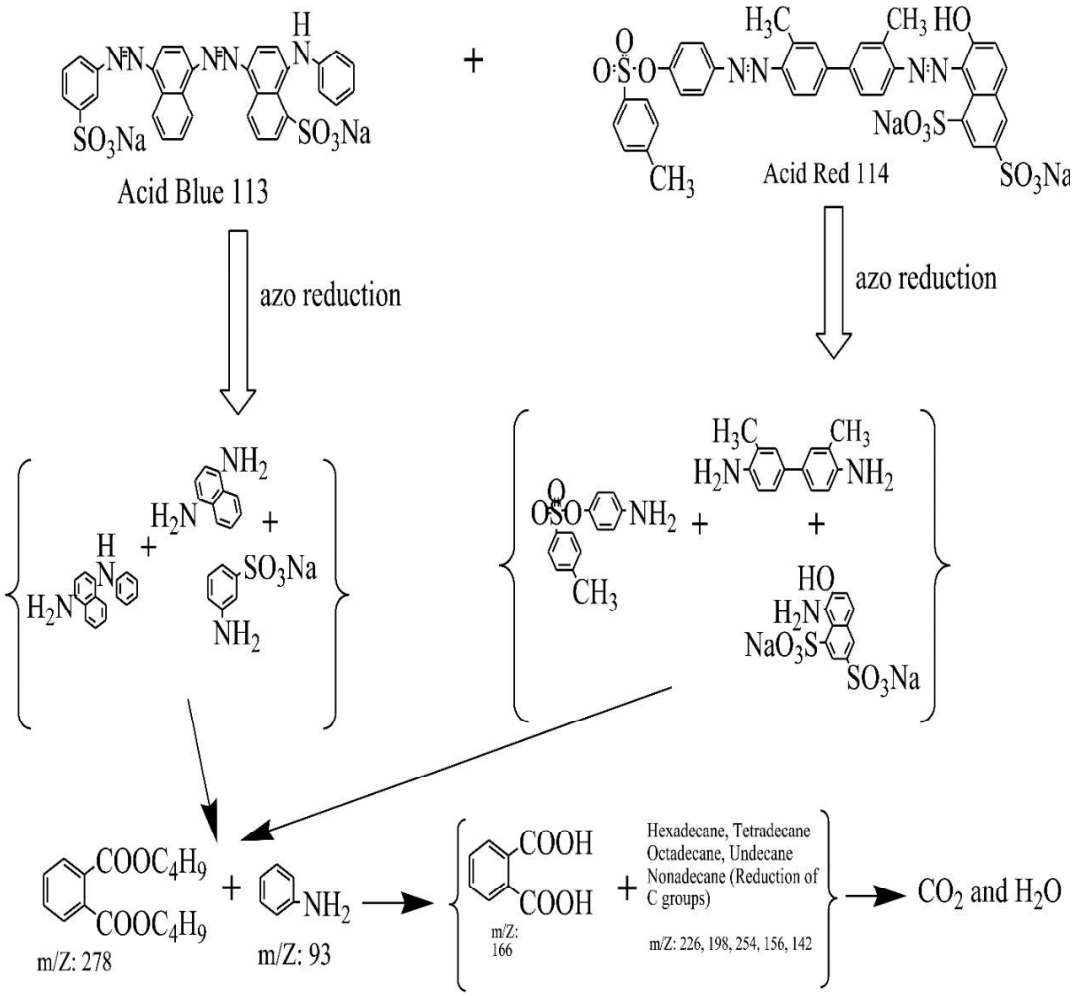

Figure 4.19 Possible reaction pathways of AB113 and AR11

4.3 Photocatalytic Study of Dyes on Metal ions Doped and Codoped TiO_2

4.3.1 Characterization of Photocatalyst

4.3.1.1 XRD Analysis

Figure 4.20 shows the X-ray diffraction patterns of the undoped, doped and codoped TiO_2. Diffraction peaks (1 0 1), (0 0 4), (2 0 0), (1 0 5), (2 1 1) and (2 0 4) have been recognized for anatase crystal phase of TiO_2 photocatalyst [239]. The X-ray diffraction pattern of anatase have a major peak at 2Theta = 25.3685° equivalent to the 101 peak. Hamadanian et al. [40] also observed the anatase crystal phase of TiO_2 corresponding to a main peak at 2Theta = 25.2° equivalent to the 101 peak.

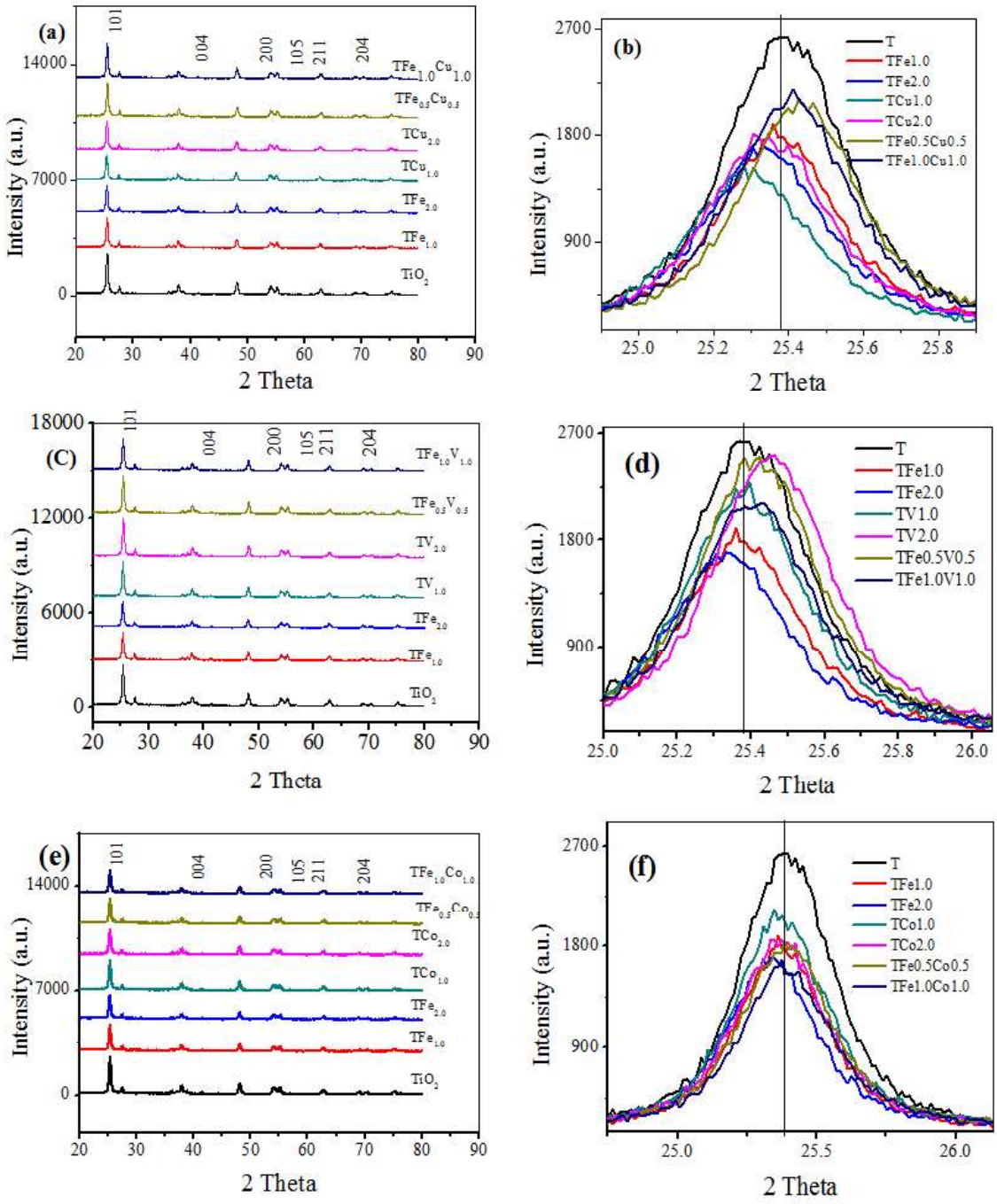

Figure 4.20 XRD pattern of (a), (c) and (e) undoped, doped and codoped TiO_2 nanoparticles; (b), (d) and (f) the shift in anatase peak (1 0 1)

Baiju et al. [240] reported the peak at 2Theta = 27.4° corresponding to (1 1 0) for rutile crystal structure and Srivatsa et al. [241] reported the peak at 2Theta = 30.8° corresponding to (1 2 1) for brookite crystal structures. These two peaks have not been identified in our XRD

patterns, indicating that brookite and rutile crystal structures are not present. In the section of 20-80°, the nature of diffraction peaks of the pure TiO_2 crystal planes is reasonably related to that of Fe and Cu doped and codoped TiO_2. The XRD patterns did not show any Fe and Cu phases so it is established that iron and copper ions are equally dispersed between the anatase crystals. Figure 4.20b, d and f show the XRD peaks of anatase crystalline plane (1 0 1) in the doped and codoped samples demonstrating a small move to the higher diffraction angle as compared to bare TiO_2 with the increase in Fe and Cu ions doping percentage. The computed values for all the doped and codoped TiO_2 samples have been shown in Table 4.17. This verdict specifies the existence of lattice alteration in the anatase arrangement by the amalgamation of the dopants with the reduced ionic radii in TiO_2 matrix.

Table 4.17 Properties of the doped and codoped TiO_2 samples

Catalyst sample	**2 θ (degree) (peak 101)**	**d-spacing (Å)**	**Crystallite size (nm)**	**Anatase lattice parameters (Å)**	
				a = b	**c**
T	25.3685	3.50808	22.80	3.7767	9.4109
$TFe_{1.0}$	25.3766	3.50955	22.16	3.7824	9.4699
$TFe_{2.0}$	25.3413	3.51454	22.45	3.7814	9.5232
$TCu_{1.0}$	25.2934	3.51381	21.06	3.7891	9.5162
$TCu_{2.0}$	25.3481	3.52063	21.89	3.7815	9.5274
$TFe_{0.5}Cu_{0.5}$	25.4367	3.50150	22.49	3.7677	9.4831
$TFe_{1.0}Cu_{1.0}$	25.4132	3.50982	22.92	3.7812	9.5333
$TV_{1.0}$	25.3821	3.49915	22.30	3.7763	9.4929
$TV_{2.0}$	25.4552	3.50886	21.88	3.7595	9.5694
$TFe_{0.5}V_{0.5}$	25.4199	3.50389	24.45	3.7777	9.4731
$TFe_{1.0}V_{1.0}$	25.4041	3.50584	22.76	3.7693	9.4949
$TCo_{1.0}$	25.3703	3.51076	22.56	3.7823	9.4359
$TCo_{2.0}$	25.3681	4.43563	23.56	3.7595	9.5680
$TFe_{0.5}Co_{0.5}$	25.3878	4.23310	23.13	3.7812	9.3954
$TFe_{1.0}Co_{1.0}$	25.3867	4.37565	22.27	3.78	9.40

The alteration in the "c" (lattice parameter) factor is reduced in metal ion codoped TiO_2 powder samples as compared to metal ion doped powder samples, possibly due to the dissimilar collaboration of dopant ions (Fe, Cu, V and Co) with the titanium ions in the codoped TiO_2 powders. The similar findings have been observed for all the doped and codoped TiO_2 samples. The average size of nanoparticles was estimated from the Scherrer equation on the anatase diffraction peak (1 0 1) [242]:

$$D = \frac{\lambda}{\beta \cos\theta} \tag{4.4}$$

where D is the crystallite size of the catalyst, λ the x-ray wavelength (1.54060 Å), β the full width at half maximum (FWHM) of the diffraction peak and θ is the diffraction angle. The average crystallite size of doped and codoped TiO_2 samples was found in the range of 21.1-24.5 nm (Table 4.17). Table 4.17 presents the lattice parameters of undoped, doped and codoped TiO_2 photocatalysts and have been computed based on anatase crystal planes of (1 0 1) from XRD peaks. A common style of the stretching the "c-axis" is perceived with enhancing the percentage of metal ion dopant concentration in all samples [43].

4.3.1.2 Fourier Transform Infrared (FTIR) Spectroscopy

The FTIR patterns of the doped and codoped TiO_2 samples are shown in Figure 4.21. The FTIR patterns have been plotted in finger print region (Figure 4.22) of 1300-400 cm^{-1} so that the reflectiveness of the bands will be expanded. The bands around 3330-3460 and 1610-1645 cm^{-1} have been found in all the doped/codoped powder samples, representing stretching vibrations of hydroxyl clusters and the bending vibrations of water molecules respectively. Lv et al. [243] also observed the same phenomena for p-doped TiO_2 nanoparticles. The band around 520-670 cm^{-1} in all samples are recognized to Ti-O-Ti stretching vibration, which moves towards the upper wavelength by accumulation of transition metal. The FTIR patterns of the doped and codoped samples have not shown any band equivalent to the doped or codoped metal oxide due to the low weight percent of metal ions in doping and codoping.

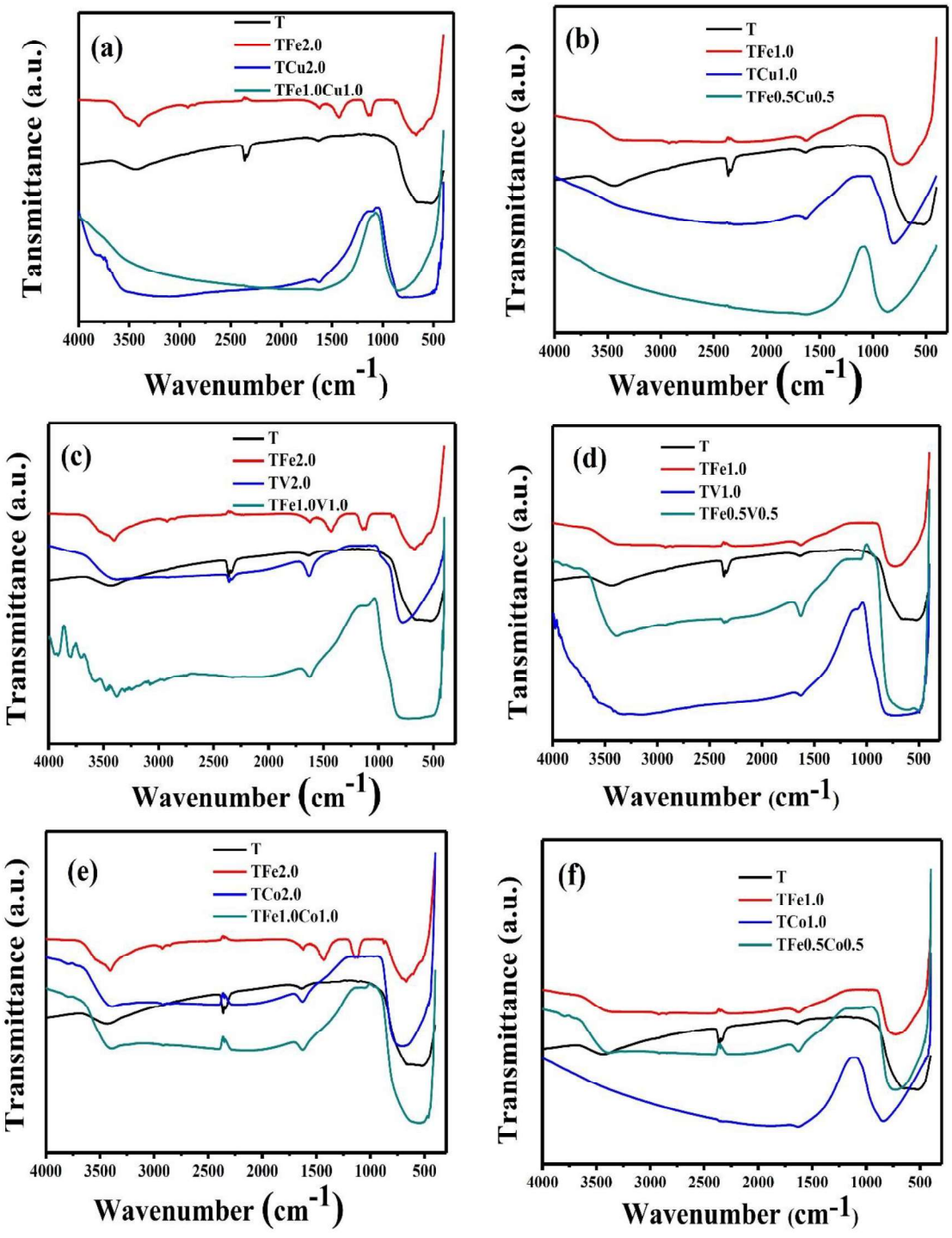

Figure 4.21 FTIR spectra of TiO_2, $TFe_{2.0}$, $TCu_{2.0}$, $TFe_{1.0}Cu_{1.0}$, $TV_{2.0}$, $TFe_{1.0}Cu_{1.0}$, $TCo_{2.0}$ and $TFe_{1.0}Co_{1.0}$

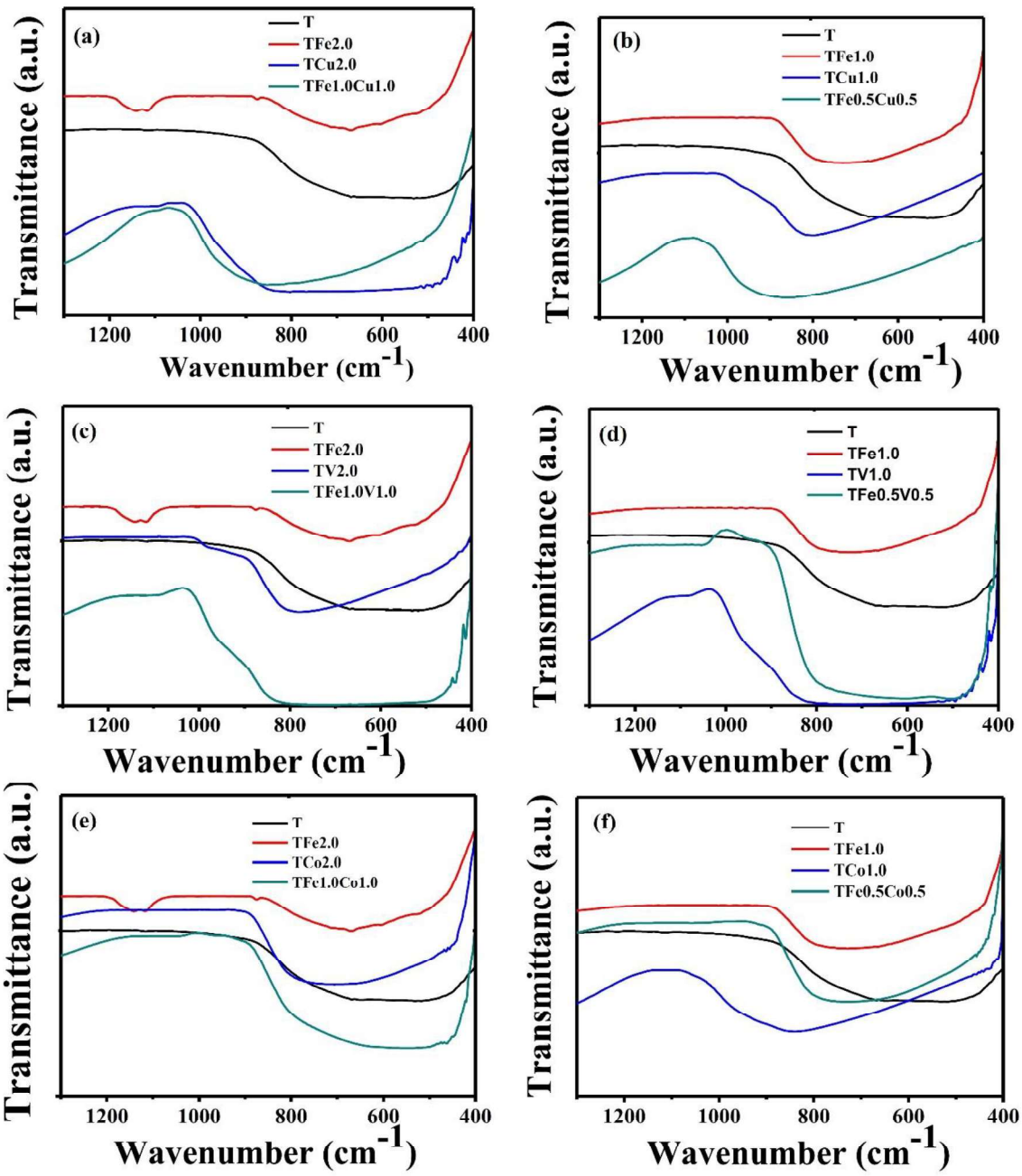

Figure 4.22 FTIR spectra of TiO_2, $TFe_{1.0}$, $TCu_{1.0}$, $TFe_{0.5}Cu_{0.5}$, $TV_{1.0}$, $TFe_{0.5}Cu_{0.5}$, $TCo_{1.0}$ and $TFe_{0.5}Co_{0.5}$

4.3.1.3 UV-Visible Diffuse Reflectance Spectroscopy (DRS)

From DRS patterns, it was found that the doped and codoped samples show outstanding absorbance in the visible range of 400-521 nm (Table 4.18). This represents their robust absorbance of visible light capability as related to bare TiO_2. Kubelka Munk function has been used to calculate the energy band gap of the samples by eq. (4.5) [244].

$$f(R) = \frac{(1-R)^2}{2R} \tag{4.5}$$

Where R is the diffuse reflectance. In the present study, $(f(R).h\nu)^{1/2}$ versus energy bad gap ($h\nu$) has been plotted and shown in Figure 4.23.

The Kubelka–Munk plots of all the samples undoped (T), doped (T, $TFe_{1.0}$, $TFe_{2.0}$, $TCu_{1.0}$, $TCu_{2.0}$, $TV_{1.0}$, $TV_{2.0}$, $TCo_{1.0}$, $TCo_{2.0}$) and codoped ($TFe_{0.5}Cu_{0.5}$, $TFe_{1.0}Cu_{1.0}$, $TFe_{0.5}V_{0.5}$, $TFe_{1.0}V_{1.0}$, $TFe_{0.5}Co_{0.5}$, $TFe_{1.0}Co_{1.0}$) TiO_2 powders have been shown in Figures 4.23 a, b and c. The energy band gap has been estimated by extrapolating the linear curve of the band until it crosses the energy band gap axis. The estimation of energy band gap by extrapolation of linear curve of three samples ($TFe_{1.0}Cu_{1.0}$, $TFe_{1.0}V_{1.0}$, and TFe1.0Co1.0) have been shown in Figure 4.23 6 d, e and f. The energy band gap and absorption wavelength have been shown in Table 4.18. From Table 4.8, it is clear that there is a decrease of the energy band gap by doping the metal ion in TiO_2. It was also observed that by increasing the weight percent of dopant, the energy band gap decreased substantially. It was observed that by decreasing the energy band gap, the wavelength of the sample is shifted towards visible region. Riaz et al., [42] also observed the shift in the absorption edge for Cu−Ni/TiO_2 photocatalysts.

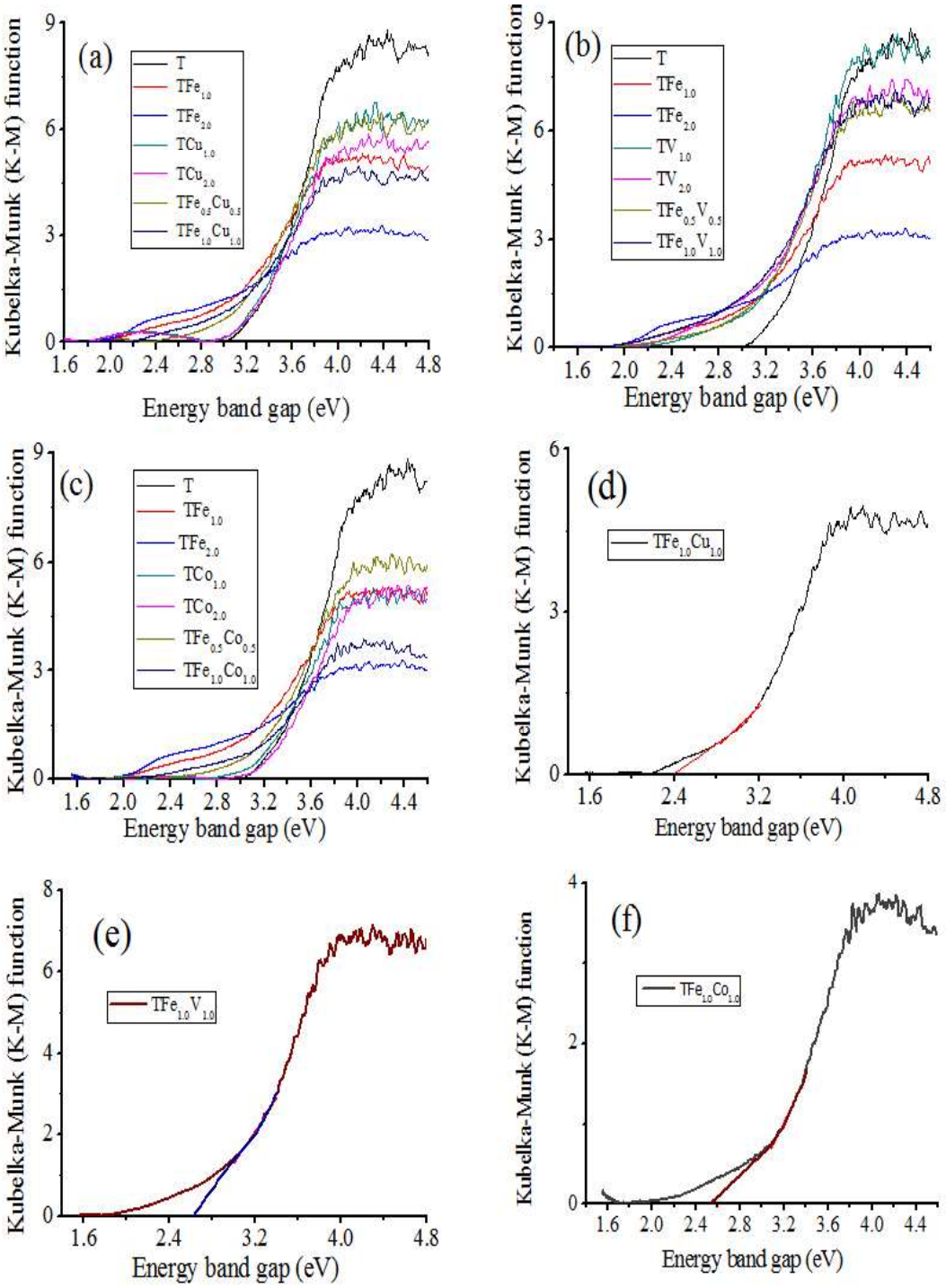

Figure 4.23 Kubelka-Munk (K-M) function plot (a) T, $TFe_{1.0}$, $TFe_{2.0}$, $TCu_{1.0}$, $TCu_{2.0}$, $TFe_{0.5}Cu_{0.5}$, $TFe_{1.0}Cu_{1.0}$, (b) T, $TFe_{1.0}$, $TFe_{2.0}$, $TV_{1.0}$, $TV_{2.0}$, $TFe_{0.5}V_{0.5}$, $TFe_{1.0}V_{1.0}$and (c) T, $TFe_{1.0}$, $TFe_{2.0}$, $TCo1_{.0}$, $TCo_{2.0}$, $TFe_{0.5}Co_{0.5}$, $TFe_{1.0}Co_{1.0}$ and estimation of energy band gap (d) $TFe_{1.0}Cu_{1.0}$ (e) $TFe_{1.0}V_{1.0}$ and (f) $TFe_{1.0}Co_{1.0}$

Table 4.18 Energy band gap and wavelength of the doped and codoped TiO_2 samples

Catalyst sample	Energy band gap (eV)	Wavelength (nm)
T	3.15	393
$TFe_{1.0}$	2.78	446
$TFe_{2.0}$	2.40	505
$TCu_{1.0}$	3.07	403
$TCu_{2.0}$	3.04	407
$TFe_{0.5}Cu_{0.5}$	2.93	422
$TFe_{1.0}Cu_{1.0}$	2.38	521
$TV_{1.0}$	2.80	454
$TV_{2.0}$	2.73	455
$TFe_{0.5}V_{0.5}$	2.91	425
$TFe_{1.0}V_{1.0}$	2.45	505
$TCo_{1.0}$	2.95	419
$TCo_{2.0}$	2.74	452
$TFe_{0.5}Co_{0.5}$	2.88	430
$TFe_{1.0}Co_{1.0}$	2.53	521

4.3.1.4 Field Emission Scanning Electron Microscopy (FESEM) Analysis

Figure 4.24 shows the FESEM micrographs of 2 weight % doping and codoping of the photocatalysts ($TFe_{2.0}$, $TCu_{2.0}$, $TFe_{1.0}Cu_{1.0}$, $TV_{2.0}$, $TFe_{1.0}V_{1.0}$, $TCo_{2.0}$ and $TFe_{1.0}Co_{1.0}$) at 250 X magnification as compared to undoped TiO_2. 1 weight % doped and codoped samples are shown in Figure 4.25. All micrographs showed asymmetrical shaped crystallite (18-24 nm) with agglomeration. It can be observed from Figure 4.24 and Figure 4.25 that the Fe, Cu, V and Co dopant metals are evenly dispersed onto the support. Riaz et al., [42] also reported similar behavior for Cu/TiO_2 prepared by using a coprecipitation method.

4.3.1.5 Transmission Electron Microscopy (TEM) Analysis

TEM images (Figure 4.26) of 2 weight % doped and codoped samples (TiO_2, $TFe_{2.0}$, $TCu_{2.0}$, $TFe_{1.0}Cu_{1.0}$, $TV_{2.0}$, $TFe_{1.0}Cu_{1.0}$, $TCo_{2.0}$ and $TFe_{1.0}Co_{1.0}$) from which the particle sizes were found to be around 11-19 nm. 1 weight % doped and codoped samples are shown in

Figure 4.27. The particle size found from XRD measurement is marginally higher as compared to the TEM measurement, which may be attributed to the enlargement of XRD peaks due to geometric reasons. It appears from Figure 4.26 and Figure 4.27 that the metal ions tend to form the complex with the surface oxygen of TiO_2 [40], which represses the growth of TiO_2 crystallite. These figures also reveal that the doping and codoping of Fe, Cu, V and Co do not leave any change in the shape of the nanoparticles.

4.3.1.6 Energy Dispersive X-ray Analysis (EDX)

The energy dispersive X-ray analysis gives both qualitative and quantitative information about elemental composition of the materials. Figure 4.28 and Figure 4.29 show the EDX pattern of the prepared systems. The EDX data show the surface composition of the modified systems. From the Figure 4.28 and Figure 4.29, it is clear that there is successive incorporation of metal ions with the TiO_2.

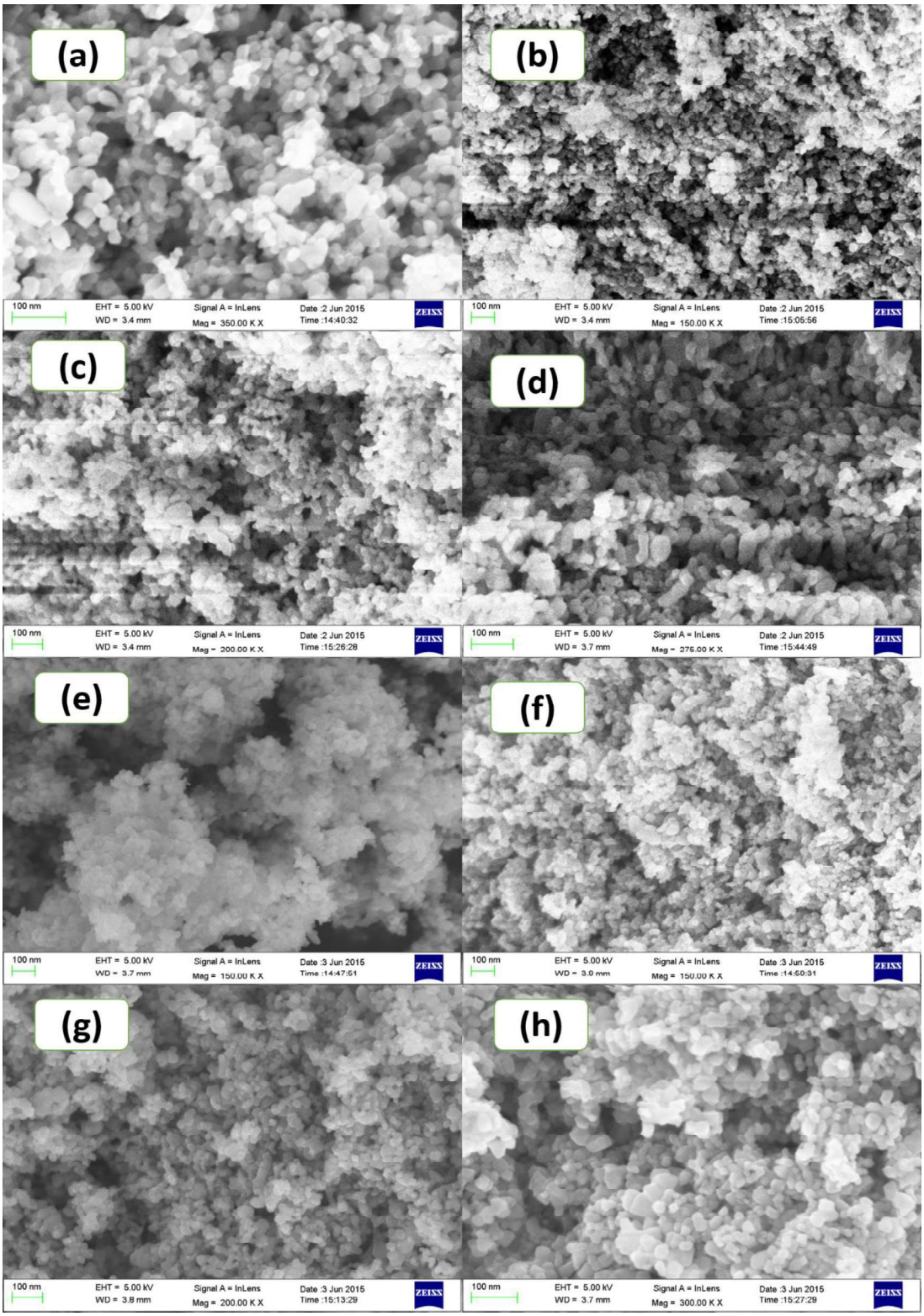

Figure 4.24 FESEM micrographs of (a) TiO_2, (b) $TFe_{2.0}$, (c) $TCu_{2.0}$, (d) $TFe_{1.0}Cu_{1.0}$, (e) $TV_{2.0}$, (f) $TFe_{1.0}Cu_{1.0}$, (g) $TCo_{2.0}$ and (h) $TFe_{1.0}Co_{1.0}$

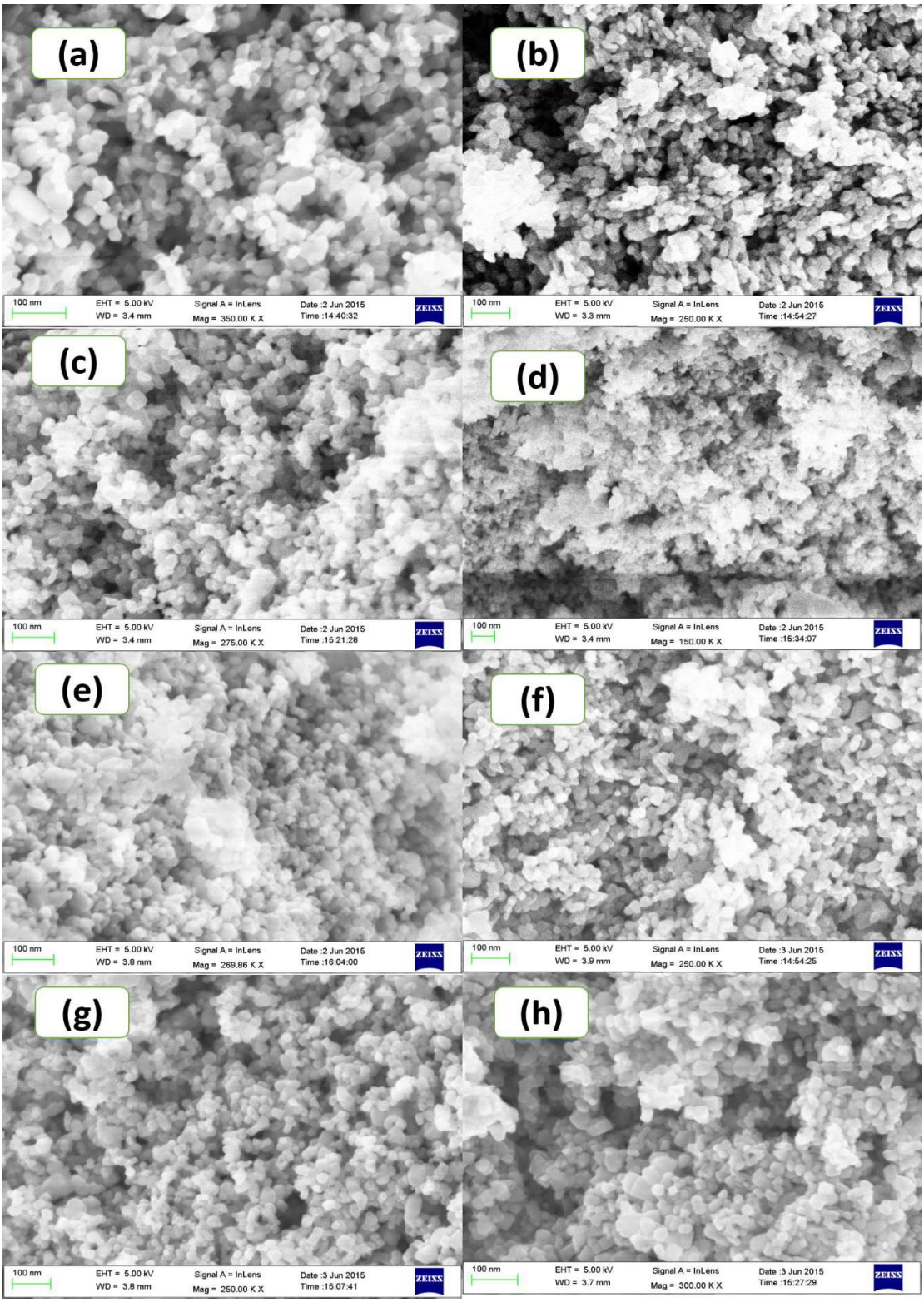

Figure 4.25 FESEM micrographs of (a) TiO_2, (b) $TFe_{1.0}$, (c) $TCu_{1.0}$, (d) $TFe_{0.5}Cu_{0.5}$, (e) $TV_{1.0}$, (f) $TFe_{0.5}Cu_{0.5}$, (g) $TCo_{1.0}$ and (h) $TFe_{0.5}Co_{0.5}$

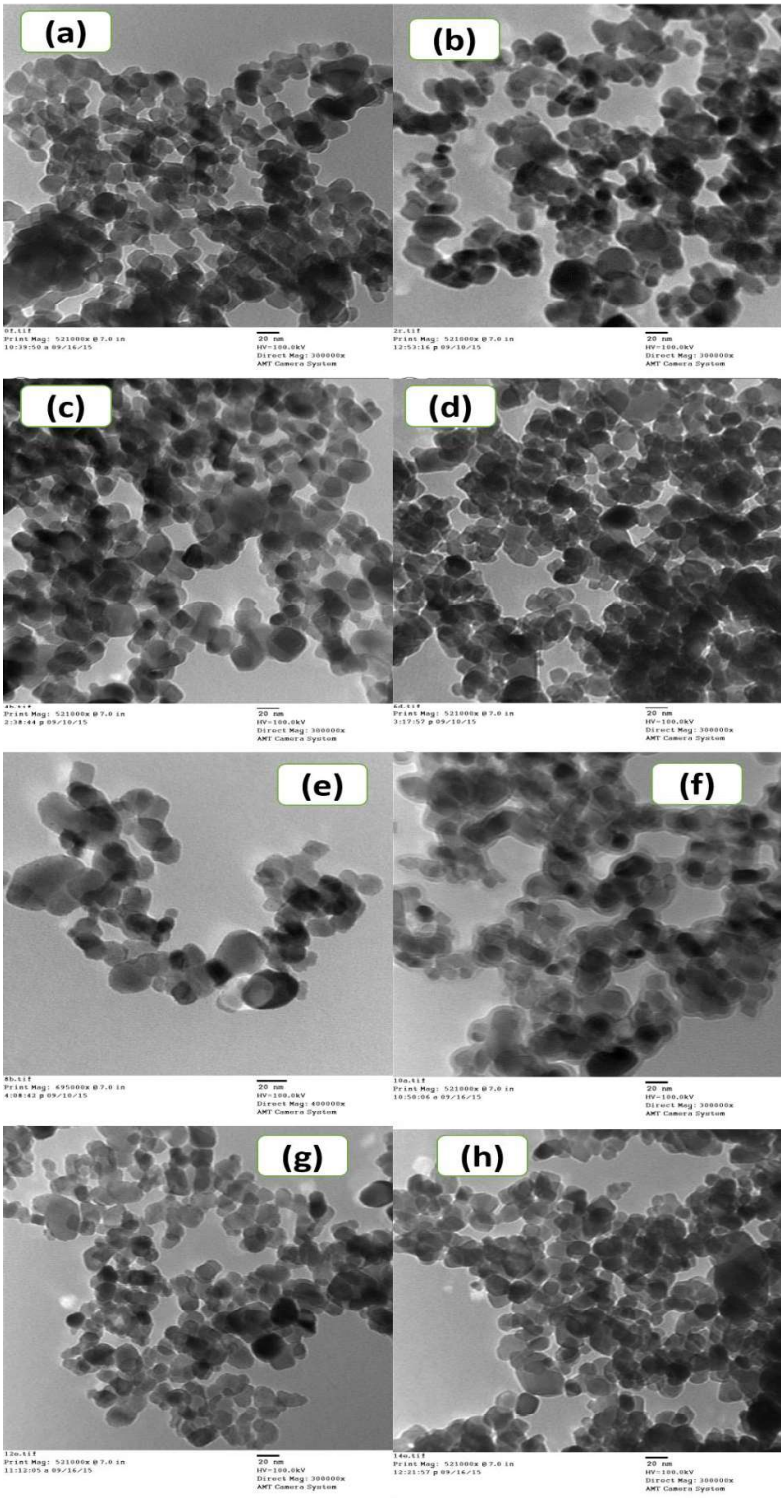

Figure 4.26 TEM micrographs of (a) TiO_2, (b) $TFe_{2.0}$, (c) $TCu_{2.0}$, (d) $TFe_{1.0}Cu_{1.0}$, (e) $TV_{2.0}$, (f) $TFe_{1.0}Cu_{1.0}$, (g) $TCo_{2.0}$ and (h) $TFe_{1.0}Co_{1.0}$

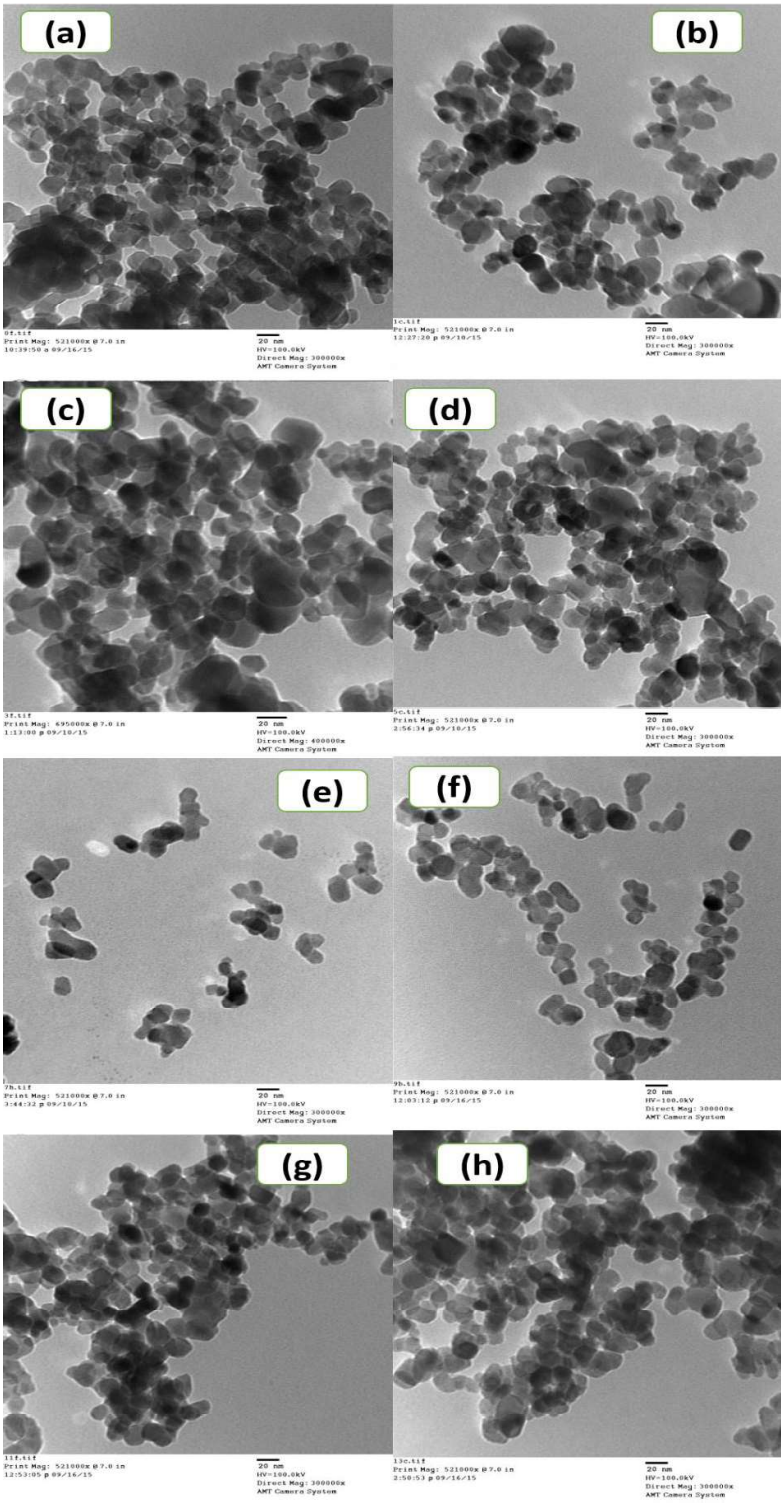

Figure 4.27 TEM micrographs of (a) TiO_2, (b) $TFe_{1.0}$, (c) $TCu_{1.0}$, (d) $TFe_{0.5}Cu_{0.5}$, (e) $TV_{1.0}$, (f) $TFe_{0.5}Cu_{0.5}$, (g) $TCo_{1.0}$ and (h) $TFe_{0.5}Co_{0.5}$

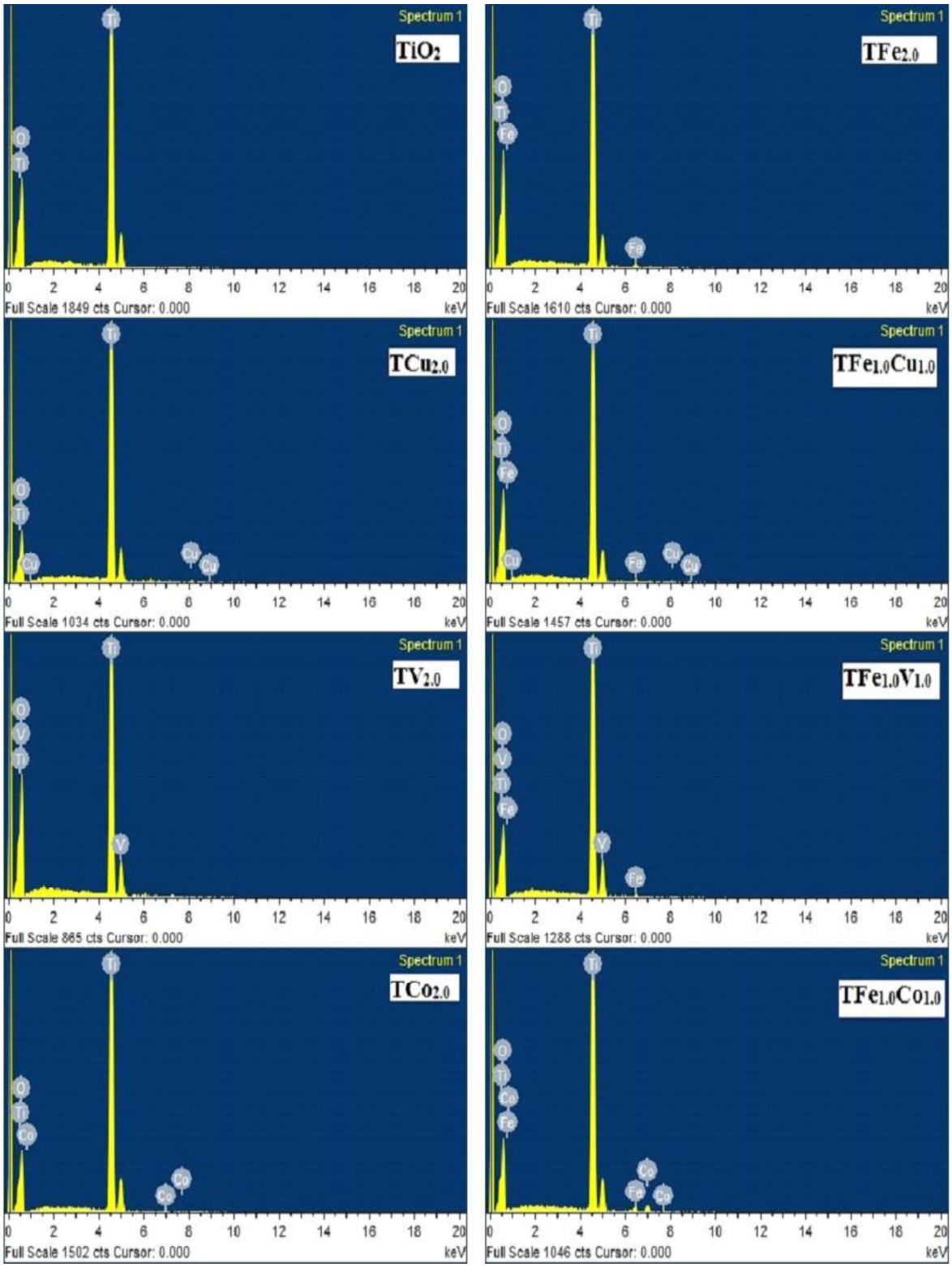

Figure 4.28 EDX mapping of TiO_2, $TFe_{2.0}$, $TCu_{2.0}$, $TFe_{1.0}Cu_{1.0}$, $TV_{2.0}$, $TFe_{1.0}Cu_{1.0}$, $TCo_{2.0}$ and $TFe_{1.0}Co_{1.0}$

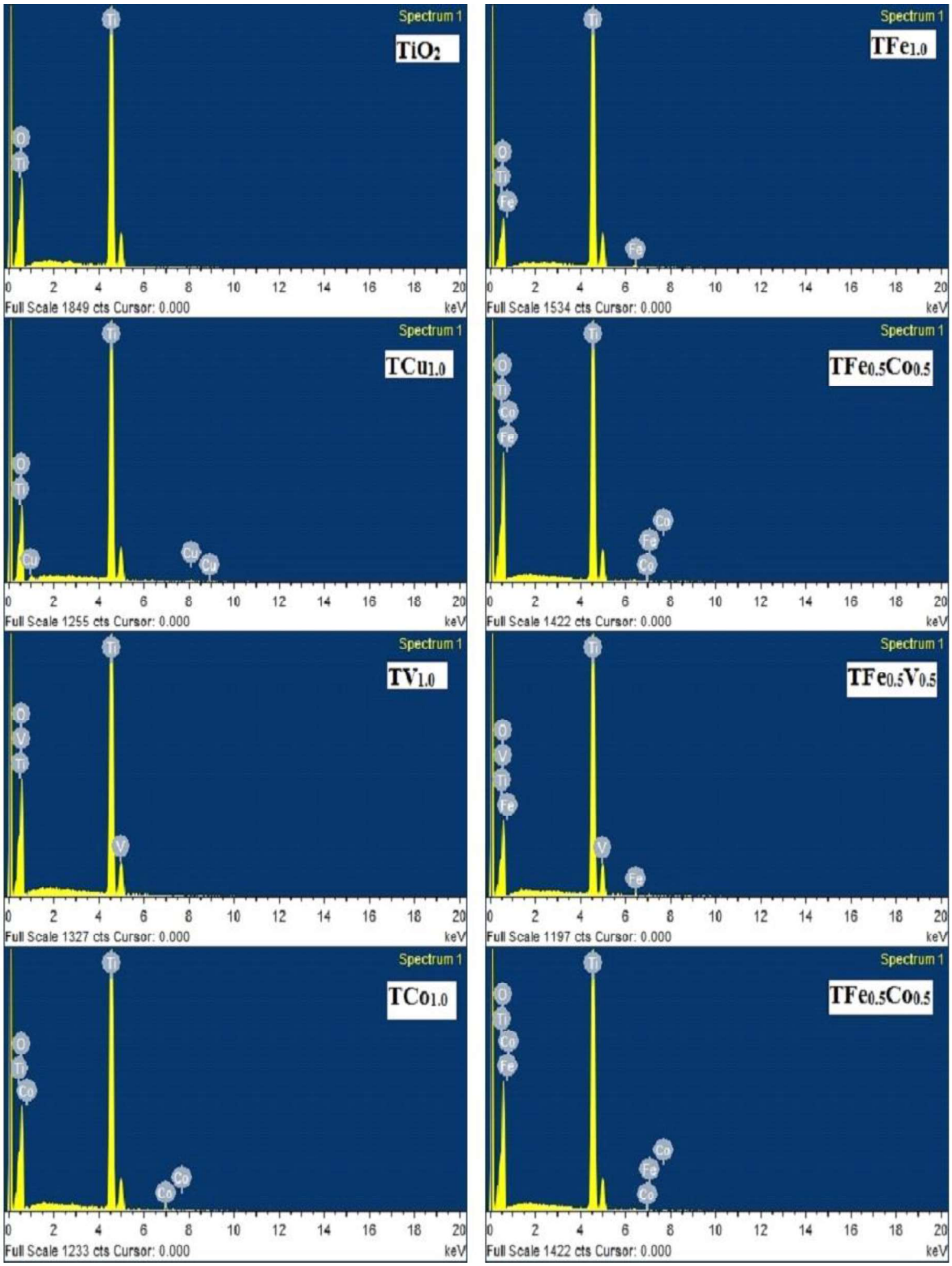

Figure 4.29 EDS mapping of TiO_2, $TFe_{1.0}$, $TCu_{1.0}$, $TFe_{0.5}Cu_{0.5}$, $TV_{1.0}$, $TFe_{0.5}Cu_{0.5}$, $TCo_{1.0}$ and $TFe_{0.5}Co_{0.5}$

4.3.1.7 X-ray Photoelectron Spectroscopy (XPS)

XPS was used to determine the elemental surface compositions and oxidation state of elements for different doped and codoped samples as shown in Figures 4.30 to 4.32. For the Ti 2 p region (Figure 4.31(a-c)), the peaks of Ti $sp_{3/2}$ and Ti $2p_{1/2}$ at 458.27 eV and 463.93 eV, respectively, they are all in good agreement with the values of Ti^{4+}. The similar observations have been reported by Apiwong-ngarm et al. [39] (i.e. the peaks of Ti $sp_{3/2}$ and Ti $2p_{1/2}$ at 458.62 eV and 464.36 eV, respectively) and Wang et al. [41] (i.e. the peaks of Ti $sp_{3/2}$ and Ti $2p_{1/2}$ at 458.6 eV and 464.3 eV, respectively). No broad FWHM of Ti $2p_{3/2}$ peak signals also indicates the only presence of Ti^{4+} species [41]. The O 1s binding energies (Figure 4.31(d-f)) of all the samples are located at 529.4 eV, which is assigned to bulk oxide (O^{2-}) in the TiO_2 lattice. Apiwong-ngarm et al. (2014) and Zhou et al. [245] reported the similar peaks for O 1s. The signals of Fe (Figure 4.32 a, b) were found to be weaker than all the others, due to the low doping amount. The peak located at 710.3 eV for Fe $2p_{3/2}$ was ascribed to the presence of Fe^{3+} ions [39]. The deconvolution of Cu $2p_{3/2}$ spectrum (Figure 4.32 c) showed a peak located at 932.1 eV assignable to Cu^{+} species. Figure 4.32 d shows the XPS spectrum for V $2p_{3/2}$ of vanadium doped and codoped TiO_2. The peak at 516.45 eV demonstrates that V is incorporated into the TiO_2 lattice. This indicated that V species exist in the lattice of V doped and codoped TiO_2 in the form of V^{5+}. Figure 4.32 (e) shows the XPS spectrum for Co 2p of cobalt doped and codoped photocatalyst samples. The peaks at 780.9 eV and 795.9 eV demonstrate that Co is fused into the lattice TiO_2. The peak at 780.9 eV indicates the Co $2p_{3/2}$ and the peak at 795.9 eV indicates the Co $2p_{1/2}$ [246].

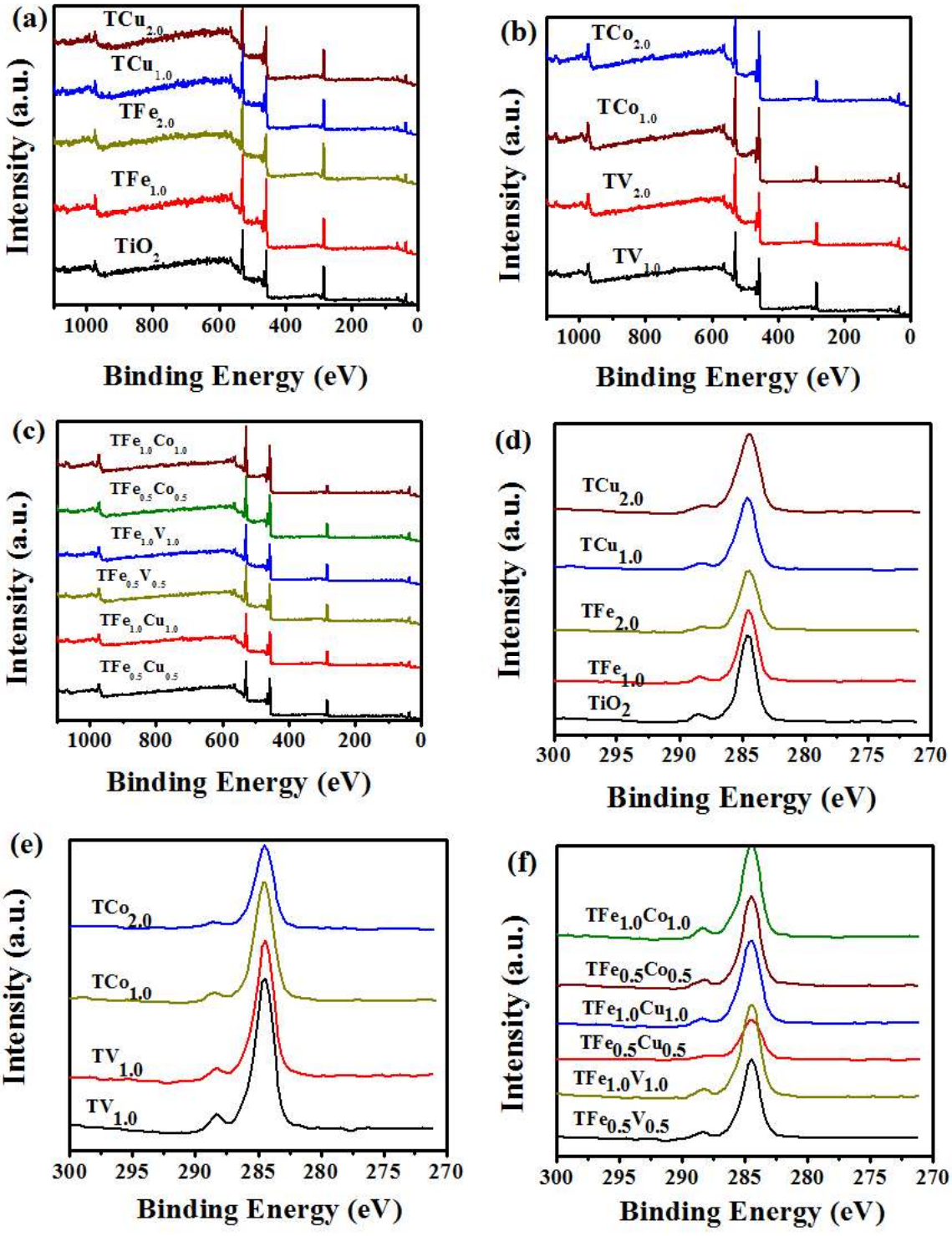

Figure 4.30 XPS of undoped, doped and codoped samples (a), (b) and (c) whole and (d), (e) and (f) C 1s

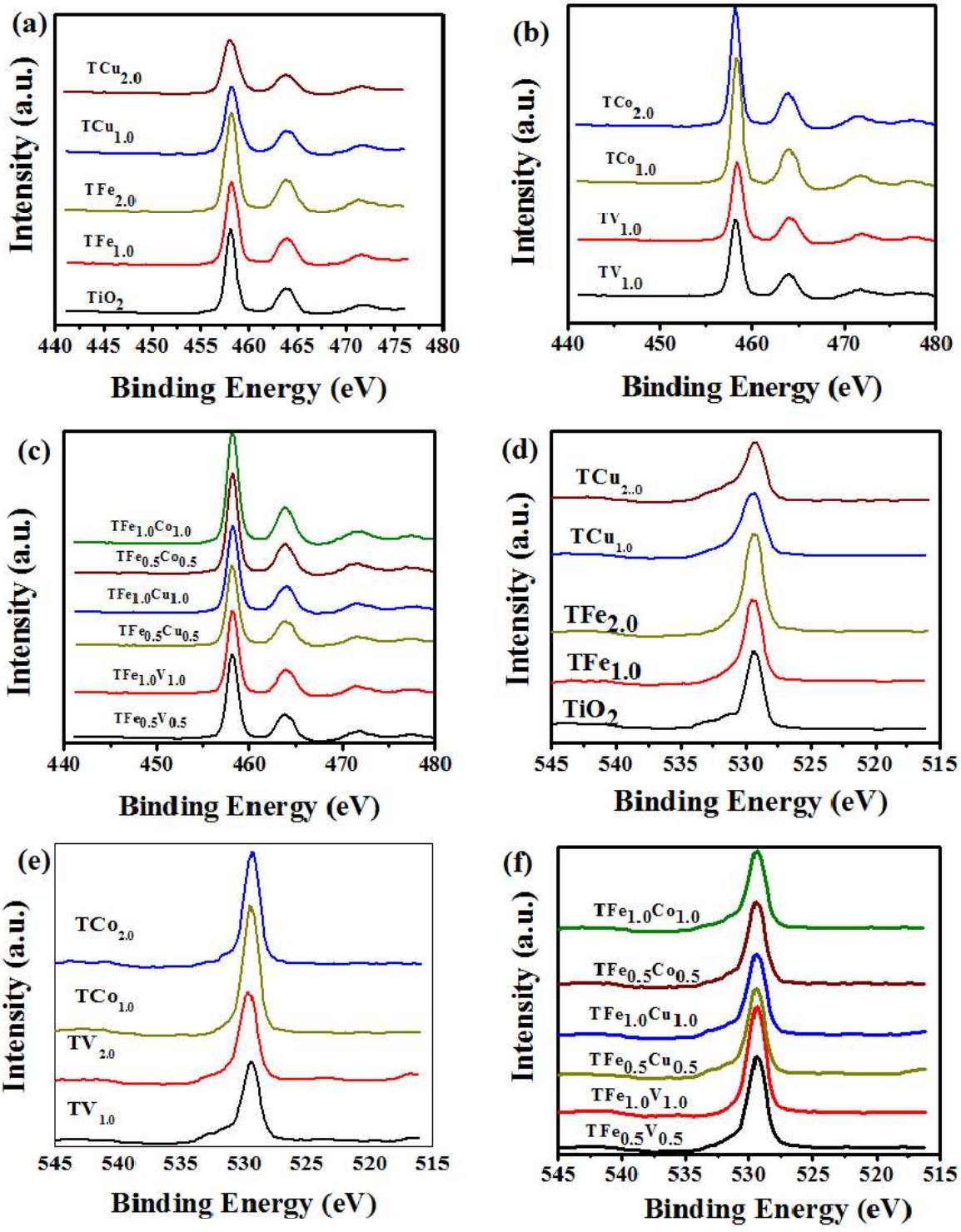

Figure 4.31 XPS of undoped, doped and codoped samples (a), (b) and (c) Ti 2p and (d), (e) and (f) O 1s

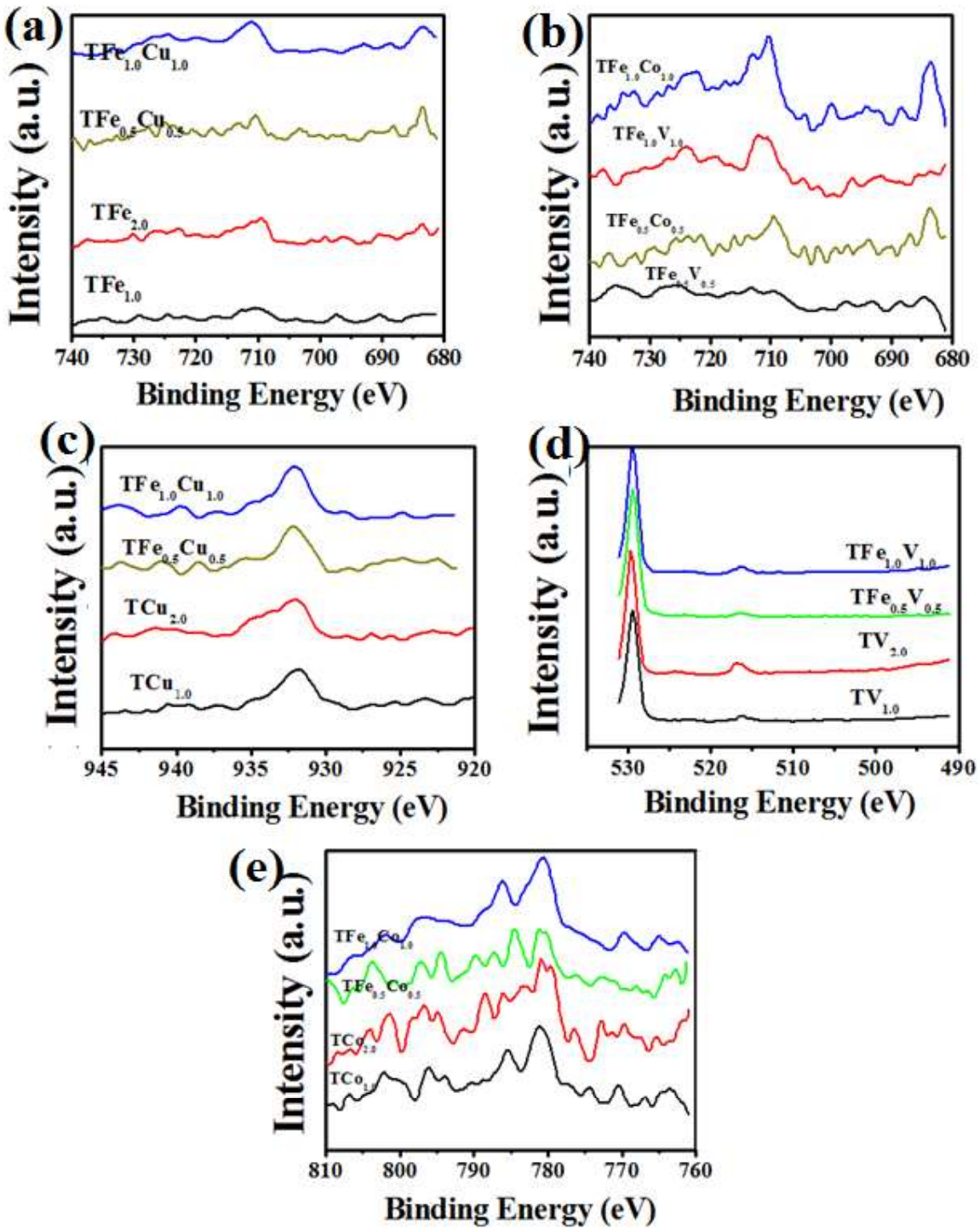

Figure 4.32 XPS of undoped, doped and codoped samples (a) and (b) Fe 2p3 (c) Cu 2p3, (d) V 2p3 and (e) Co 2p3

4.3.2 Effect of Doping and Codoping on Photocatalytic Decolorization of Textile Dyes

Photocatalytic performance of the samples was determined by studying the decolorization rate (C/C_o) and reaction kinetics of the photodecolorization reaction of RB5,

AR114 and AB113 in aqueous suspensions under visible light. Degussa P25 is used as reference to that of the doped and codoped TiO_2. Figure 4.33(a), Figure 4.34(a) and Figure 4.35(a) show a comparison of the decolorization rate (C/C_o) of RB5, AR114 and AB113 respectively with different catalysts under visible light. Decolorization of all the three dyes without a catalyst was also investigated. As can be seen from Figure 4.33(a), Figure 4.34(a) and Figure 4.35(a) that the self-decolorization of dyes is negligible as compared with the doped and codoped photocatalyst, showing that the dyes decolorization have photocatalyst as prerequisites. It is also seen from Figure 4.33a, Figure 4.34a and Figure 4.35a that the decolorization of all the dyes under Degussa P25 alone is not much significant. It is clear that the codoped TiO_2 shows the highest photocatalytic decolorization activity than doped and Degussa P25 under visible light, indicating that the photocatalytic activity of the codoped nanoparticles has a brilliant visible light response [41].

For the comparison of reaction rate among different catalysts and dyes, the first-order kinetic model was presented, $\ln C = -kt + \ln C_o$, where C is the dye concentration at time t, k is the reaction rate constant and C_o is the initial concentration of dye. Under the experimental conditions used, we assume that concentration of dyes after adsorption-desorption equilibrium is the initial concentration C_o. Figure 4.33b, Figure 4.34b and Figure 4.35b show the decolorization of RB5, AR114 and AB113 as a function of time in presence of different catalysts under visible-light irradiation. According to the above kinetic model, the rate constants k, has been plotted for different catalysts and shown in Figure 4.36.

It has been observed from Figure 4.36 that the reaction rate constant for all the three dyes with undoped TiO_2 is very low with comparison to doped and codoped TiO_2 photocatalysts. It was observed that reaction rate constant for decolorization of all the three dyes increases with the increase in the concentration of dopant from 1% to 2 % and the reaction rate also increases significantly with codoped photocatalysts. This is due to low energy band gap and absorbance of large visible light photons.

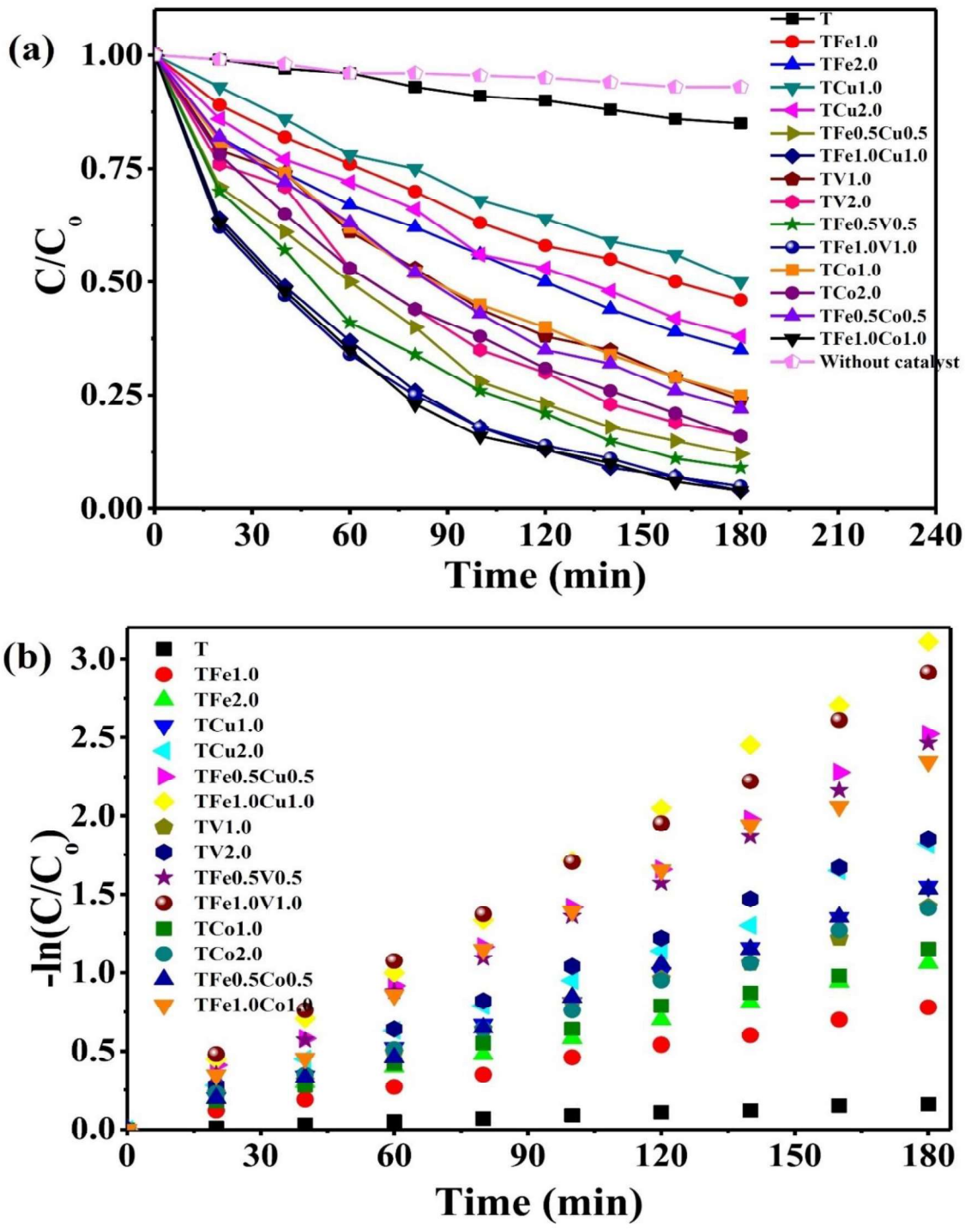

Figure 4.33 (a) Photocatalytic decolorization (b) reaction kinetics of RB5 using undoped, Fe and Cu, V and Co doped and codoped TiO_2 (Photocatalyst = 2.0 g l^{-1}, $[RB5]_o$ = 100 mg l^{-1},pH = 4)

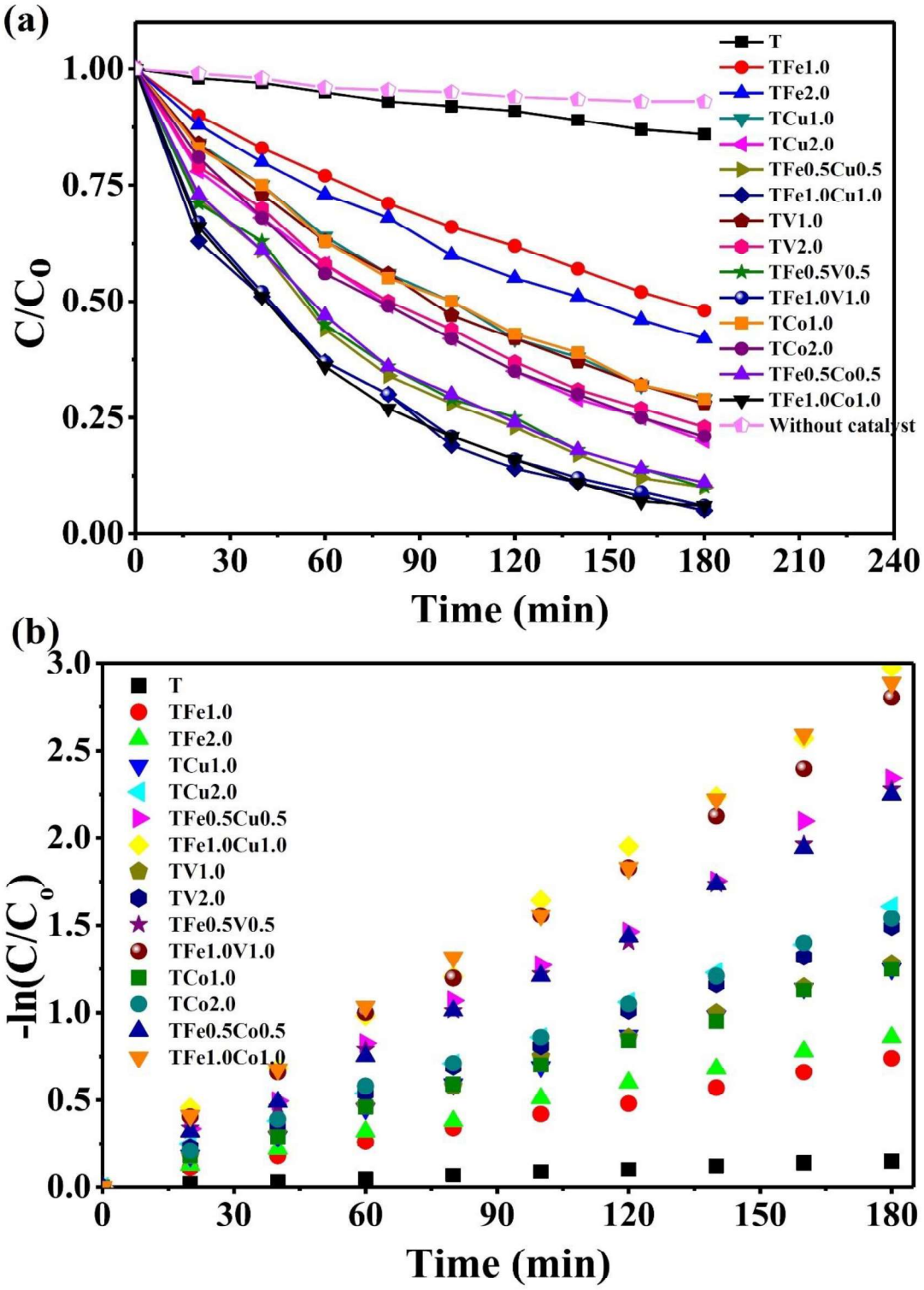

Figure 4.34 (a) Photocatalytic decolorization (b) reaction kinetics of AB113 using undoped, Fe and Cu, V and Co doped and codoped TiO_2 (Photocatalyst = 1.5 g l^{-1}, $[AB113]_o$ = 80 mg l^{-1},pH = 4)

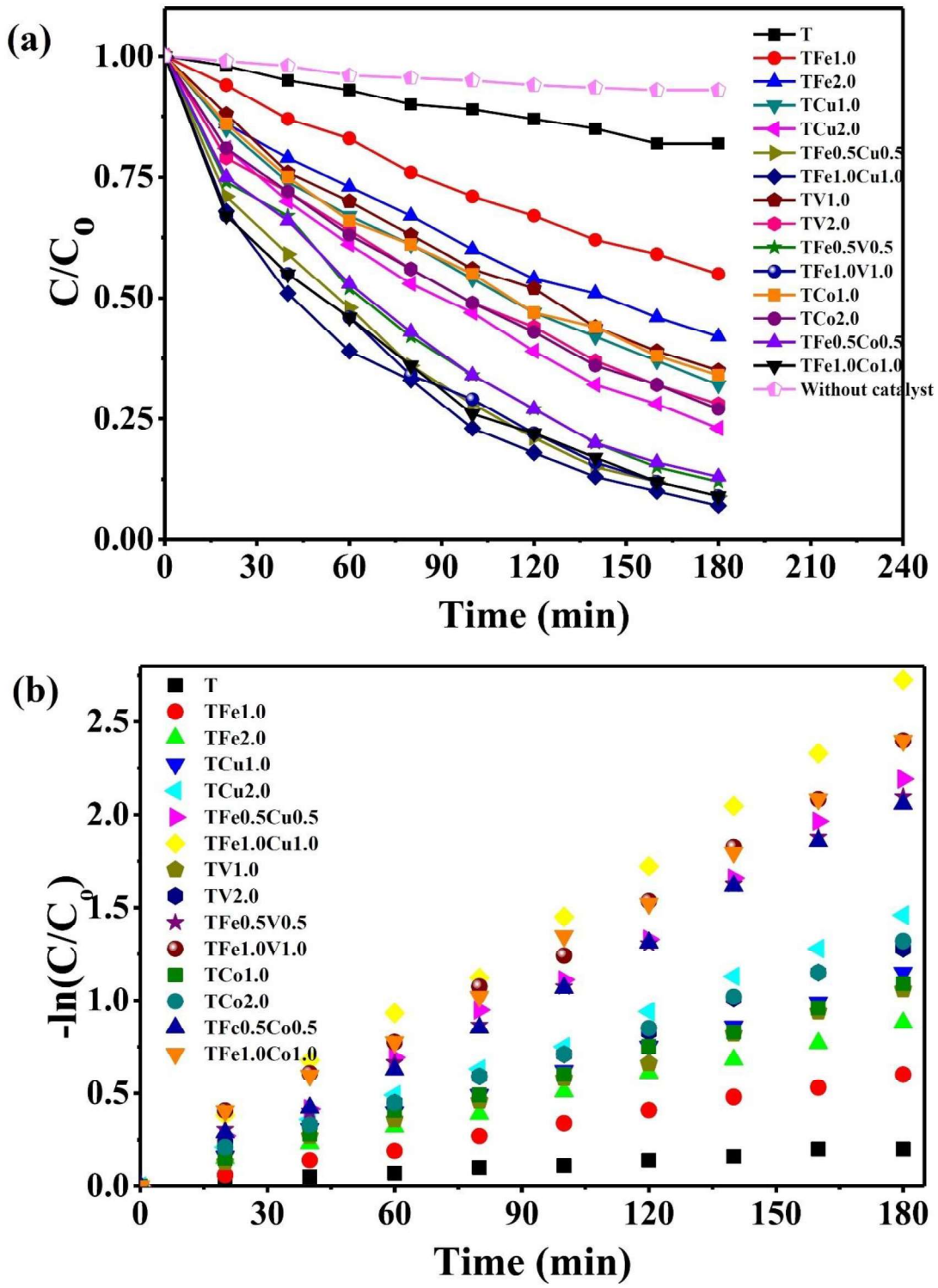

Figure 4.35 (a) Photocatalytic decolorization (b) reaction kinetics of AR114 using undoped, Fe and Cu, V and Co doped and codoped TiO_2 (Photocatalyst = 1.5 g l^{-1}, $[AR114]_o$ = 100 mg l^{-1},pH = 4)

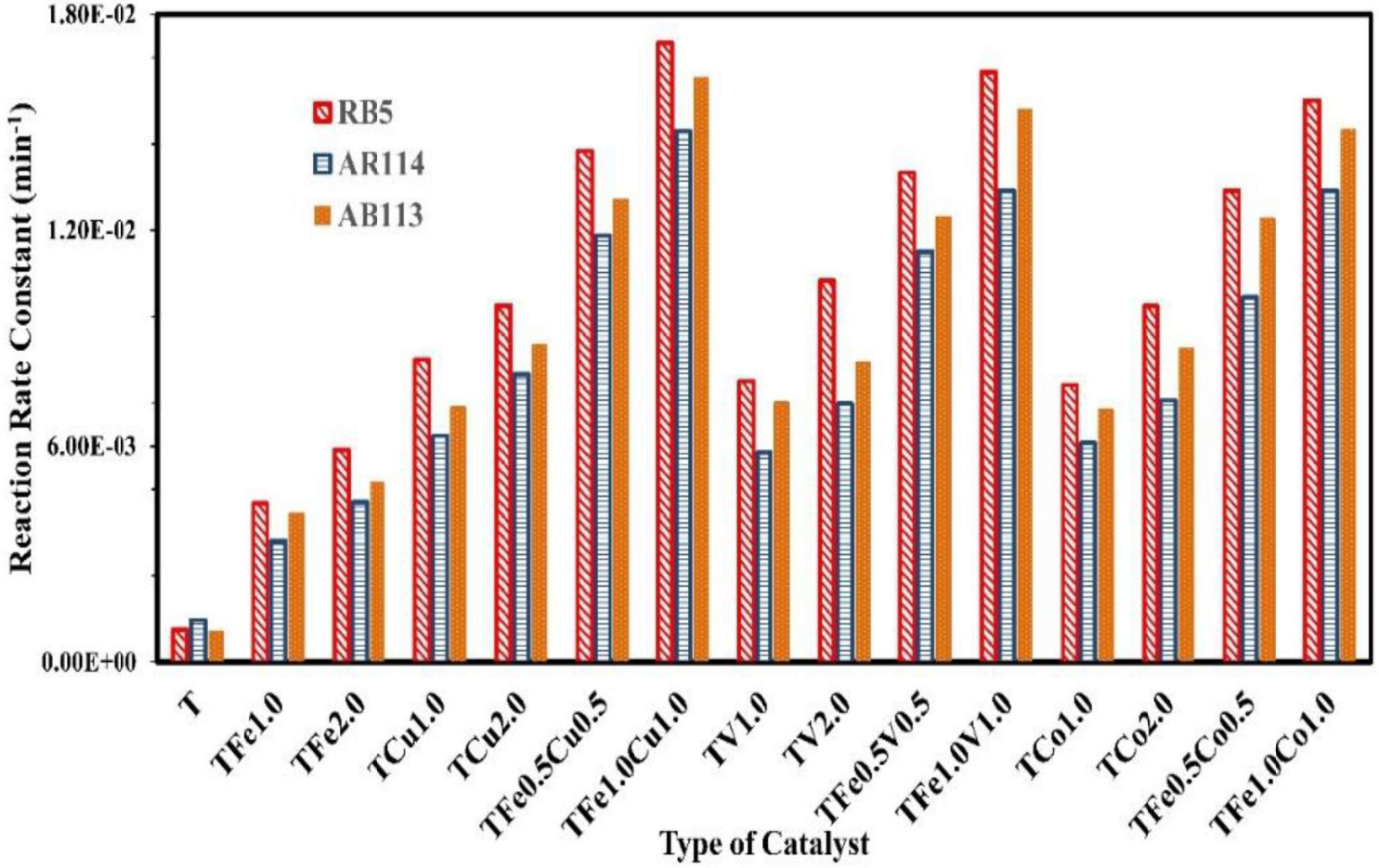

Figure 4.36 The kinetic constants (min^{-1}) for the photo decolorization of dyes with different catalysts at optimum conditions (ref Table 4.6)

4.4 Effect of Immobilization of TiO_2 over Cement Beads on Photocatalytic decolorization of Textile Dyes

4.4.1 Preliminary Study

Firstly, experiments with immobilization support were performed using blank cement beads under UV light in batch reactor (Figure 4.37). A small photo decolorization (approx. 6 %) for all the dyes was achieved due to adsorption of dye on the surface of cement beads. Further adsorption experiments with Degussa P25 have been performed, showing 18 % dye decolorization after 5 h of UV light irradiations. In slurry mode, all the dyes have been degraded after 3 h of UV light irradiation but with immobilized TiO_2 on cement beads under UV light, photo decolorization was recorded up to 90%.

4.4.1 Stability studies

The main aim of this study was the application of immobilized TiO_2 on cement beads in baffled fixed bed reactor and to check the strength of the catalyst on support. In the current study, the focus has been made to check the strength of TiO_2 coated cement beads for the photodecolorization of textile dyes. The cement beads were successfully reused for more than 25 times with a very short reduction in the decolorization of textile dyes (Figure 4.38).

SEM images with their EDX mapping of the immobilized beads after different recycles of use have been shown in Figure 4.39, which reveal that the immobilization was undamaged even after more than 25 cycles of use, ensuring the durability of immobilization. Thus, these beads will work efficiently even after 25 recycles. After each recycle, the immobilized beads were reactivated after drying in oven at 100^{o}C for 1-2 h.

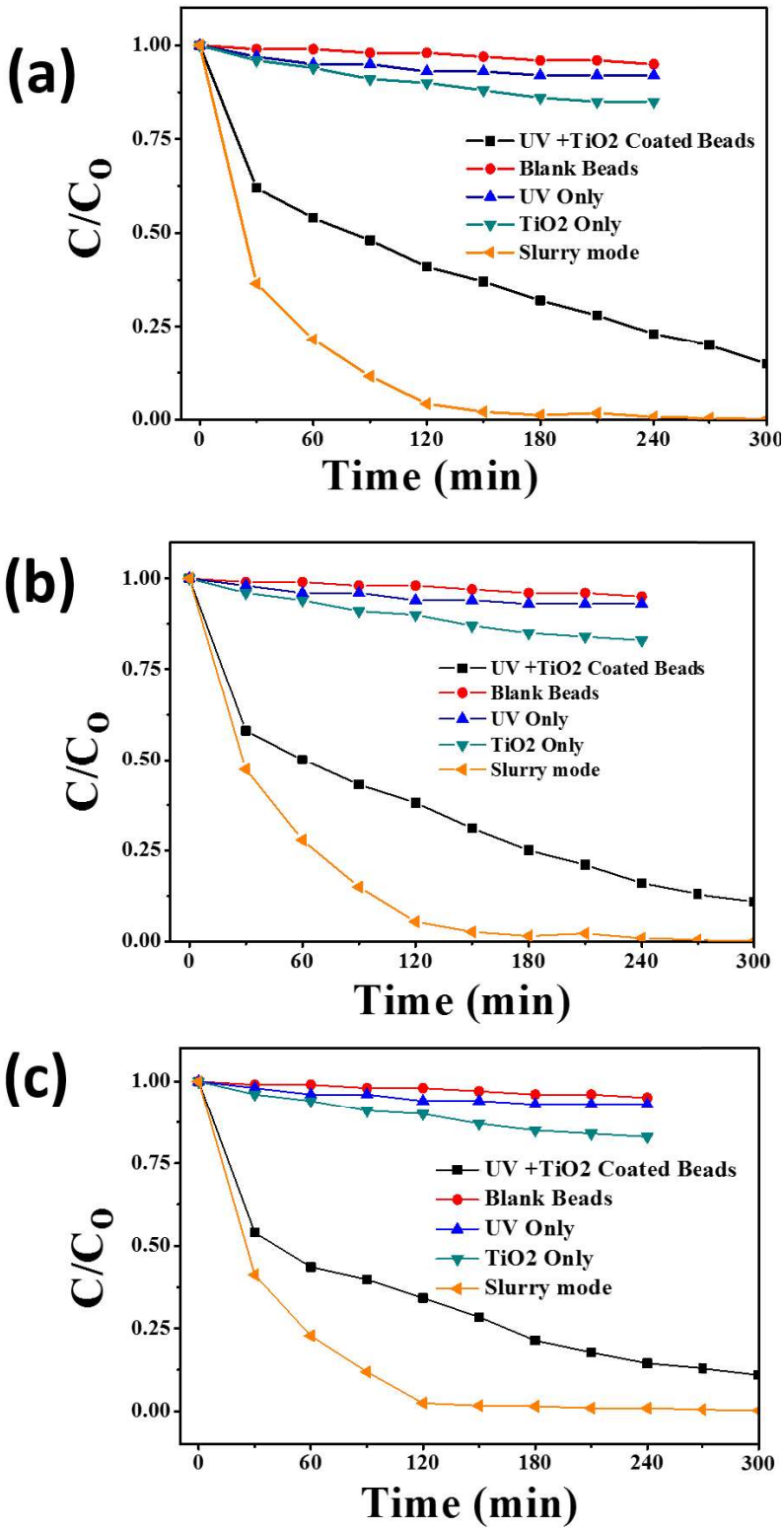

Figure 4.37 Primary study of immobilized supports for the decolorization of (a) RB5, (b) AB113 and (c) AR114

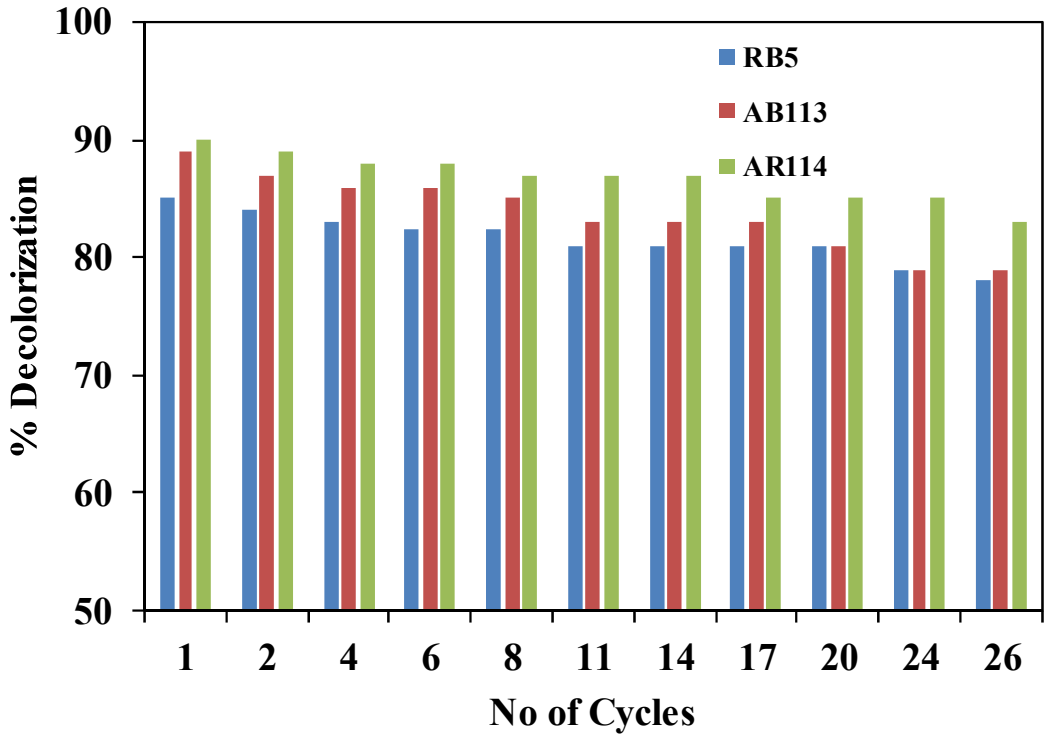

Figure 4.38 Stability study of catalyst for the photo-decolorization of three textile dyes

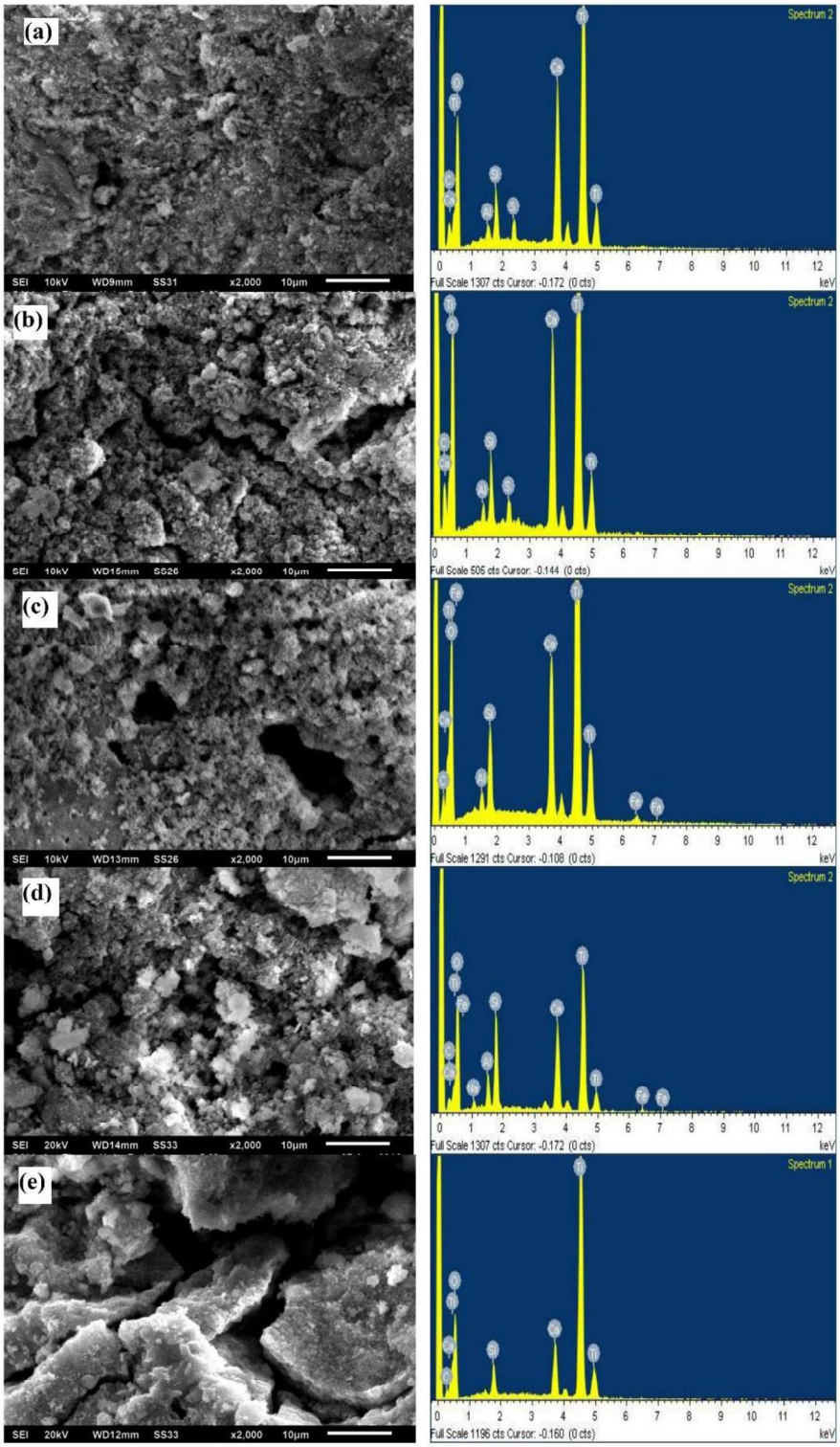

Figure 4.39 SEM images of (a) fresh coated TiO_2, (b) after 3rd cycle, (c) after 7th cycle, (d) after 16th cycle and (e) after 25th cycle along with their EDX mappings

4.4.3 Baffled Fixed Bed Reactor Study

Several complications such as agglomeration of the particles during the process are caused due to usage of TiO_2 in the form of photocatalyst, which reduces the efficiency of photocatalytic process. Hence, recovering of photocatalyst from wastewater by TiO_2 slurry needs costly microfiltration processes [247]. Light transport limitation appears with a high catalyst loading. Besides, it is difficult to separate the small TiO_2 particles from water after treatment where the particle size of fine P25 Degussa TiO_2 powders is about 21 nm and, in the aqueous phase, the particles form aggregates within the micron range. With the slurry TiO_2 system, an additional process step would need to be entailed for post-separation of the catalysts. This separation process is crucial to avoid the loss of catalyst particles and introduction of the new pollutant of TiO_2 in the treated water. Hence a fixed bed reactor was used to avoid these problems. This, however, may lower the oxidation potential per volume of water compared to the dispersed-phase system due to mass transfer limitation and light transport limitation caused by (i) the presence of substrate that absorbs light and (ii) a lower catalyst surface-to-volume ratio.

Hence, immobilization of catalyst was done on cement beads. The treatment process was carried out in baffled fixed bed reactor. For Fixed bed reactor, the time taken for the decolorization (pH 4 and dye concentration 100 mg l^{-1}) was 8 h at the flow rate of 500 ml h^{-1}. The percentage decolorization was found to be 85% for RB5 and 89% for AB113 and AR114 (Figure 4.40).

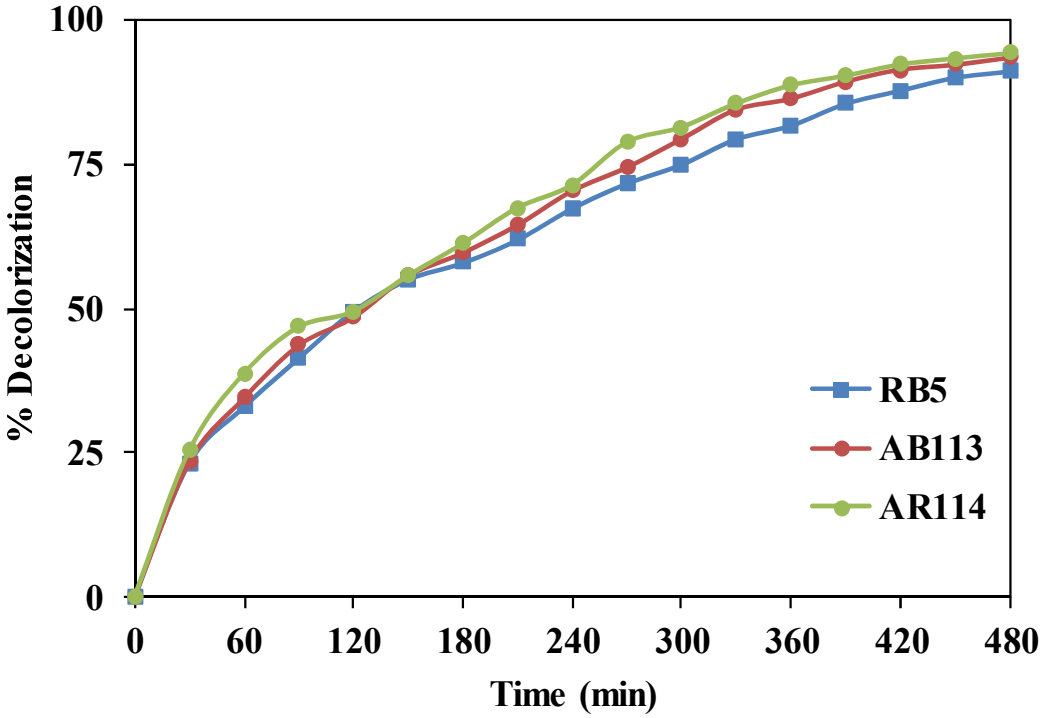

Figure 4.40 % decolorization of textile dyes in the baffled fixed bed reactor

4.4.3.1 Kinetic Study

The decolorization of RB5, AB113 and AR114 in baffled fixed bed reactor can be described by a power law kinetic model. The first order reaction kinetics in relations to decolorization efficiency of RB5, AB113 and AR114 can be described by eq.(4.1).

A graph of ln C_o/C versus t for photocatalytic decolorization of RB5, AB113 and AR114 is presented in Figure 4.41. A linear correlation between ln C_o/C and time was obtained. The reaction rate constants were 0.0049 min^{-1}, 0.0056 min^{-1} and 0.0059 min^{-1} with the values of R^2 0.9896, 0.9899 and 0.9901 for the decolorization of RB5, AB113 and AR114 respectively. [248]

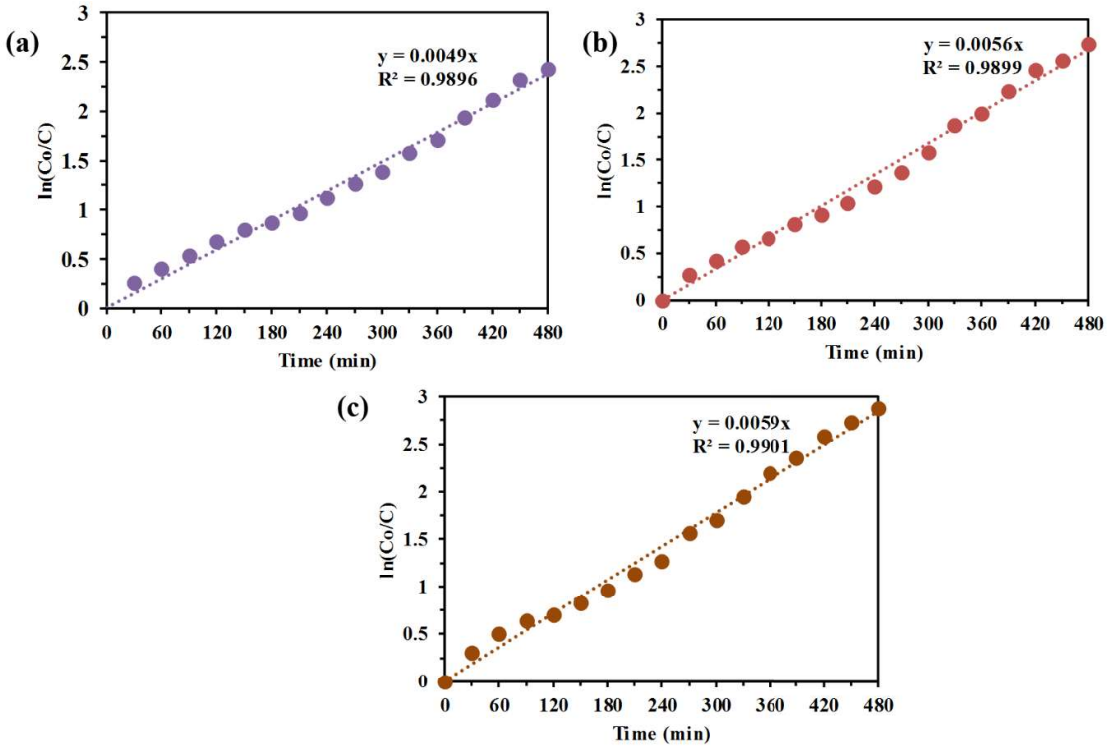

Figure 4.41 Decolorization kinetics of (a) RB5, (b) AB113 and (c) AR114 dyes in baffled fixed bed reactor

Chapter 5 CONCLUSIONS AND RECOMMONDATIONS

5.1 Conclusions

5.1.1 Modeling and Optimization of Photocatalytic Activity of RB5, AB113 and AR114 Dyes by ANN and RSM

From the photocatalytic degradation of RB5, AB113 and AR114 using the UV/TiO_2, the following conclusions are drawn:

1. The MSE is found minimum with eight, ten and ten neurons for RB5, AB113 and AR114 respectively for both (decolorization and degradation efficiency) cases by using the tan-sigmoid transfer function with three-layered feed forward back propagation in ANN network.
2. Model F values predicted by ANOVA are 17.03 and 14.29, 15.28 and 16.17, and 12.89 and 11.53 for decolorization and degradation efficiency of RB5, AB113 and AR114 respectively, implying that the three-level model is significant.
3. TiO_2 concentration, initial dye concentration, pH and time are the highly significant parameters for both decolorization and degradation of RB5, AB113 and AR114.
4. The maximum decolorization and degradation of the dyes take place in the pH range of 2-4.
5. The decolorization and degradation efficiency increases with increase in A/V ratio of the reactor.
6. There is a rapid increase in decolorization and degradation efficiency up to 135 min, irrespective of the initial dye concentration, after that there is little increase in decolorization and degradation efficiency.
7. The first order rate constants for the decolorization of RB5, AB113 and AR114 are found to be 0.0515 min^{-1}, 0.0470 min^{-1} and 0.0542 min^{-1} respectively and for the

degradation of RB5, AB113 and AR114 are found to be 0.0246 min^{-1}, 0.0205 min^{-1} and 0.0253 min^{-1}, respectively.

8. The mineralization of all the dyes has also been confirmed by removal of TOC as well as GC-MS analysis at optimum condition.

5.1.2 Photocatalytic Activity of Binary Dye Mixture of AB113 and AR114

From the photocatalytic decolorization of binary dye mixture of AB113 and AR114 using the UV/TiO_2, the following conclusions are drawn:

1. Both the calibration methods, (i) first order derivative spectrophotometric technique and (ii) multivariate calibration technique, are suitable to quantify individual dye concentrations in binary dye mixture.
2. The optimized neurons for the photocatalytic decolorization of the mixture of AB113 and AR114 dyes are ten using the three layered feed-forward back propagation type ANN structure.
3. Model F values predicted by ANOVA are 52.63 and 54.50 for decolorization of AB113 and AR114 respectively, indicating that the five level model is significant.
4. The TiO_2 loading, initial concentration of dyes, initial pH, time and the interaction of TiO_2 loading to initial concentration of dyes etc. are found highly significant parameters for decolorization efficiency of AB113 and AR114.
5. The decolorization efficiency of AB113 and AR114 first increases with increasing TiO_2 dose, up to a value of 200 mg l^{-1}, after that no change has been observed for decolorization efficiency of AB113 and AR114.
6. On increase in TiO_2 concentration beyond a certain value, photocatalytic decolorization decreases.
7. The decolorization efficiency of AB113 and AR114 increases with decreasing the pH.

8. The optimized process parameters are found to be TiO_2 dose 200 mg l^{-1}, pH 5 and time 180 min for a dye concentration of 20 mg l^{-1}.
9. The first order rate constants for the decolorization of AB113 and AR114 in binary dye mixture are found to be 0.0164 min^{-1} and 0.0228 min^{-1} respectively.
10. The mineralization of the dyes has also been confirmed by removal of TOC as well as GC-MS analysis.

5.1.3 Preparation, Characterization and Photocatalytic Study of Dyes on Metal Ions Doped and Codoped TiO_2

From the photocatalytic decolorization of RB5, AB113 and AR114 using the metal ion doped and codoped TiO_2, the following conclusions are drawn:

1. Transition metal ions doped and codoped TiO_2 nanoparticles have been successfully prepared through a simple wet impregnation method.
2. The structural characterization (by XRD) revealed the presence of anatase phase of metal ions doped and codoped TiO_2 nanoparticles. It has been noted that there is no evidence of secondary or impurity related peaks in all the transition metal ions doped and codoped TiO_2 samples.
3. The stretching vibrations of hydroxyl clusters, the bending vibrations of water molecules and Ti-O-Ti stretching vibration in the doped and codoped samples have been recognized by FTIR spectroscopy.
4. UV-Vis DRS patterns of the doped and codoped samples show the absorption edge shift towards the higher wavelength region (red shift) upon increase in transition metal dopant concentrations.

5. The metal ions doped and codoped TiO_2 nanoparticles are asymmetrical shaped crystallites as per FESEM analysis.
6. From TEM images of the nanoparticles, particle sizes are found to be around 11-19 nm of all the doped and codoped samples.
7. Photocatalytic study of textile dyes shows that the self- decolorization of dyes is negligible as compared to the doped and codoped photocatalyst, indicating that the dyes decolorization have photocatalyst as prerequisite.
8. The photodecolorization of textile dyes under visible light with all synthesized catalyst samples follows the first order reaction kinetics.
9. The reaction rate constants for the decolorization of all the three dyes with undoped TiO_2 are very low as compared to doped and codoped TiO_2 photocatalysts.
10. It was observed that the reaction rate constant for decolorization of all the three dyes increases with the increase in the concentration of dopant from 1% to 2 % and the reaction rate also increases significantly with codoped photocatalysts.
11. It was observed that the reaction rate constant for decolorization of all the three dyes was maximum with codoping of Fe and Cu on TiO_2.

5.1.4 Effect of Immobilization of TiO_2 on Cement Beads on Photocatalytic Decolorization of Textile Dyes

From the photocatalytic decolorization of RB5, AB113 and AR114 using immobilized TiO_2 on cement beads, the following conclusions are drawn:

1. TiO_2 nanoparticles have been successfully coated on cement beads.
2. In batch reactor with immobilized TiO_2 on cement beads and UV light, photodecolorization of dyes up to 90% is achieved.
3. TiO_2 coated cement beads are stable for more than 25 cycles and can be reused.

4. The percentage decolorization is found to be 85% for RB5 and 89% for AB113 and AR114 in 8 h using the baffled fixed bed reactor at the flow rate of 500 ml h^{-1}.
5. The decolorization of all the three dyes follows the first order reaction kinetics.

5.2 Recommendations

The present work marks the steps towards synthesis and assessment of photocatalytic activity of doped, codoped and immobilized TiO_2 under UV light and visible light, the modeling and optimization. This study lays the foundation for many future works, some of which are listed below:

- Study for the possibility of replacing the artificial light sources with solar irradiation as well as LED device.
- Non-metal, Alkaline earth metal, rare earth metal and noble metal can be doped on TiO_2 materials and the structural and electronic properties of the materials can be studied for different applications of photocatalysis.
- Although the photocatalytic degradation of organic pollutants and treatment of waste water have been extensively studied and consolidated its benefits. The industrial use of this technology has been linked due to lack of suitable large scale reactor or treatment plant. The potential of total mineralization of wastewater that can accrue with the use of this technology has not been fully exploited by the industry so far. Therefore, a better understanding of the design of these systems is required.
- Although cement is a low cost material for immobilization of TiO_2 but there is a lot of scope for finding other materials for immobilization of TiO_2.
- Decolorization of the dye wastewaters is one central objective of TiO_2-mediated photocatalytic treatment as well as that of the current study. Total mineralization of the dye is an equally important end goal. Thus, along with monitoring absorbance changes

during the course of the photocatalytic remediation process, other complementary measurements like HPLC must be carried out to get a complete outcome of the process efficiency.

- The photocatalytic activity of the developed photocatalysts can be investigated with other recalcitrant contaminants, such as endocrine disrupting compounds (EDC), phenolic compounds, halophenols and pesticides.
- Effects of various parameters such as light wavelength, light intensity, reaction temperature, dissolved oxygen, etc. in addition to that have been studied in the current work would help in further modeling and optimization and enhancement in the efficiencies of the TiO_2 photocatalysts.

REFERENCES

222[1] S. Malato, J. Blanco, A. Vidal, C. Richter, Photocatalysis with solar energy at a pilot-plant scale: An overview, Applied Catalysis B: Environmental, 37 (2002) 1-15.

[2] S. Das, V.C. Srivastava, Recent advances in fabrication of photocatalytic micro-reactor, Materials Science Forum, 855 (2016) 156-167.

[3] A. Yadav, S. Mukherji, A. Garg, Removal of chemical oxygen demand and color from simulated textile wastewater using a combination of chemical/physicochemical processes, Industrial & Engineering Chemistry Research, 52 (2013) 10063-10071.

[4] E. Bizani, K. Fytianos, I. Poulios, V. Tsiridis, Photocatalytic decolorization and degradation of dye solutions and wastewaters in the presence of titanium dioxide, Journal of Hazardous Materials, 136 (2006) 85-94.

[5] V.S. Mane, I.D. Mall, V.C. Srivastava, Use of bagasse fly ash as an adsorbent for the removal of brilliant green dye from aqueous solution, Dyes and Pigments, 73 (2007) 269-278.

[6] T. Aye, M. Mehrvar, W.A. Anderson, Effects of photocatalysis on the biodegradability of Cibacron Brilliant Yellow 3G-P (Reactive Yellow 2), Journal of Environmental Science and Health, Part A, 39 (2004) 113-126.

[7] C.-Y. Chen, J.-C. Chang, A.-H. Chen, Competitive biosorption of azo dyes from aqueous solution on the templated crosslinked-chitosan nanoparticles, Journal of Hazardous Materials, 185 (2011) 430-441.

[8] M. Turabik, Adsorption of basic dyes from single and binary component systems onto bentonite: Simultaneous analysis of Basic Red 46 and Basic Yellow 28 by first order derivative spectrophotometric analysis method, Journal of Hazardous Materials, 158 (2008) 52-64.

[9] V.K. Gupta, M. Sharma, R.K. Vyas, Hydrothermal modification and characterization of bentonite for reactive adsorption of methylene blue: An ESI-MS study, Journal of Environmental Chemical Engineering, 3 (2015) 2172-2179.

[10] J. Sharma, I.M. Mishra, V. Kumar, Mechanistic study of photo-oxidation of bisphenol-A (BPA) with hydrogen peroxide (H_2O_2) and sodium persulfate (SPS), Journal of Environmental Management, 166 (2016) 12-22.

[11] J. Sharma, I.M. Mishra, V. Kumar, Degradation and mineralization of bisphenol A (BPA) in aqueous solution using advanced oxidation processes: UV/H_2O_2 and UV/$S_2O_8^-$ oxidation systems, Journal of Environmental Management, 156 (2015) 266-275.

[12] T. Robinson, G. McMullan, R. Marchant, P. Nigam, Remediation of dyes in textile effluent: A critical review on current treatment technologies with a proposed alternative, Bioresource Technology, 77 (2001) 247-255.

[13] R. Andreozzi, V. Caprio, A. Insola, R. Marotta, Advanced oxidation processes (AOP) for water purification and recovery, Catalysis Today, 53 (1999) 51-59.

[14] I. Casero, D. Sicilia, S. Rubio, D. Pérez-Bendito, Chemical degradation of aromatic amines by Fenton's reagent, Water Research, 31 (1997) 1985-1995.

[15] S.J. Masten, S.H.R. Davies, The use of ozonation to degrade organic contaminants in wastewaters, Environmental Science and Technology, 28 (1994) 180A-185A.

[16] L.W. Miller, M.I. Tejedor-Tejedor, M.A. Anderson, Titanium dioxide-coated silica waveguides for the photocatalytic oxidation of formic acid in water, Environmental Science & Technology, 33 (1999) 2070-2075.

[17] W.H. Glaze, J.W. Kang, Advanced oxidation processes. Description of a kinetic model for the oxidation of hazardous materials in aqueous media with ozone and hydrogen peroxide in a semibatch reactor, Industrial and Engineering Chemistry Research, 28 (1989) 1573-1580.

[18] J. Hoigné, H. Bader, Rate constants of reactions of ozone with organic and inorganic compounds in water-I: Non-dissociating organic compounds, Water Research, 17 (1983) 173-183.

[19] J. Hoigné, H. Bader, Rate constants of reactions of ozone with organic and inorganic compounds in water-II: Dissociating organic compounds, Water Research, 17 (1983) 185-194.

[20] G.R. Peyton, F.Y. Huang, J.L. Burleson, W.H. Glaze, Destruction off pollutants in water with ozone in combination with ultraviolet radiation. 1: General principles and oxidation of tetrachloroethylene, Environmental Science and Technology, 16 (1982) 448-453.

[21] D. Robert, S. Malato, Solar photocatalysis: A clean process for water detoxification, Science of The Total Environment, 291 (2002) 85-97.

[22] W.R. Haag, C.C. David Yao, Rate constants for reaction of hydroxyl radicals with several drinking water contaminants, Environmental Science and Technology, 26 (1992) 1005-1013.

[23] W.H. Glaze, J.-W. Kang, D.H. Chapin, The chemistry of water treatment processes involving ozone, hydrogen peroxide and ultraviolet radiation, Ozone: Science & Engineering, 9 (1987) 335-352.

[24] M. Pera-Titus, V. García-Molina, M.A. Baños, J. Giménez, S. Esplugas, Degradation of chlorophenols by means of advanced oxidation processes: A general review, Applied Catalysis B: Environmental, 47 (2004) 219-256.

[25] E. Rezaei, J. Soltan, N. Chen, Catalytic oxidation of toluene by ozone over alumina supported manganese oxides: Effect of catalyst loading, Applied Catalysis B: Environmental, 136–137 (2013) 239-247.

[26] R. Keykavoos, R. Mankidy, H. Ma, P. Jones, J. Soltan, Mineralization of bisphenol A by catalytic ozonation over alumina, Separation and Purification Technology, 107 (2013) 310-317.

[27] A.M.T. Silva, E. Nouli, Â.C. Carmo-Apolinário, N.P. Xekoukoulotakis, D. Mantzavinos, Sonophotocatalytic/H_2O_2 degradation of phenolic compounds in agro-industrial effluents, Catalysis Today, 124 (2007) 232-239.

[28] J. Moreira, B. Serrano, A. Ortiz, H. de Lasa, A unified kinetic model for phenol photocatalytic degradation over TiO_2 photocatalysts, Chemical Engineering Science, 78 (2012) 186-203.

[29] Metcalf, Eddy, Wastewater Enggineering: Treatmtment & Reuse, Tata McGraw-Hill Education Private Limited, (2009).

[30] M.R. Hoffmann, S.T. Martin, W. Choi, D.W. Bahnemann, Environmental applications of semiconductor photocatalysis, Chemical Reviews, 95 (1995) 69-96.

[31] G. Rothenberger, J. Moser, M. Graetzel, N. Serpone, D.K. Sharma, Charge carrier trapping and recombination dynamics in small semiconductor particles, Journal of the American Chemical Society, 107 (1985) 8054-8059.

[32] N. Serpone, E. Pelizzetti, Photocatalysis: Fundamentals and Applications, Wiley, New York, (1989).

[33] N. Serpone, D. Lawless, J. Disdier, J.-M. Herrmann, Spectroscopic, photoconductivity, and photocatalytic studies of TiO_2 colloids: Naked and with the lattice doped with Cr^{3+}, Fe^{3+}, and V^{5+} cations, Langmuir, 10 (1994) 643-652.

[34] M. Kocher, T.K. Däubler, E. Harth, U. Scherf, A. Gügel, D. Neher, Photoconductivity of an inorganic/organic composite containing dye-sensitized nanocrystalline titanium dioxide, Applied Physics Letters, 72 (1998) 650-652.

[35] K.R. Gopidas, M. Bohorquez, P.V. Kamat, Photophysical and photochemical aspects of coupled semiconductors: charge-transfer processes in colloidal cadmium sulfide-titania and cadmium sulfide-silver(I) iodide systems, The Journal of Physical Chemistry, 94 (1990) 6435-6440.

[36] J.C.S. Wu, C.-H. Chen, A visible-light response vanadium-doped titania nanocatalyst by sol–gel method, Journal of Photochemistry and Photobiology A: Chemistry, 163 (2004) 509-515.

[37] R. Khan, S.W. Kim, T.-J. Kim, C.-M. Nam, Comparative study of the photocatalytic performance of boron–iron Co-doped and boron-doped TiO_2 nanoparticles, Materials Chemistry and Physics, 112 (2008) 167-172.

[38] J. Liu, Z. Zhang, L. Yang, Y. Zhang, S. Deng, The Degradation of Reactive Black Wastewater by Fe/Cu Co-doped TiO_2, International Journal of Chemistry, 3 (2011) 87-92.

[39] K. Apiwong-ngarm, P. Pongwan, B. Inceesungvorn, S. Phanichphant, K. Wetchakun, N. Wetchakun, Photocatalytic activities of Fe–Cu/TiO_2 on the mineralization of oxalic acid and formic acid under visible light irradiation, Powder Technology, 266 (2014) 447-455.

[40] M. Hamadanian, A. Reisi-Vanani, A. Majedi, Synthesis, characterization and effect of calcination temperature on phase transformation and photocatalytic activity of Cu,S-codoped TiO_2 nanoparticles, Applied Surface Science, 256 (2010) 1837-1844.

[41] Q. Wang, S. Xu, F. Shen, Preparation and characterization of TiO_2 photocatalysts co-doped with iron (III) and lanthanum for the degradation of organic pollutants, Applied Surface Science, 257 (2011) 7671-7677.

[42] N. Riaz, F.K. Chong, Z.B. Man, M.S. Khan, B.K. Dutta, Photodegradation of Orange II under visible light using Cu–Ni/TiO_2: influence of Cu:Ni mass composition, preparation, and calcination temperature, Industrial & Engineering Chemistry Research, 52 (2013) 4491-4503.

[43] H. Khan, D. Berk, Characterization and mechanistic study of Mo^{+6} and V^{+5} codoped TiO_2 as a photocatalyst, Journal of Photochemistry and Photobiology A: Chemistry, 294 (2014) 96-109.

[44] M.F.J. Dijkstra, A. Michorius, H. Buwalda, H.J. Panneman, J.G.M. Winkelman, A.A.C.M. Beenackers, Comparison of the efficiency of immobilized and suspended systems in photocatalytic degradation, Catalysis Today, 66 (2001) 487-494.

[45] M. Fathinia, A.R. Khataee, M. Zarei, S. Aber, Comparative photocatalytic degradation of two dyes on immobilized TiO_2 nanoparticles: Effect of dye molecular structure and response surface approach, Journal of Molecular Catalysis A: Chemical, 333 (2010) 73-84.

[46] A.K. Ray, A.A.C.M. Beenackers, Novel photocatalytic reactor for water purification, AIChE Journal, 44 (1998) 477-483.

[47] M.P. Seabra, E. Rego, A. Ribeiro, J.A. Labrincha, Photodegradation of Orange II solutions by TiO_2 active layers jet sprayed on aluminium sheets, Chemical Engineering Journal, 171 (2011) 175-180.

[48] A. Rachel, M. Subrahmanyam, P. Boule, Comparison of photocatalytic efficiencies of TiO_2 in suspended and immobilised form for the photocatalytic degradation of nitrobenzenesulfonic acids, Applied Catalysis B: Environmental, 37 (2002) 301-308.

[49] N. Prakash, S.A. Manikandan, L. Govindarajan, V. Vijayagopal, Prediction of biosorption efficiency for the removal of copper (II) using artificial neural networks, Journal of Hazardous Materials, 152 (2008) 1268-1275.

[50] F. Despagne, D. Luc Massart, Neural networks in multivariate calibration, Analyst, 123 (1998) 157R-178R.

[51] W. Daosud, P. Thitiyasook, A. Arpornwichanop, P. Kittisupakorn, M.A. Hussain, Neural network inverse model-based controller for the control of a steel pickling process, Computers & Chemical Engineering, 29 (2005) 2110-2119.

[52] D.P.B.T.B. Strik, A.M. Domnanovich, L. Zani, R. Braun, P. Holubar, Prediction of trace compounds in biogas from anaerobic digestion using the MATLAB neural network toolbox, Environmental Modelling & Software, 20 (2005) 803-810.

[53] U.I. Gaya, Heterogeneous photocatalysis using inorganic semiconductor solids, Springer Netherlands, (2014).

[54] J. Hagen, Heterogeneous catalysis: Fundamentals, Wiley-VCH Verlag GmbH & Co. KGaA, (2006).

[55] D.S. Bhatkhande, V.G. Pangarkar, A.A.C.M. Beenackers, Photocatalytic degradation for environmental applications - A review, Journal of Chemical Technology & Biotechnology, 77 (2002) 102-116.

[56] M.V. Dozzi, Improving the photocatalytic activity of TiO_2 for environmental application: Effects of doping and of surface modification, Ph.D. thesis, The University of Milan, Italy, (2011).

[57] C.-H. Wu, C.-L. Chang, Decolorization of Reactive Red 2 by advanced oxidation processes: Comparative studies of homogeneous and heterogeneous systems, Journal of Hazardous Materials, 128 (2006) 265-272.

[58] A. Fujishima, K. Honda, Electrochemical photolysis of water at a semiconductor electrode, Nature, 238 (1972) 37-38.

[59] O. Carp, C.L. Huisman, A. Reller, Photoinduced reactivity of titanium dioxide, Progress in Solid State Chemistry, 32 (2004) 33-177.

[60] K. Mori, Photo-functionalized materials using nanoparticles: Photocatalysis, Kona, 41 (2004) 750-756.

[61] N. Serpone, P. Maruthamuthu, P. Pichat, E. Pelizzetti, H. Hidaka, Exploiting the interparticle electron transfer process in the photocatalysed oxidation of phenol, 2-chlorophenol and pentachlorophenol: chemical evidence for electron and hole transfer between coupled semiconductors, Journal of Photochemistry and Photobiology A: Chemistry, 85 (1995) 247-255.

[62] B. Neppolian, H.C. Choi, S. Sakthivel, B. Arabindoo, V. Murugesan, Solar/UV-induced photocatalytic degradation of three commercial textile dyes, Journal of Hazardous Materials, 89 (2002) 303-317.

[63] R. Comparelli, E. Fanizza, M.L. Curri, P.D. Cozzoli, G. Mascolo, A. Agostiano, UV-induced photocatalytic degradation of azo dyes by organic-capped ZnO nanocrystals immobilized onto substrates, Applied Catalysis B: Environmental, 60 (2005) 1-11.

[64] C.-H. Wu, G.-P. Chang-Chien, W.-S. Lee, Photodegradation of polychlorinated dibenzo-p-dioxins: comparison of photocatalysts, Journal of Hazardous Materials, 114 (2004) 191-197.

[65] M.A. Fox, M.T. Dulay, Heterogeneous photocatalysis, Chemical Reviews, 93 (1993) 341-357.

[66] L.B. Khalil, W.E. Mourad, M.W. Rophael, Photocatalytic reduction of environmental pollutant Cr (VI) over some semiconductors under UV/visible light illumination, Applied Catalysis B: Environmental, 17 (1998) 267-273.

[67] T. Ohno, F. Tanigawa, K. Fujihara, S. Izumi, M. Matsumura, Photocatalytic oxidation of water on TiO_2-coated WO_3 particles by visible light using Iron (III) ions as electron acceptor, Journal of Photochemistry and Photobiology A: Chemistry, 118 (1998) 41-44.

[68] J.-M. Herrmann, Heterogeneous photocatalysis: State of the art and present applications, Topics in Catalysis, 34 (2005) 49-65.

[69] A. Ramakrishnan, S. Neubert, B. Mei, J. Strunk, L. Wang, M. Bledowski, M. Muhler, R. Beranek, Enhanced performance of surface-modified TiO_2 photocatalysts prepared via a visible-light photosynthetic route, Chemical Communications, 48 (2012) 8556-8558.

[70] O.K. Dalrymple, E. Stefanakos, M.A. Trotz, D.Y. Goswami, A review of the mechanisms and modeling of photocatalytic disinfection, Applied Catalysis B: Environmental, 98 (2010) 27-38.

[71] V.A. Sakkas, M.A. Islam, C. Stalikas, T.A. Albanis, Photocatalytic degradation using design of experiments: A review and example of the Congo Red degradation, Journal of Hazardous Materials, 175 (2010) 33-44.

[72] I. Arslan-Alaton, A review of the effects of dye-assisting chemicals on advanced oxidation of reactive dyes in wastewater, Coloration Technology, 119 (2003) 345-353.

[73] J. Zhao, X. Yang, Photocatalytic oxidation for indoor air purification: A literature review, Building and Environment, 38 (2003) 645-654.

[74] I.K. Konstantinou, T.A. Albanis, TiO2-assisted photocatalytic degradation of azo dyes in aqueous solution: kinetic and mechanistic investigations: A review, Applied Catalysis B: Environmental, 49 (2004) 1-14.

[75] H. Gerischer, F. Willig, Reaction of Excited Dye Molecules at Electrodes, in Physical and Chemical Applications of Dyestuffs, Springer Berlin / Heidelberg, (1976) 31-84.

[76] K. Soutsas, V. Karayannis, I. Poulios, A. Riga, K. Ntampegliotis, X. Spiliotis, G. Papapolymerou, Decolorization and degradation of reactive azo dyes via heterogeneous photocatalytic processes, Desalination, 250 (2010) 345-350.

[77] V. Augugliaro, C. Baiocchi, A. Bianco Prevot, E. García-López, V. Loddo, S. Malato, G. Marcí, L. Palmisano, M. Pazzi, E. Pramauro, Azo-dyes photocatalytic degradation in aqueous suspension of TiO_2 under solar irradiation, Chemosphere, 49 (2002) 1223-1230.

[78] O. Legrini, E. Oliveros, A.M. Braun, Photochemical processes for water treatment, Chemical Reviews, 93 (1993) 671-698.

[79] S. Singh, H. Mahalingam, P.K. Singh, Polymer-supported titanium dioxide photocatalysts for environmental remediation: A review, Applied Catalysis A: General, 462–463 (2013) 178-195.

[80] S. Riyas, V.A. Yasir, P.N.M. Das, Crystal structure transformation of TiO_2 in presence of Fe_2O_3 and NiO in air atmosphere, Bulletin of Materials Science, 25 (2002) 267-273.

[81] A.R. Khataee, M.B. Kasiri, Photocatalytic degradation of organic dyes in the presence of nanostructured titanium dioxide: Influence of the chemical structure of dyes, Journal of Molecular Catalysis A: Chemical, 328 (2010) 8-26.

[82] A.R. Khataee, G.A. Mansoori, Nanostructured Titanium Dioxide Materials: Properties, Preparation and Applications, World Scientific Publishing Co. Pte. Ltd., Singapore, (2012).

[83] H. Kazuhito, I. Hiroshi, F. Akira, TiO_2 photocatalysis: A historical overview and future prospects, Japanese Journal of Applied Physics, 44 (2005) 8269.

[84] Y. Ao, J. Xu, D. Fu, X. Shen, C. Yuan, Low temperature preparation of anatase TiO_2-activated carbon composite film, Applied Surface Science, 254 (2008) 4001-4006.

[85] K. Wilke, H.D. Breuer, The influence of transition metal doping on the physical and photocatalytic properties of titania, Journal of Photochemistry and Photobiology A: Chemistry, 121 (1999) 49-53.

[86] A.G. Agrios, P. Pichat, State of the art and perspectives on materials and applications of photocatalysis over TiO_2, Journal of Applied Electrochemistry, 35 (2005) 655-663.

[87] U.I. Gaya, A.H. Abdullah, Heterogeneous photocatalytic degradation of organic contaminants over titanium dioxide: A review of fundamentals, progress and problems, Journal of Photochemistry and Photobiology C: Photochemistry Reviews, 9 (2008) 1-12.

[88] F. Sayılkan, M. Asiltürk, P. Tatar, N. Kiraz, Ş. Şener, E. Arpaç, H. Sayılkan, Photocatalytic performance of Sn-doped TiO_2 nanostructured thin films for photocatalytic degradation of malachite green dye under UV and Vis-lights, Materials Research Bulletin, 43 (2008) 127-134.

[89] J. Liqiang, S. Xiaojun, X. Baifu, W. Baiqi, C. Weimin, F. Honggang, The preparation and characterization of La doped TiO_2 nanoparticles and their photocatalytic activity, Journal of Solid State Chemistry, 177 (2004) 3375-3382.

[90] M. Kang, Synthesis of Fe/TiO_2 photocatalyst with nanometer size by solvothermal method and the effect of H_2O addition on structural stability and photodecomposition of methanol, Journal of Molecular Catalysis A: Chemical, 197 (2003) 173-183.

[91] B.-Y. Lee, S.-H. Park, M. Kang, S.-C. Lee, S.-J. Choung, Preparation of Al/TiO_2 nanometer photo-catalyst film and the effect of H_2O addition on photo-catalytic performance for benzene removal, Applied Catalysis A: General, 253 (2003) 371-380.

[92] M.K. Seery, R. George, P. Floris, S.C. Pillai, Silver doped titanium dioxide nanomaterials for enhanced visible light photocatalysis, Journal of Photochemistry and Photobiology A: Chemistry, 189 (2007) 258-263.

[93] M. Zhou, J. Yu, B. Cheng, Effects of Fe-doping on the photocatalytic activity of mesoporous TiO_2 powders prepared by an ultrasonic method, Journal of Hazardous Materials, 137 (2006) 1838-1847.

[94] S.S. Lee, H.J. Kim, K.T. Jung, H.S. Kim, Y.G. Shul, Photocatalytic activity of metal ion (Fe or W) doped titania, Korean Journal of Chemical Engineering, 18 (2001) 914-918.

[95] N. Sobana, M. Muruganadham, M. Swaminathan, Nano-Ag particles doped TiO_2 for efficient photodegradation of Direct azo dyes, Journal of Molecular Catalysis A: Chemical, 258 (2006) 124-132.

[96] M. Subramanian, S. Vijayalakshmi, S. Venkataraj, R. Jayavel, Effect of cobalt doping on the structural and optical properties of TiO_2 films prepared by sol–gel process, Thin Solid Films, 516 (2008) 3776-3782.

[97] Y. Yang, X.-J. Li, J.-T. Chen, L.-Y. Wang, Effect of doping mode on the photocatalytic activities of Mo/TiO_2, Journal of Photochemistry and Photobiology A: Chemistry, 163 (2004) 517-522.

[98] J. Lee, W. Choi, Effect of platinum deposits on TiO_2 on the anoxic photocatalytic degradation pathways of alkylamines in water: Dealkylation and n-alkylation, Environmental Science & Technology, 38 (2004) 4026-4033.

[99] S. Kim, S.-J. Hwang, W. Choi, Visible light active platinum-ion-doped TiO_2 photocatalyst, The Journal of Physical Chemistry B, 109 (2005) 24260-24267.

[100] Y. Wang, H. Cheng, L. Zhang, Y. Hao, J. Ma, B. Xu, W. Li, The preparation, characterization, photoelectrochemical and photocatalytic properties of lanthanide metal-ion-doped TiO_2 nanoparticles, Journal of Molecular Catalysis A: Chemical, 151 (2000) 205-216.

[101] W.-C. Hung, S.-H. Fu, J.-J. Tseng, H. Chu, T.-H. Ko, Study on photocatalytic degradation of gaseous dichloromethane using pure and iron ion-doped TiO_2 prepared by the sol–gel method, Chemosphere, 66 (2007) 2142-2151.

[102] N. Venkatachalam, M. Palanichamy, V. Murugesan, Sol–gel preparation and characterization of alkaline earth metal doped nano TiO_2: Efficient photocatalytic degradation of 4-chlorophenol, Journal of Molecular Catalysis A: Chemical, 273 (2007) 177-185.

[103] J. Zhou, M. Takeuchi, A.K. Ray, M. Anpo, X.S. Zhao, Enhancement of photocatalytic activity of P25 TiO_2 by vanadium-ion implantation under visible light irradiation, Journal of Colloid and Interface Science, 311 (2007) 497-501.

[104] J. Chen, M. Yao, X. Wang, Investigation of transition metal ion doping behaviors on TiO_2 nanoparticles, Journal of Nanoparticle Research, 10 (2007) 163-171.

[105] S. Liu, X. Chen, A visible light response TiO_2 photocatalyst realized by cationic S-doping and its application for phenol degradation, Journal of Hazardous Materials, 152 (2008) 48-55.

[106] M. Crişan, A. Brăileanu, M. Răileanu, M. Zaharescu, D. Crişan, N. Drăgan, M. Anastasescu, A. Ianculescu, I. Niţoi, V.E. Marinescu, S.M. Hodorogea, Sol–gel S-doped TiO_2 materials for environmental protection, Journal of Non-Crystalline Solids, 354 (2008) 705-711.

[107] D. Jiang, Y. Xu, B. Hou, D. Wu, Y. Sun, Synthesis of visible light-activated TiO_2 photocatalyst via surface organic modification, Journal of Solid State Chemistry, 180 (2007) 1787-1791.

[108] R.S. Sonawane, B.B. Kale, M.K. Dongare, Preparation and photo-catalytic activity of Fe-TiO_2 thin films prepared by sol–gel dip coating, Materials Chemistry and Physics, 85 (2004) 52-57.

[109] T. Bak, J. Nowotny, M. Rekas, C.C. Sorrell, Photo-electrochemical hydrogen generation from water using solar energy. Materials-related aspects, International Journal of Hydrogen Energy, 27 (2002) 991-1022.

[110] R. Asahi, T. Morikawa, T. Ohwaki, K. Aoki, Y. Taga, Visible-light photocatalysis in nitrogen-doped titanium oxides, Science, 293 (2001) 269-271.

[111] J.C. Yu, Jiaguo, Wingkei, Zitao, Lizhi, Effects of F^- doping on the photocatalytic activity and microstructures of nanocrystalline TiO_2 powders, Chemistry of Materials, 14 (2002) 3808-3816.

[112] S. Sakthivel, H. Kisch, Daylight photocatalysis by carbon-modified titanium dioxide, Angewandte Chemie International Edition, 42 (2003) 4908-4911.

[113] O. Diwald, T.L. Thompson, E.G. Goralski, S.D. Walck, J.T. Yates, The effect of nitrogen ion implantation on the photoactivity of TiO_2 rutile single crystals, The Journal of Physical Chemistry B, 108 (2004) 52-57.

[114] J.H. Park, S. Kim, A.J. Bard, Novel carbon-doped TiO_2 nanotube arrays with high aspect ratios for efficient solar water splitting, Nano Letters, 6 (2006) 24-28.

[115] L. Dong, G.-x. Cao, Y. Ma, X.-l. Jia, G.-t. Ye, S.-k. Guan, Enhanced photocatalytic degradation properties of nitrogen-doped titania nanotube arrays, Transactions of Nonferrous Metals Society of China, 19 (2009) 1583-1587.

[116] Y. Ao, J. Xu, S. Zhang, D. Fu, A one-pot method to prepare N-doped titania hollow spheres with high photocatalytic activity under visible light, Applied Surface Science, 256 (2010) 2754-2758.

[117] A. Fujishima, X. Zhang, D.A. Tryk, TiO_2 photocatalysis and related surface phenomena, Surface Science Reports, 63 (2008) 515-582.

[118] M. Pelaez, N.T. Nolan, S.C. Pillai, M.K. Seery, P. Falaras, A.G. Kontos, P.S.M. Dunlop, J.W.J. Hamilton, J.A. Byrne, K. O'Shea, M.H. Entezari, D.D. Dionysiou, A review on the visible light active titanium dioxide photocatalysts for environmental applications, Applied Catalysis B: Environmental, 125 (2012) 331-349.

[119] S.M. Gupta, M. Tripathi, A review of TiO_2 nanoparticles, Chinese Science Bulletin, 56 (2011) 1639-1657.

[120] R.S.K. Wong, J. Feng, X. Hu, P.L. Yue, Discoloration and mineralization of non-biodegradable azo dye Orange II by copper-doped TiO_2 nanocatalysts, Journal of Environmental Science and Health, Part A, 39 (2004) 2583-2595.

[121] W.K. Wong, M.A. Malati, Doped TiO_2 for solar energy applications, Solar Energy, 36 (1986) 163-168.

[122] J. Papp, H.S. Shen, R. Kershaw, K. Dwight, A. Wold, Titanium(IV) oxide photocatalysts with palladium, Chemistry of Materials, 5 (1993) 284-288.

[123] K. Adachi, K. Ohta, T. Mizuno, Photocatalytic reduction of carbon dioxide to hydrocarbon using copper-loaded titanium dioxide, Solar Energy, 53 (1994) 187-190.

[124] A.V. Rupa, D. Divakar, T. Sivakumar, Titania and noble metals deposited titania catalysts in the photodegradation of tartazine, Catalysis Letters, 132 (2009) 259-267.

[125] D. Heeskens, P. Aghaei, S. Kaluza, J. Strunk, M. Muhler, Selective oxidation of ethanol in the liquid phase over Au/TiO_2, physica status solidi (b), 250 (2013) 1107-1118.

[126] A. Sclafani, J.-M. Herrmann, Influence of metallic silver and of platinum-silver bimetallic deposits on the photocatalytic activity of titania (anatase and rutile) in organic

and aqueous media, Journal of Photochemistry and Photobiology A: Chemistry, 113 (1998) 181-188.

[127] C.-y. Wang, C.-y. Liu, X. Zheng, J. Chen, T. Shen, The surface chemistry of hybrid nanometer-sized particles I. Photochemical deposition of gold on ultrafine TiO_2 particles, Colloids and Surfaces A: Physicochemical and Engineering Aspects, 131 (1998) 271-280.

[128] V. Subramanian, E. Wolf, P.V. Kamat, Semiconductor−metal composite nanostructures. To what extent do metal nanoparticles improve the photocatalytic activity of TiO_2 films?, The Journal of Physical Chemistry B, 105 (2001) 11439-11446.

[129] K.V.S. Rao, B. Lavédrine, P. Boule, Influence of metallic species on TiO_2 for the photocatalytic degradation of dyes and dye intermediates, Journal of Photochemistry and Photobiology A: Chemistry, 154 (2003) 189-193.

[130] A.K. Gupta, A. Pal, C. Sahoo, Photocatalytic degradation of a mixture of Crystal Violet (Basic Violet 3) and Methyl Red dye in aqueous suspensions using Ag^+ doped TiO_2, Dyes and Pigments, 69 (2006) 224-232.

[131] F. Han, V.S.R. Kambala, M. Srinivasan, D. Rajarathnam, R. Naidu, Tailored titanium dioxide photocatalysts for the degradation of organic dyes in wastewater treatment: A review, Applied Catalysis A: General, 359 (2009) 25-40.

[132] W. Choi, A. Termin, M.R. Hoffmann, The role of metal ion dopants in quantum-sized TiO_2: Correlation between photoreactivity and charge carrier recombination dynamics, The Journal of Physical Chemistry, 98 (1994) 13669-13679.

[133] X. Yang, C. Cao, L. Erickson, K. Hohn, R. Maghirang, K. Klabunde, Photo-catalytic degradation of Rhodamine B on C-, S-, N-, and Fe-doped TiO_2 under visible-light irradiation, Applied Catalysis B: Environmental, 91 (2009) 657-662.

[134] J. Zhu, J. Ren, Y. Huo, Z. Bian, H. Li, Nanocrystalline Fe/TiO_2 visible photocatalyst with a mesoporous structure prepared via a nonhydrolytic sol−gel route, The Journal of Physical Chemistry C, 111 (2007) 18965-18969.

[135] S. Klosek, D. Raftery, Visible Light Driven V-Doped TiO_2 Photocatalyst and Its Photooxidation of Ethanol, The Journal of Physical Chemistry B, 105 (2001) 2815-2819.

[136] S. Ghasemi, S. Rahimnejad, S.R. Setayesh, S. Rohani, M.R. Gholami, Transition metal ions effect on the properties and photocatalytic activity of nanocrystalline TiO_2 prepared in an ionic liquid, Journal of Hazardous Materials, 172 (2009) 1573-1578.

[137] N. Gupta, B. Pal, Photocatalytic activity of transition metal and metal ions impregnated TiO_2 nanostructures for iodide oxidation to iodine formation, Journal of Molecular Catalysis A: Chemical, 371 (2013) 48-55.

[138] D. Zhang, Enhanced photocatalytic activity for titanium dioxide by co-modification with copper and iron, Transition Metal Chemistry, 35 (2010) 933-938.

[139] P. Yang, C. Lu, N. Hua, Y. Du, Titanium dioxide nanoparticles co-doped with Fe^{3+} and Eu^{3+} ions for photocatalysis, Materials Letters, 57 (2002) 794-801.

[140] M.A. Behnajady, H. Eskandarloo, Silver and copper co-impregnated onto TiO_2-P25 nanoparticles and its photocatalytic activity, Chemical Engineering Journal, 228 (2013) 1207-1213.

[141] N. Daneshvar, D. Salari, A.R. Khataee, Photocatalytic degradation of azo dye acid red 14 in water on ZnO as an alternative catalyst to TiO_2, Journal of Photochemistry and Photobiology A: Chemistry, 162 (2004) 317-322.

[142] K. Selvam, M. Muruganandham, I. Muthuvel, M. Swaminathan, The influence of inorganic oxidants and metal ions on semiconductor sensitized photodegradation of 4-fluorophenol, Chemical Engineering Journal, 128 (2007) 51-57.

[143] R.A. Damodar, K. Jagannathan, T. Swaminathan, Decolourization of reactive dyes by thin film immobilized surface photoreactor using solar irradiation, Solar Energy, 81 (2007) 1-7.

[144] A.R. Khataee, M. Zarei, M. Fathinia, M.K. Jafari, Photocatalytic degradation of an anthraquinone dye on immobilized TiO_2 nanoparticles in a rectangular reactor: Destruction pathway and response surface approach, Desalination, 268 (2011) 126-133.

[145] S. Karcher, A. Kornmüller, M. Jekel, Anion exchange resins for removal of reactive dyes from textile wastewaters, Water Research, 36 (2002) 4717-4724.

[146] D. Chatterjee, A. Mahata, Visible light induced photodegradation of organic pollutants on dye adsorbed TiO2 surface, Journal of Photochemistry and Photobiology A: Chemistry, 153 (2002) 199-204.

[147] F. Herrera, A. Lopez, J. Kiwi, Photochemically activated degradation of reactive dyes: Statistical modeling of the reactor performance, Journal of Photochemistry and Photobiology A: Chemistry, 135 (2000) 45-51.

[148] I. Poulios, I. Tsachpinis, Photodegradation of the textile dye Reactive Black 5 in the presence of semiconducting oxides, Journal of Chemical Technology & Biotechnology, 74 (1999) 349-357.

[149] T.C.K. Yang, S.-F. Wang, S.H.Y. Tsai, S.-Y. Lin, Intrinsic photocatalytic oxidation of the dye adsorbed on TiO_2 photocatalysts by diffuse reflectance infrared Fourier transform spectroscopy, Applied Catalysis B: Environmental, 30 (2001) 293-301.

[150] A. Garg, V.K. Sangal, P.K. Bajpai, Decolorization and degradation of Reactive Black 5 dye by photocatalysis: Modeling, optimization and kinetic study, Desalination and Water Treatment, 57 (2016) 18003-18015.

[151] D. Chatterjee, V.R. Patnam, A. Sikdar, P. Joshi, R. Misra, N.N. Rao, Kinetics of the decoloration of reactive dyes over visible light-irradiated TiO_2 semiconductor photocatalyst, Journal of Hazardous Materials, 156 (2008) 435-441.

[152] S.K. Kansal, N. Kaur, S. Singh, Photocatalytic degradation of two commercial reactive dyes in aqueous phase using nanophotocatalysts, Nanoscale Research Letters, 4 (2009) 709-716.

[153] O.K. Mahadwad, P.A. Parikh, R.V. Jasra, C. Patil, Photocatalytic degradation of reactive black-5 dye using TiO_2 impregnated ZSM-5, Bulletin of Materials Science, 34 (2011) 551-556.

[154] M. Muneer, R. Philip, S. Das, Photocatalytic degradation of waste water pollutants. Titanium dioxidemediated oxidation of a textile dye, Acid Blue 40, Research on Chemical Intermediates, 23 (1997) 233-246.

[155] C. Bauer, P. Jacques, A. Kalt, Photooxidation of an azo dye induced by visible light incident on the surface of TiO_2, Journal of Photochemistry and Photobiology A: Chemistry, 140 (2001) 87-92.

[156] C. Galindo, P. Jacques, A. Kalt, Photochemical and photocatalytic degradation of an indigoid dye: A case study of acid blue 74 (AB74), Journal of Photochemistry and Photobiology A: Chemistry, 141 (2001) 47-56.

[157] A. Houas, H. Lachheb, M. Ksibi, E. Elaloui, C. Guillard, J.-M. Herrmann, Photocatalytic degradation pathway of methylene blue in water, Applied Catalysis B: Environmental, 31 (2001) 145-157.

[158] M. Saquib, M. Muneer, TiO_2-mediated photocatalytic degradation of a triphenylmethane dye (gentian violet), in aqueous suspensions, Dyes and Pigments, 56 (2003) 37-49.

[159] M. Qamar, M. Saquib, M. Muneer, Photocatalytic degradation of two selected dye derivatives, Chromotrope 2B and Amido Black 10B, in aqueous suspensions of titanium dioxide, Dyes and Pigments, 65 (2005) 1-9.

[160] M.M.H. Khalil, A.A. Abdel-Shafi, M.S.A. Abdel-Mottaleb, Photocatalytic degradation of some toxic analytical reagents with TiO_2, International Journal of Photoenergy, 1 (1999) 85-88.

[161] K. Vinodgopal, P.V. Kamat, Electrochemically assisted photocatalysis using nanocrystalline semiconductor thin films, Solar Energy Materials and Solar Cells, 38 (1995) 401-410.

[162] B. Neppolian, H.C. Choi, S. Sakthivel, B. Arabindoo, V. Murugesan, Solar light induced and TiO_2 assisted degradation of textile dye Reactive Blue 4, Chemosphere, 46 (2002) 1173-1181.

[163] I.A. Alaton, I.A. Balcioglu, Photochemical and heterogeneous photocatalytic degradation of waste vinylsulphone dyes: a case study with hydrolyzed Reactive Black 5, Journal of Photochemistry and Photobiology A: Chemistry, 141 (2001) 247-254.

[164] C.A.K. Gouvêa, F. Wypych, S.G. Moraes, N. Durán, N. Nagata, P. Peralta-Zamora, Semiconductor-assisted photocatalytic degradation of reactive dyes in aqueous solution, Chemosphere, 40 (2000) 433-440.

[165] W. Baran, A. Makowski, W. Wardas, The influence of $FeCl_3$ on the photocatalytic degradation of dissolved azo dyes in aqueous TiO_2 suspensions, Chemosphere, 53 (2003) 87-95.

[166] B. Zielińska, J. Grzechulska, A.W. Morawski, Photocatalytic decomposition of textile dyes on TiO_2-Tytanpol A11 and TiO_2-Degussa P25, Journal of Photochemistry and Photobiology A: Chemistry, 157 (2003) 65-70.

[167] B. Neppolian, S. Sakthivel, B. Arabindoo, M. Palanichamy, V. Murugesan, Degradation of textile dye by solar light using TiO_2 and ZnO photocatalysts, Journal of Environmental Science and Health, Part A, 34 (1999) 1829-1838.

[168] S.K. Sharma, H. Bhunia, P.K. Bajpai, Photocatalytic decolorization kinetics and mineralization of Reactive Black 5 aqueous solution by UV/TiO_2 nanoparticles, CLEAN – Soil, Air, Water, 40 (2012) 1290-1296.

[169] M. Nikazar, K. Gholivand, K. Mahanpoor, Photocatalytic degradation of azo dye Acid Red 114 in water with TiO_2 supported on clinoptilolite as a catalyst, Desalination, 219 (2008) 293-300.

[170] M.J. Pawar, A.D. Khajone, A.B. Ingale, M.D. Gaonar, Sol-gel synthesis of nanosized α-Fe_2O_3 and photodegradation of Acid Red 114 Dye, International Journal of Advanced Scientific Research and Technology, 3 (2012) 600-605.

[171] J.-M. Lee, M.-S. Kim, B. Hwang, W. Bae, B.-W. Kim, Photodegradation of Acid Red 114 dissolved using a photo-Fenton process with TiO_2, Dyes and Pigments, 56 (2003) 59-67.

[172] C. Sahoo, A.K. Gupta, A. Pal, Photocatalytic degradation of Crystal Violet (C.I. Basic Violet 3) on silver ion doped TiO2, Dyes and Pigments, 66 (2005) 189-196.

[173] T.B. Nguyen, M.-J. Hwang, K.-S. Ryu, Synthesis and high photocatalytic activity of Zn-doped TiO_2 nanoparticles by sol-gel and ammonia-evaporation method, Bulletin of the Korean Chemical Society, 33 (2012) 243-247.

[174] Y. Lu, Q. Sun, T. Liu, D. Yang, Y. Liu, J. Li, Fabrication, characterization and photocatalytic properties of millimeter-long TiO_2 fiber with nanostructures using cellulose fiber as a template, Journal of Alloys and Compounds, 577 (2013) 569-574.

[175] J. Virkutyte, V. Jegatheesan, R.S. Varma, Visible light activated TiO_2/microcrystalline cellulose nanocatalyst to destroy organic contaminants in water, Bioresource Technology, 113 (2012) 288-293.

[176] M.J. Uddin, F. Cesano, F. Bonino, S. Bordiga, G. Spoto, D. Scarano, A. Zecchina, Photoactive TiO_2 films on cellulose fibres: Synthesis and characterization, Journal of Photochemistry and Photobiology A: Chemistry, 189 (2007) 286-294.

[177] L. Bouna, B. Rhouta, F. Maury, Physicochemical study of photocatalytic activity of TiO_2 supported palygorskite clay mineral, International Journal of Photoenergy, 2013 (2013) 6.

[178] M. Cristina Yeber, J. Rodríguez, J. Freer, N. Durán, H. D. Mansilla, Photocatalytic degradation of cellulose bleaching effluent by supported TiO_2 and ZnO, Chemosphere, 41 (2000) 1193-1197.

[179] M.A. Behnajady, N. Modirshahla, N. Daneshvar, M. Rabbani, Photocatalytic degradation of an azo dye in a tubular continuous-flow photoreactor with immobilized TiO_2 on glass plates, Chemical Engineering Journal, 127 (2007) 167-176.

[180] S. Sakthivel, M.V. Shankar, M. Palanichamy, B. Arabindoo, V. Murugesan, Photocatalytic decomposition of leather dye: Comparative study of TiO_2 supported on alumina and glass beads, Journal of Photochemistry and Photobiology A: Chemistry, 148 (2002) 153-159.

[181] A.R. Khataee, M. Zarei, Photocatalysis of a dye solution using immobilized ZnO nanoparticles combined with photoelectrochemical process, Desalination, 273 (2011) 453-460.

[182] D.F. Ollis, E. Pelizzetti, N. Serpone, Photocatalyzed destruction of water contaminants, Environmental Science & Technology, 25 (1991) 1522-1529.

[183] L.C. Chen, T.C. Chou, Kinetics of photodecolorization of methyl orange using titanium dioxide as catalyst, Industrial & Engineering Chemistry Research, 32 (1993) 1520-1527.

[184] V.K. Pareek, A.A. Adesina, Handbook of Photochemistry and Photobiology, American Scientific Publishers, H.S. Nalwa, Editor, Stevenson Ranch: CA., (2003) 345-412.

[185] I. Michael, E. Hapeshi, C. Michael, D. Fatta-Kassinos, Solar Fenton and solar TiO_2 catalytic treatment of ofloxacin in secondary treated effluents: Evaluation of operational and kinetic parameters, Water Research, 44 (2010) 5450-5462.

[186] M. Sleiman, D. Vildozo, C. Ferronato, J.-M. Chovelon, Photocatalytic degradation of azo dye Metanil Yellow: Optimization and kinetic modeling using a chemometric approach, Applied Catalysis B: Environmental, 77 (2007) 1-11.

[187] T.A. McMurray, J.A. Byrne, P.S.M. Dunlop, J.G.M. Winkelman, B.R. Eggins, E.T. McAdams, Intrinsic kinetics of photocatalytic oxidation of formic and oxalic acid on immobilised TiO_2 films, Applied Catalysis A: General, 262 (2004) 105-110.

[188] S. Hwang, M.C. Lee, W. Choi, Highly enhanced photocatalytic oxidation of CO on titania deposited with Pt nanoparticles: kinetics and mechanism, Applied Catalysis B: Environmental, 46 (2003) 49-63.

[189] C.M. So, M.Y. Cheng, J.C. Yu, P.K. Wong, Degradation of azo dye Procion Red MX-5B by photocatalytic oxidation, Chemosphere, 46 (2002) 905-912.

[190] G.A. Epling, C. Lin, Photoassisted bleaching of dyes utilizing TiO_2 and visible light, Chemosphere, 46 (2002) 561-570.

[191] A.F. Martins, M.L. Wilde, C. Da Silveira, Photocatalytic degradation of Brilliant Red dye and textile wastewater, Journal of Environmental Science and Health, Part A, 41 (2006) 675-685.

[192] U.G. Akpan, B.H. Hameed, Parameters affecting the photocatalytic degradation of dyes using TiO_2-based photocatalysts: A review, Journal of Hazardous Materials, 170 (2009) 520-529.

[193] A. Bianco Prevot, C. Baiocchi, M.C. Brussino, E. Pramauro, P. Savarino, V. Augugliaro, G. Marcì, L. Palmisano, Photocatalytic degradation of Acid Blue 80 inaqueous solutions containing TiO_2 suspensions, Environmental Science & Technology, 35 (2001) 971-976.

[194] H. Lachheb, E. Puzenat, A. Houas, M. Ksibi, E. Elaloui, C. Guillard, J.-M. Herrmann, Photocatalytic degradation of various types of dyes (Alizarin S, Crocein Orange G, Methyl Red, Congo Red, Methylene Blue) in water by UV-irradiated titania, Applied Catalysis B: Environmental, 39 (2002) 75-90.

[195] M. Stylidi, D.I. Kondarides, X.E. Verykios, Pathways of solar light-induced photocatalytic degradation of azo dyes in aqueous TiO_2 suspensions, Applied Catalysis B: Environmental, 40 (2003) 271-286.

[196] S. Tunesi, M. Anderson, Influence of chemisorption on the photodecomposition of salicylic acid and related compounds using suspended titania ceramic membranes, The Journal of Physical Chemistry, 95 (1991) 3399-3405.

[197] C. Guillard, J. Disdier, C. Monnet, J. Dussaud, S. Malato, J. Blanco, M.I. Maldonado, J.-M. Herrmann, Solar efficiency of a new deposited titania photocatalyst: Chlorophenol, pesticide and dye removal applications, Applied Catalysis B: Environmental, 46 (2003) 319-332.

[198] K. Okamoto, Y. Yamamoto, H. Tanaka, A. Itaya, Kinetics of heterogeneous photocatalytic decomposition of phenol over anatase TiO_2 powder, Bulletin of the Chemical Society of Japan, 58 (1985) 2023-2028.

[199] R.W. Matthews, S.R. McEvoy, A comparison of 254 nm and 350 nm excitation of TiO_2 in simple photocatalytic reactors, Journal of Photochemistry and Photobiology A: Chemistry, 66 (1992) 355-366.

[200] A.R. Soleymani, J. Saien, H. Bayat, Artificial neural networks developed for prediction of dye decolorization efficiency with UV/$K_2S_2O_8$ process, Chemical Engineering Journal, 170 (2011) 29-35.

[201] A. Aleboyeh, M.B. Kasiri, M.E. Olya, H. Aleboyeh, Prediction of azo dye decolorization by UV/H_2O_2 using artificial neural networks, Dyes and Pigments, 77 (2008) 288-294.

[202] S. Dutta, S.A. Parsons, C. Bhattacharjee, S. Bandhyopadhyay, S. Datta, Development of an artificial neural network model for adsorption and photocatalysis of reactive dye on TiO_2 surface, Expert Systems with Applications, 37 (2010) 8634-8638.

[203] M. Vaez, A. Zarringhalam Moghaddam, S. Alijani, Optimization and modeling of photocatalytic degradation of azo dye using a response surface methodology (RSM) based on the central composite design with immobilized titania nanoparticles, Industrial & Engineering Chemistry Research, 51 (2012) 4199-4207.

[204] S. Göb, E. Oliveros, S.H. Bossmann, A.M. Braun, R. Guardani, C.A.O. Nascimento, Modeling the kinetics of a photochemical water treatment process by means of artificial neural networks, Chemical Engineering and Processing: Process Intensification, 38 (1999) 373-382.

[205] P. Calza, V.A. Sakkas, A. Villioti, C. Massolino, V. Boti, E. Pelizzetti, T. Albanis, Multivariate experimental design for the photocatalytic degradation of imipramine: Determination of the reaction pathway and identification of intermediate products, Applied Catalysis B: Environmental, 84 (2008) 379-388.

[206] V.K. Pareek, M.P. Brungs, A.A. Adesina, R. Sharma, Artificial neural network modeling of a multiphase photodegradation system, Journal of Photochemistry and Photobiology A: Chemistry, 149 (2002) 139-146.

[207] M.B. Kasiri, H. Aleboyeh, A. Aleboyeh, Modeling and optimization of heterogeneous photo-fenton process with response surface methodology and artificial neural networks, Environmental Science & Technology, 42 (2008) 7970-7975.

[208] A.R. Khataee, Photocatalytic removal of C.I. Basic Red 46 on immobilized TiO_2 nanoparticles: Artificial neural network modelling, Environmental Technology, 30 (2009) 1155-1168.

[209] M. Zarei, A.R. Khataee, R. Ordikhani-Seyedlar, M. Fathinia, Photoelectro-Fenton combined with photocatalytic process for degradation of an azo dye using supported TiO_2 nanoparticles and carbon nanotube cathode: Neural network modeling, Electrochimica Acta, 55 (2010) 7259-7265.

[210] G.E.P. Box, J.S. Hunter, Multi-Factor Experimental Designs For Exploring Response Surfaces, (1957) 195-241.

[211] G.E.P. Box, D.W. Behnken, Some new three level designs for the study of quantitative variables, Technometrics, 2 (1960) 455-475.

[212] S.J. Kalil, F. Maugeri, M.I. Rodrigues, Response surface analysis and simulation as a tool for bioprocess design and optimization, Process Biochemistry, 35 (2000) 539-550.

[213] S. Mannan, A. Fakhru'l-Razi, M.Z. Alam, Optimization of process parameters for the bioconversion of activated sludge by Penicillium corylophilum, using response surface methodology, Journal of Environmental Sciences, 19 (2007) 23-28.

[214] A. Kumar, B. Prasad, I.M. Mishra, Process parametric study for ethene carboxylic acid removal onto powder activated carbon using Box-Behnken design, Chemical Engineering & Technology, 30 (2007) 932-937.

[215] K. Tarangini, A. Kumar, G.R. Satpathy, V.K. Sangal, Statistical optimization of process parameters for Cr (VI) biosorption onto mixed cultures of pseudomonas aeruginosa and bacillus subtilis, CLEAN – Soil, Air, Water, 37 (2009) 319-327.

[216] I.-H. Cho, K.-D. Zoh, Photocatalytic degradation of azo dye (Reactive Red 120) in TiO_2/UV system: Optimization and modeling using a response surface methodology (RSM) based on the central composite design, Dyes and Pigments, 75 (2007) 533-543.

[217] A.R. Khataee, M. Zarei, L. Moradkhannejhad, Application of response surface methodology for optimization of azo dye removal by oxalate catalyzed photoelectro-Fenton process using carbon nanotube-PTFE cathode, Desalination, 258 (2010) 112-119.

[218] A.R. Khataee, M. Zarei, L. Moradkhannejhad, S. Nourie, B. Vahid, Nitrogen doping of commercial TiO_2 nanoparticles for enhanced photocatalytic degradation of dye under visible light: Central composite design approach, Advanced Chemistry Letters, 1 (2013) 24-31.

[219] T.A. Carlson, Photoelectron and Auger Spectroscopy, Plenum Press, (1975).

[220] A. Verma, N.T. Prakash, A.P. Toor, An efficient TiO_2 coated immobilized system for the degradation studies of herbicide isoproturon: Durability studies, Chemosphere, 109 (2014) 7-13.

[221] J. Saien, A.R. Soleymani, H. Bayat, Modeling Fentonic advanced oxidation process decolorization of Direct Red 16 using artificial neural network technique, Desalination and Water Treatment, 40 (2012) 174-182.

[222] P. Kaur, V.K. Sangal, J.P. Kushwaha, Modeling and evaluation of electro-oxidation of dye wastewater using artificial neural networks, RSC Advances, 5 (2015) 34663-34671.

[223] V.K. Sangal, V. Kumar, I.M. Mishra, Process parametric optimization of a divided wall distillation column, Chemical Engineering Communications, 201 (2014) 72-87.

[224] M. Muthukumar, D. Mohan, M. Rajendran, Optimization of mix proportions of mineral aggregates using Box Behnken design of experiments, Cement and Concrete Composites, 25 (2003) 751-758.

[225] M. Evans, Optimization of manufacturing processes: A response surface approach, Maney Materials Science, London, (2003).

[226] V.K. Sangal, V. Kumar, I.M. Mishra, Optimization of structural and operational variables for the energy efficiency of a divided wall distillation column, Computers & Chemical Engineering, 40 (2012) 33-40.

[227] C. Sahoo, A.K. Gupta, Optimization of photocatalytic degradation of methyl blue using silver ion doped titanium dioxide by combination of experimental design and response surface approach, Journal of Hazardous Materials, 215–216 (2012) 302-310.

[228] N. Barka, S. Qourzal, A. Assabbane, A. Nounah, Y. Ait-Ichou, Photocatalytic degradation of an azo reactive dye, Reactive Yellow 84, in water using an industrial titanium dioxide coated media, Arabian Journal of Chemistry, 3 (2010) 279-283.

[229] B. Gözmen, M. Turabik, A. Hesenov, Photocatalytic degradation of Basic Red 46 and Basic Yellow 28 in single and binary mixture by UV/TiO_2/periodate system, Journal of Hazardous Materials, 164 (2009) 1487-1495.

[230] R.S. Juang, S.H. Lin, P.Y. Hsueh, Removal of binary azo dyes from water by UV-irradiated degradation in TiO_2 suspensions, Journal of Hazardous Materials, 182 (2010) 820-826.

[231] S.K. Sharma, H. Bhunia, P.K. Bajpai, Photocatalytic decolorization kinetics and adsorption isotherms of a mixture of two anionic azo dyes: Reactive Red 120 and Reactive Black 5, Desalination and Water Treatment, 44 (2012) 261-268.

[232] P. Singh, A. Dhir, V.K. Sangal, Optimization of photocatalytic process parameters for the degradation of acrylonitrile using Box Behnken Design, Desalination and Water Treatment, 55 (2014) 1501-1508.

[233] S. Ghafari, H.A. Aziz, M.H. Isa, A.A. Zinatizadeh, Application of response surface methodology (RSM) to optimize coagulation–flocculation treatment of leachate using poly-aluminum chloride (PAC) and alum, Journal of Hazardous Materials, 163 (2009) 650-656.

[234] S. Bansal, J.P. Kushwaha, V.K. Sangal, Electrochemical treatment of Reactive Black 5 textile wastewater: optimization, kinetics, and disposal study, Water Environment Research, 85 (2013) 2294-2306.

[235] J.M. Dostanić, D.R. Lončarević, P.T. Banković, O.G. Cvetković, D.M. Jovanović, D.Ž. Mijin, Influence of process parameters on the photodegradation of synthesized azo pyridone dye in TiO_2 water suspension under simulated sunlight, Journal of Environmental Science and Health, Part A, 46 (2011) 70-79.

[236] M. Muruganandham, N. Sobana, M. Swaminathan, Solar assisted photocatalytic and photochemical degradation of Reactive Black 5, Journal of Hazardous Materials, 137 (2006) 1371-1376.

[237] B. Zielińska, J. Grzechulska, B. Grzmil, A.W. Morawski, Photocatalytic degradation of Reactive Black 5: A comparison between TiO_2-Tytanpol A11 and TiO_2-Degussa P25 photocatalysts, Applied Catalysis B: Environmental, 35 (2001) L1-L7.

[238] N. Wang, J. Li, L. Zhu, Y. Dong, H. Tang, Highly photocatalytic activity of metallic hydroxide/titanium dioxide nanoparticles prepared via a modified wet precipitation process, Journal of Photochemistry and Photobiology A: Chemistry, 198 (2008) 282-287.

[239] M. Hamadanian, A. Reisi-Vanani, A. Majedi, Sol-gel preparation and characterization of Co/TiO_2 nanoparticles: application to the degradation of Methyl Orange, Journal of the Iranian Chemical Society, 7 (2010) S52-S58.

[240] K.V. Baiju, P. Shajesh, W. Wunderlich, P. Mukundan, S.R. Kumar, K.G.K. Warrier, Effect of tantalum addition on anatase phase stability and photoactivity of aqueous sol–gel derived mesoporous titania, Journal of Molecular Catalysis A: Chemical, 276 (2007) 41-46.

[241] K.M.K. Srivatsa, M. Bera, A. Basu, Pure brookite titania crystals with large surface area deposited by Plasma Enhanced Chemical Vapour Deposition technique, Thin Solid Films, 516 (2008) 7443-7446.

[242] K. Umar, A. Aris, T. Parveen, J. Jaafar, Z. Abdul Majid, A. Vijaya Bhaskar Reddy, J. Talib, Synthesis, characterization of Mo and Mn doped ZnO and their photocatalytic activity for the decolorization of two different chromophoric dyes, Applied Catalysis A: General, 505 (2015) 507-514.

[243] Y. Lv, L. Yu, H. Huang, H. Liu, Y. Feng, Preparation, characterization of P-doped TiO_2 nanoparticles and their excellent photocatalystic properties under the solar light irradiation, Journal of Alloys and Compounds, 488 (2009) 314-319.

[244] K. Umar, M.M. Haque, M. Muneer, T. Harada, M. Matsumura, Mo, Mn and La doped TiO_2: Synthesis, characterization and photocatalytic activity for the decolourization of three different chromophoric dyes, Journal of Alloys and Compounds, 578 (2013) 431-438.

[245] Z. Wenfang, L. Qingju, Z. Zhongqi, Z. Ji, Preparation and properties of vanadium-doped TiO_2 photocatalysts, Journal of Physics D: Applied Physics, 43 (2010) 035301-035306.

[246] J. Tian, H. Gao, H. Kong, P. Yang, W. Zhang, J. Chu, Influence of transition metal doping on the structural, optical, and magnetic properties of TiO2 films deposited on Si substrates by a sol–gel process, Nanoscale Research Letters, 8 (2013) 1-11.

[247] M. Rastegar, K.R. Shadbad, A.R. Khataee, R. Pourrajab, Optimization of photocatalytic degradation of sulphonated diazo dye C.I. Reactive Green 19 using ceramic-coated TiO_2 nanoparticles, Environmental Technology, 33 (2012) 995-1003.

[248] M.A. Nawi, Y.S. Ngoh, S.M. Zain, Photoetching of immobilized TiO_2-ENR50-PVC composite for improved photocatalytic activity, International Journal of Photoenergy, DOI: 10.1155/2012/859294 (2012).

PUBLICATIONS

In Peer Reviewed Journals

1. Alok Garg, Vikas K. Sangal, Pramod K. Bajpai, Decolorization and degradation of Reactive Black 5 dye by photocatalysis: Modeling, optimization and kinetic study, Desalination and Water Treatment, 57 (2016) 18003-18015.
2. Alok Garg, Vikas K. Sangal, Pramod K. Bajpai, Photocatalytic treatment of binary mixture of dyes using UV/TiO2 process: Calibration, modeling, optimization and mineralization study, International Journal of Chemical Reactor Engineering (Accepted DOI: 10.1515/ijcre-2015-0220).
3. Alok Garg, Vikas K. Sangal, Pramod K. Bajpai, Ashish Kumar, Photocatalytic dyes degradation under visible light irradiation over nano (Fe/TiO_2, Cu/TiO_2 and $Fe\text{-}Cu/TiO_2$) catalysts, Catalysis Letters (Communicated, Manuscript id: CATLET-2016-0919).
4. Alok Garg, Vikas K. Sangal, Pramod K. Bajpai, Photocatalytic Degradation of three Textile Dyes using TiO_2 Nanoparticles immobilized on Cement Beads (under preparation).

In Conferences

1. Alok Garg, Vikas K Sangal, Pramod K Bajpai, Adsorption and Photocatalytic Degradation of Acid Blue 113 Catalyzed by TiO_2 Photocatalyst, Second National Conference on Advanced Oxidation Processes-2015 (AOP2015) (Oct 15, 2015 to Oct 16, 2016) Hosted by: Dr. S. S. Bhatnagar UICT, Punjab University, Chandigarh, India
2. Alok Garg, Vikas K Sangal, Pramod K Bajpai, Photodegradation of Reactive Black 5 Textile Dye Effluent using Doped and Undoped TiO_2 Photocatalyst, Fourth international Conference on Advanced Oxidation Processes-2016 (AOP2016) (Dec 17 – 20 2016) Hosted by: BITS – Pilani (Goa campus) India (Abstract accepted).